A MODIS-BASED ALGORITHM TO DETECT FOREST DEGRADATION: A CASE STUDY IN MEXICO

by

Yunuen Reygadas Langarica, M.A.

A dissertation submitted to the Graduate Council of
Texas State University in partial fulfillment
of the requirements for the degree of
Doctor of Philosophy
with a Major in Geographic Information Science
December 2019

Committee Members:

Jennifer L. R. Jensen, Chair

Nate Currit

Edwin T. Chow

Gretchen G. Moisen

FAIR USE AND AUTHOR'S PERMISSION STATEMENT

Fair Use

Duplication Permission

ACKNOWLEDGEMENTS

I would like to express my deepest gratitude and appreciation to my advisor, Dr. Jennifer Jensen, for her unconditional support through my entire academic journey at Texas State University. Her guidance was not limited to my specific research field, she mentored me on many ways, from how to organize and teach a Remote Sensing course to how to deal with the most subtle details of the academic world. I am sincerely grateful for the role she played as my advisor and for her inspiring example as a successful woman in science. I would also like to extend my sincere thanks to my committee members, Dr. Nate Currit, Dr. Edwin Chow, and Dr. Gretchen Moisen, whose valuable experience, suggestions, and comments greatly improved this work.

I also wish to thank the *Comisión Nacional Forestal* (CONAFOR) for providing me with reference data to validate the results of this research. In particular, I would like to thank David Quiroz, who kindly walked me through the data acquisition process. A warm thank you goes to Diego Reygadas for his guidance at the earliest stage of this process.

I must express my profound gratitude to my colleagues of the Department of Geography for the company, the deep and diverse conversations, and for the insightful feedback that strengthened the foundations of my research.

I cannot thank my parents, Martha Langarica and Efrain Reygadas, enough for providing me with the adequate personal tools to overcome the challenges of being a

Ph.D. student in a foreign country. Also, thanks to my sister, Yoa, for understanding me without having to use words. A special thanks to Aldo for motivating me and supporting me to pursue a Ph.D. in the United States. My profound acknowledgment to Trins and Cyn for holding my back and feeding my spirit in a daily basis through “Once upon a time”. Lastly, I would like to thank to my always-present childhood friends.

TABLE OF CONTENTS

Page

LIST OF TABLES

Table **Page**

LIST OF FIGURES

Figure Page

ABSTRACT

With global warming becoming a major concern worldwide, forest degradation impacts on environmental services, especially those related to climate regulation through carbon sequestration, have received increasing attention among the scientific community. However, monitoring forest degradation has not been easy to accomplish due to the non-discrete nature of the process, in which changes are subtle and alter vegetation gradually. This research proposes an algorithm to detect forest degradation using Moderate Resolution Imaging Spectroradiometer (MODIS) images collected over Central Mexico (tile h08v06) between 2002 and 2017. The underlying assumption of a constant negative relationship between vegetation greenness and surface temperature, which has guided several studies that aim to identify ecosystem disturbances, was discarded as a foundation on which to build the algorithm. An evaluation of the annual and intraseasonal relationship between Leaf Area Index (LAI) and Land Surface Temperature (LST) demonstrated that the relationship between these two variables in the study area is not constant and its nature (i.e., sign) varies depending on the temporal scale and forest type under analysis. The use of LAI was proposed to facilitate consideration of the structural changes evident from degradation though not necessarily observable through widely used vegetation spectral indices, such as Normalized Difference Vegetation Index (NDVI)and Enhanced Vegetation Index (EVI). Thus, the proposed algorithm focused on vegetation greenness and overcame the challenge of detecting subtle and gradual vegetation changes through a trend analysis of LAI. Overall, the results indicate that 52% of the study area has experienced increasing LAI trends, 37% has remained unchanged, and 11% exhibits some level of forest degradation (i.e., decreasing LAI trends). Particularly, the algorithm estimated that 0.6% (385 km^2) is highly degraded, 5.3% (3,406 km^2) moderately degraded, and 5.1% (3,245 km^2) slightly degraded. The non-degraded (89%) and degraded (11%) areas served as scenarios to

investigate the effect of precipitation on LAI in the context of forest degradation conditions. The results showed that the response of LAI to precipitation is predominantly positive and its occurrence is higher in non-degraded pixels (43%) than in degraded pixels (28%). This dissertation contributes to the body of knowledge focused on monitoring forest degradation and comprehending vegetation-climate feedbacks at regional scales.

1. INTRODUCTION

1.1. Background

With global warming becoming a major concern worldwide, forest degradation impacts on environmental services, especially those related to climate regulation through carbon sequestration, have received increasing attention among the scientific community (Jenkins and Schaap 2018). However, monitoring forest degradation has not been easy to accomplish due to the non-discrete nature of the process, in which changes are subtle and alter vegetation gradually. This slow transition from a healthy to an unhealthy condition slightly modifies the spectral response of vegetation across remotely sensed observations. Detecting the trajectory of those slight spectral variations has been a challenging task for environmental remote sensing specialists.

1.1.1. Forest and forest degradation

The understanding of forest degradation strongly depends on what is considered "forest". National and international organizations, countries, and private institutions have established different forest definitions that respond to particular purposes and specific criteria (Table 1.1). International forest policy has been ruled by the definition of the United Nations Food and Agriculture Organization (FAO; Chazdon et al. 2016), which describes forests as lands, not primarily classified under agricultural or urban land use, of more than 0.5 hectares, with a tree canopy cover of more than 10%, and trees capable to reach a minimum height of 5 meters *in situ* (FAO 2001). The United Nations Framework Convention on Climate Change (UNFCC) follows similar parameters, but allows each

country participating in the Clean Development Mechanisms (CDM) of the Kyoto Protocol to select minimum thresholds of canopy cover (10-30%), area (0.05-1.0 hectares), and height (2-5 meters; Putz and Redford 2010). Despite being widely used, these definitions have been criticized because considerable quantities of carbon and other environmental values could be lost if some areas remain classified as forest even if 70% of their canopy cover is removed or the entire tree cover is replaced by plantations that technically qualify as forest (Chazdon et al. 2016; Sasaki and Putz 2009).

Table 1.1. Forest definitions established by selected national and international organizations

Institution	Definition	Source
United Nations Food and Agriculture Organization (FAO)	"…includes natural forests and forest plantations. It is used to refer to land with a tree canopy cover of more than 10 percent and area of more than 0.5 ha. Forests are determined both by the presence of trees and the absence of other predominant land uses. The trees should be able to reach a minimum height of 5 m. Young stands that have not yet but are expected to reach a crown density of 10 percent and tree height of 5 m are included under forest, as are temporarily unstocked areas. The term includes forests used for purposes of production, protection, multiple-use or conservation (i.e. forest in national parks, nature reserves and other protected areas), as well as forest stands on agricultural lands (e.g. windbreaks and shelterbelts of trees with a width of more than 20 m), and rubberwood plantations and cork oak stands. The term specifically excludes stands of trees established primarily for agricultural production, for example fruit tree plantations. It also excludes trees planted in agroforestry systems"	FAO 2001
United Nations Framework Convention on Climate Change (UNFCC)	"… minimum area of land of 0.05-1.0 hectares with tree crown cover (or equivalent stocking level) of more than 10-30 per cent with trees with the potential to reach a minimum height of 2-5 meters at maturity in situ. A forest may consist either of closed forest formations where trees of various storeys and undergrowth cover a high proportion of the ground or open forest. Young natural stands and all plantations which have yet to reach a crown density of 10-30 per cent or tree height of 2-5 meters are included under forest, as are areas normally forming part of the forest area which are temporarily unstocked as a result of human intervention such as harvesting or natural causes but which are expected to revert to forest"	Kant 2006

Table 1.1. Continued

Institution	Definition	Source
International Union of Forestry Research Organizations (IUFRO)	"A land area with a minimum 10 % tree crown coverage (or equivalent stocking level), or formerly having such tree cover and that is being naturally or artificially regenerated or that is being afforested"	IUFRO 1994
United Nations Convention on Biological Diversity (UN-CBD)	"… a forest is a land area of more than 0.5 ha, with a tree canopy cover of more than 10%, which is not primarily under agricultural or other specific non-forest land use. In the case of young forests or regions where tree growth is climatically suppressed, the trees should be capable of reaching a height of 5 m *in situ*, and of meeting the canopy cover requirement"	CBD 2001
Mexico´s National Forest Comission *(Comisión Nacional Forestal;* CONAFOR)	"Vegetation, generally in temperate zones, with a prevalence of woody perennial species, a tree canopy cover of more than 10 percent, and an area of more than 1,500 square meters"	DOF 2005
United States Department of Agriculture/Forest Service (US Forest Service)	"Land that has at least 10 percent crown cover by live tally trees of any size or has had at least 10 percent canopy cover of live tally species in the past, based on the presence of stumps, snags, or other evidence. To qualify, the area must be at least 1.0 acre in size and 120.0 feet wide. Forest land includes transition zones, such as areas between forest and nonforest lands that meet the minimal tree stocking/cover and forest areas adjacent to urban and built—up lands. Roadside, streamside, and shelterbelt strips of trees must have a width of at least 120 feet and continuous length of at least 363 feet to qualify as forest land. Unimproved roads and trails, streams, and clearings in forest areas are classified as forest if they are less than 120 feet wide or less than an acre in size. Tree-covered areas in agricultural production settings, such as fruit orchards, or tree—covered areas in urban settings, such as city parks, are not considered forest land"	USDA 2016

While a robust definition is required for local forest assessment, a simple definition grounded in basic parameters is acceptable, and even needed, for regional and global studies (Sasaki and Putz 2009; Putz and Redford 2010). In this context, and to be consistent with the input Moderate Resolution Imaging Spectroradiometer (MODIS) data, this research adopts the definition used by the MODIS land cover product, which states

that forests are “lands dominated by woody vegetation with a percent cover of more than 60 percent and height exceeding 2 meters” (Strahler et al. 1999). This definition has its origins in the Land Cover Units System developed by the International Geosphere-Biosphere Programme Data and Information System (IGBP-DIS) with the purpose of creating a global land cover classification based on 1-kilometer Advanced Very High Resolution Radiometer (AVHRR) data (Belward, Estes and Kline 1999).

Similarly to the discussion around the definition of “forest”, there has been an extensive debate behind the concept of “forest degradation”. Among the international organizations that have establish a definition (Table 1.2), FAO describes forest degradation as “changes within the forest which negatively affect the structure or function of the stand or site, and thereby lower the capacity to supply products and/or services” (FAO 2001). Unlike the Intergovernmental Panel on Climate Change (IPCC) or the Verified Carbon Standard (VCS) Association which specify that forest degradation is human-driven (Table 1.2), FAO does not mention the causes of the process in the definition.

Table 1.2. Forest degradation definitions established by selected international organizations

Institution	Definition	Source
United Nations Food and Agriculture Organization (FAO)	“Changes within the forest which negatively affect the structure or function of the stand or site, and thereby lower the capacity to supply products and/or services”	FAO 2001
Intergovernmental Panel on Climate Change (IPCC)	“A direct, human-induced, long-term loss (persisting for X years or more) or at least Y% of forest carbon stocks [and forest values] since time T and not qualifying as deforestation”	GOFC-GOLD 2009
United Nations Environment Programme/Convention on Biological Diversity (UNEP/CBD)	“… a secondary forest that has lost, through human activities, the structure, function, species composition or productivity normally associated with a natural forest type expected on that site. Hence, a degraded forest delivers a reduced supply of goods and services from the given site and maintains only limited biological diversity. Biological diversity of degraded	Schoene et al. 2007

Table 1.2. Continued

Institution	Definition	Source
	forests includes many non-tree components, which may dominate in the under-canopy vegetation"	
United Nations/Millennium Ecosystem Assessment (UN/MEA)	"…results when forests remain forests but lose their ability to provide ecosystem services or suffer major changes in species composition due to overexploitation, exotic species invasion, pollution, fires, or other factors"	Sasaki and Putz 2009
Verified Carbon Standard (VCS) Association	"the persistent reduction of canopy cover and/or carbon stocks in a forest due to human activities such as animal grazing, fuel-wood extraction, timber removal or other such activities, but which does not result in the conversion of forest to non-forest land (which would be classified as deforestation), and qualifies as forests remaining as forests, such as set out under the IPCC 2003 Good Practice Guidance"	Shoch, Eaton, and Settelmyer 2013

Regardless of the drivers, the decrease in vegetation density is probably the most noticeable negative change that can be documented through time series of satellite imagery (Chazdon et al. 2016). In the remote sensing field, forest degradation is usually associated with the study of forest disturbances, which are considered drivers of a forest's state and function that range from high-impact events (e.g., caused by fires, windstorms, deforestation) to subtle and gradual processes (e.g., caused by insects, diseases, acid rain; Cohen et al. 2017). According to this description, forest degradation can be considered a type of disturbance and other disturbances can potentially lead to forest degradation processes. Therefore, this research defines forest degradation as any negative monotonic (i.e., single-direction), not necessarily linear, trend in vegetation greenness. This comprises any disturbances, including deforestation, that are not associated with a recovery process during the period of observation. However, section 3.4.2. describes a way to separate or identify potential deforestation events from pixels classified as degraded.

1.1.2. Forest degradation impacts on the carbon cycle

Forest ecosystems play an essential role in keeping the carbon cycle balance because they are able to store carbon (Brown et al. 1996). A considerable number of studies have quantitatively estimated carbon stocks in forest vegetation (Kauppi 2003; Fang et al. 2007), forest soil (Powers and Schlesinger 2002; Stevens et al. 2006), and in forest as a whole (Ramachandran et al. 2007; Sharma et al. 2011; Ullah and Al-Amin 2012). However, when these ecosystems are disturbed, the stored carbon is released as carbon dioxide (CO_2) into the atmosphere (Figure 1.1), where it contributes to global warming by absorbing heat and impeding transmission to space. In other words, CO_2,

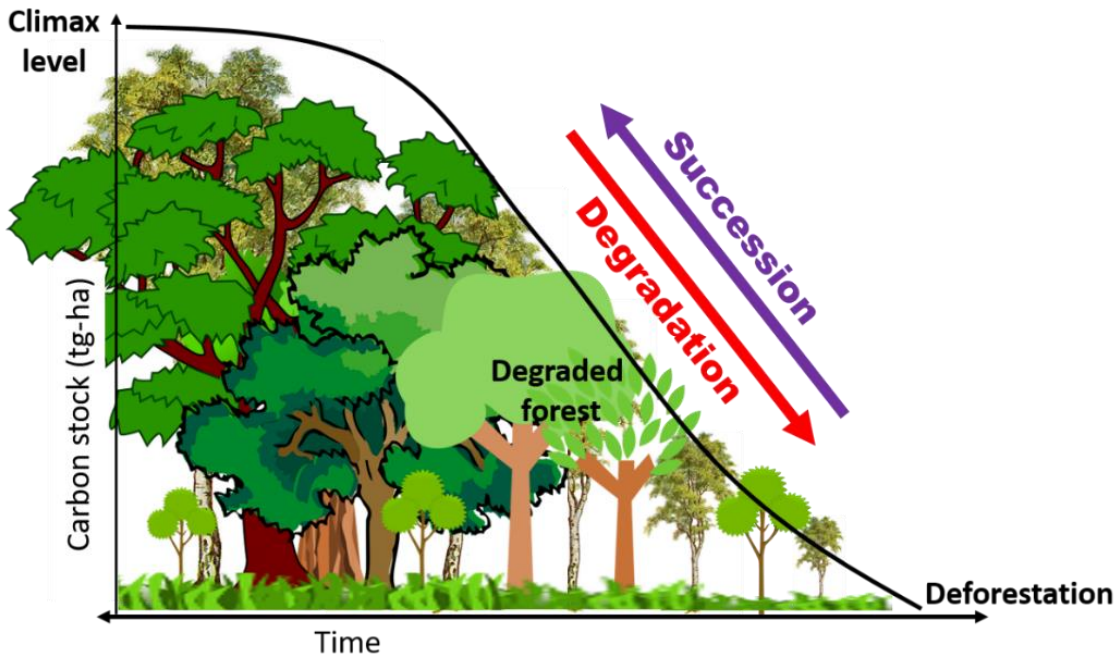

Figure 2.1. Relationship between carbon stock and forest degradation conditions. Adapted from Eckert et al. 2011

together with other greenhouse gases (GHGs) and the Earth's surface, helps to maintain the planet warm enough for living beings because it absorbs sunlight, but when its concentration rises, the process of heat absorption is abnormally enhanced (i.e., greenhouse effect) and leads to global warming (Karl et al. 2009).

Although deforestation has received more attention among the scientific community, there is evidence that forest degradation contributes to carbon stock losses in almost the same proportion as deforestation (Erb et al. 2018). In this context, Reducing Emissions from Deforestation and Forest Degradation (REDD+) is a program, of which Mexico is partner, developed by Parties to the UNFCC to create a financial value for the carbon stored in forests. REDD+ offers incentives for developing countries to reduce emissions from forested lands and invest in low-carbon paths to encourage sustainable development (FAO, UNDP, and UNEP 2015). However, there is uncertainty regarding how degradation has been, or will be, systematically measured by the more than 60 partner countries of the program. The spatio-temporal scale in which forest degradation can be measured varies across countries and, more importantly, the subtle and gradual changes inherent to forest degradation processes have traditionally been hard to monitor.

1.2. Literature review

The forest degradation definition that guides this research considers any disturbance not associated with a recovery process during the period of observation as a degradation process (see section 1.1.1). Thus, this literature review builds on remote sensing studies that aim to detect changes in vegetation from either perspective, forest

degradation or forest disturbances. Both approaches have been studied at different scales through a variety of remote sensing instruments (Table 1.3). According to the spatial resolution of the product used to perform the study, the related research can be grouped as follows:

A. Coarse spatial resolution (more than 100 meters). The most widely used sensors at this resolution are AVHRR and MODIS. By means of regression modeling, Eckert et al. (2015) demonstrated that trend analysis of MODIS Normalized Difference Vegetation Index (NDVI) successfully detect vegetation change areas, as well as land degradation and regeneration. Gao et al. (2013) show that the comparison of MODIS Percent Tree Cover (PTC) values at two different dates seems to be more appropriate to identify known degraded sites than known deforested patches. A second study indicates that a single-date PCT does not show significant difference between forest of different conservation states and concludes that the identification of forest degradation requires multi-temporal datasets with higher spatial resolution (Gao et al. 2015).

Based on the assumption about a constant negative relationship between surface temperature and surface greenness, time series of MODIS Land Surface Temperature (LST) and MODIS Enhanced Vegetation Index (EVI) have been used to detect vegetation disturbances (Mildrexler et al. 2007; Coops, Wulder, and Iwanicka 2009; Mildrexler, Zhao, and Running 2009). AVHRR Fraction Absorbed of Photosynthetically Active Radiation (FPAR) time series have also been used to

characterize major ecosystem disturbance regimes at regional (Potter et al. 2005, 2007) and global (Potter et al. 2003) scales.

Coarse spatial resolution products have some limitations that become evident when compared with higher spatial resolution imagery. For example, the application of Modified Soil Adjusted Vegetation Index (MSAVI) on MODIS and Landsat canopy fractional cover demonstrated that Landsat has higher accuracy for assessing tropical forest degradation (Hashim, Beiranvand, and Wei 2014). However, the use of coarse resolution imagery allows researchers to perform regional and global scale studies that would be otherwise almost impossible to handle computationally.

B. Moderate spatial resolution (10-99 meters). At this resolution, Landsat has been the most widely used sensor. Landsat-based algorithms have made use of shortwave-infrared spectral regions (Moisen et al. 2016; Schroeder et al. 2017), Tasseled Cap transformations (Jin and Sader 2005; Healey et al. 2005; Brooks et al. 2014; Griffiths et al. 2014), human interpretations (Cohen et al. 2016), and a variety of spectral indexes, such as the NDVI (Vogelmann et al. 2012), the Normalized Burned Ratio (NBR; Kennedy, Yang, and Cohen 2010; Huang et al. 2010), the Normalized Difference Fraction Index (NDFI; Sofan et al. 2016), the Normalized Difference Moisture Index (NDMI; Jin and Sader 2005; Hughes 2014), the MSAVI (Matricardi, Skole and Pedlowski 2010; Hashim, Beiranvand, and Wei 2014), and the Integrated Forest Z-score (IFZ; Huang et al. 2010).

Among the most popular and highly automatized Landsat-based algorithms, the Landsat-based detection of Trends in Disturbance and Recovery (LandTrendr) relies on NBR (Kennedy, Yang, and Cohen 2010), the Vegetation Change Tracker (VCT) is based on NBR and z-scores of forest spectral values (Huang et al. 2010), and the Continuous Change Detection and Classification (CCDC) uses visible, near-infrared, shortwave-infrared, and thermal spectral regions to identify surface changes, which are subsequently assigned to a land cover class through a random forest classifier (Zhu and Woodcock 2014). As a response to the need of validating the outputs from this type of algorithms, Cohen, Yang, and Kennedy (2010) created the TimeSync tool, which allows users to assess the quality of the results by syncing algorithms and human interpretations of Landsat time series.

Active sensors have also been a good source of data at this scale. Long-wavelength radar backscatter data from the Phased Array Type L-band Synthetic Aperture Radar sensor onboard the Advanced Land Observing Satellite (ALOS PALSAR) have been used to detect deforestation, forest degradation, and successional dynamics (Ryan et al. 2012; Joshi et al. 2015). Lucas et al. (2014) integrated ALOS PALSAR and Landsat-derived foliage projective cover data to map forest regrowth and degradation stages. Similarly, Tanase et al. (2015) demonstrated that the combination of the Radar Topography Mission (SRTM) and TanDEM-X mission (TDM) datasets allows not only for the identification of forest change but also for the estimation of magnitude of change.

Although the methodologies and outcomes derived from these studies have proved to be useful, very low intensity forest degradation resulting from non-mechanized logging or charcoal harvesting cannot be effectively monitored using Landsat, ALOS PALSAR, or similar products (Souza et al. 2013). For those purposes, more detailed (i.e., finer spatial resolution) remote sensing product have to be considered.

C. Fine spatial resolution (up to 9 meters). Within this category, the NDFI applied to a combination of Landsat and *Satellite Pour l'Observation de la Terre* (SPOT) datasets showed higher accuracy to detect forest degradation than NBR or NDVI (Sofan et al. 2016). Morales-Barquero et al. (2015) identified drivers and correlates of forest degradation by combining biophysical and socio-economic variables through spatially-explicit binary logistic regression, where the model covariates were obtained from SPOT 5 images, surveys, and semi-structured interviews. Dons et al. (2015) applied a supervised classification and adaptive thresholding to a pansharpened QuickBird image to detect kiln burn marks resulting from charcoal production. Huang et al. (2008) developed a change analysis method, which automatically creates samples to train a support machine vector algorithm that classifies multi-temporal IKONOS images. As for active sensors, Weishampe et al. (2012) used the below-canopy view that lidar technology enables to determine the degree of forest degradation along the Guatemala-Belize border, while Ogbodo, Oke, and Dagba (2015) found that TerraSAR images at 1 and 3-meters spatial

resolution are the most effective to detect logging roads and clearcuts, although clearcuts are also detectable with 8-meter RADARSAT images.

The use of fine resolution imagery has allowed researchers to identify more specific processes related to forest disturbances, such as the presence of kiln burn marks (Dons et al. 2015) and logging roads (Ogbodo, Oke, and Dagba 2015). However, not many studies incorporate high spatial resolution products as their main source of information. Instead, a common practice has been to use fine resolution imagery to validate results from coarser resolution products.

According to this literature review, Landsat and MODIS time series have been the most widely used data to assess forest disturbances/degradation (Table 1.3). Within the list of spectral indexes employed by Landsat and MODIS studies (i.e., NDVI, EVI, NBR, NDFI, NDMI, MSAVI), Leaf Area Index (LAI) is lacking. Among the MODIS-based algorithms, a few have relied on the assumption of constant strong negative relationship between surface greenness and surface temperature (Mildrexler et al. 2007; Coops, Wulder, and Iwanicka 2009; Mildrexler, Zhao, and Running 2009). The relationship between LAI and surface temperature has been scarcely addressed in the related literature (Yan et al. 2016), therefore, the potential of these two variables to detect forest degradation has not been investigated. Based on this gap, the MODIS-based algorithm proposed in this research is expected to contribute, with a new and effective procedure, to body of knowledge that aims to monitor forest degradation at regional scale.

Table 1.3. Selected forest degradation/disturbances studies at different scales

Spatial resolution	Sensor	Studies
Coarse (more than 100 meters)	MODIS	Jin and Sader 2005
		Mildrexler et al. 2007
		Coops, Wulder, and Iwanicka 2009
		Mildrexler, Zhao, and Running 2009
		Pouliot et al. 2009
		Vandecar et al. 2011
		Xin et al. 2013
		Hammer et al. 2014
		Hashim, Beiranvand, and Wei 2014
		Sulla-Menashe et al. 2014
		Eckert et al. 2015
		Gao et al. 2013
		Gao et al. 2015
		de Beurs, Owsley, and Julian 2016
		Tran et al. 2016
	AVHRR	Potter et al. 2003
		Potter et al. 2005
		Potter et al. 2007
Moderate (10-99 meters)	Landsat	Kovacs, Wang, and Blanco-Correa 2001
		Healey et al. 2005
		Jin and Sader 2005
		Kennedy, Yang, and Cohen 2010
		Huang et al. 2010
		Cohen, Yang, and Kennedy 2010
		Matricardi, Skole and Pedlowski 2010
		Vogelmann et al. 2012
		Souza et al. 2013
		Brooks et al. 2014
		Griffiths et al. 2014
		Hashim, Beiranvand, and Wei 2014
		Hughes 2014
		Zhu and Woodcock 2014
		Cohen et al. 2016
		Moisen et al. 2016
		Sofan et al. 2016
		Schroeder et al. 2017
		Romero-Sánchez and Ponce-Hernandez 2017
	ALOS PALSAR	Ryan et al. 2012
		Lucas et al. 2014
		Joshi et al. 2015
	SRTM and TDM	Tanase et al. 2015
Fine (up to 9 meters)	SPOT	Morales-Barquero et al. 2015
		Sofan et al. 2016
	QuickBird	Dons et al. 2015
	IKONOS	Huang et al. 2008
	Lidar	Weishampe et al. 2012
	TerraSAR/RADARSAT	Ogbodo, Oke, and Dagba 2015

1.3. Research objectives

The overall purpose of this research is to develop an algorithm to detect forest degradation using time series of MODIS images collected over Central Mexico between 2002 and 2017. The specific objectives drawn from the general objective are the following:

1. Evaluate the relationship between vegetation greenness (i.e., MODIS-LAI) and surface temperature (i.e., MODIS-LST) to determine the potential of this relationship to detect forest degradation.
2. Develop an algorithm to detect forest degradation thought a trend analysis of the MODIS variable(s) selected according to the findings of the first objective.
3. Evaluate the vegetation greenness (i.e., MODIS-LAI) response to precipitation in the context of the forest degradation conditions estimated by the proposed algorithm.

Each of these objectives is addressed in a single chapter (i.e., Chapters 2-4) following the format of a journal article (i.e., introduction, methods and data, results, discussion, and conclusions). The final chapter (i.e., Chapter 5) summarizes how the objectives were achieved, the major findings, the limitations, and the future directions of this research.

1.4. Study area

The study area comprises all zones within the MODIS tile h08v06 that were covered by forest at least one year between 2002 and 2017. According to the MODIS Land Cover product (MCD12Q1, type 3), whose spatial resolution is 500-m, these zones extend over 63,964 km^2 and are primarily distributed over the *Sierra Madre Occidental* (west mountain range) and *Sierra Madre Oriental* (east mountain range). Deciduous broadleaf forest covers 60% of the area, evergreen broadleaf 36%, and evergreen needleleaf 4% (Figure 1.2). Due to the coarser spatial resolution (i.e., 1-km) of one of the input variables, the extent of the study area used to achieve the first objective of this research differs from the extent just mentioned, which was employed for the remaining objectives. Specific information of the area analyzed in each objective can be found in the study area section of each of the chapters.

A MODIS title within Mexico was selected as the study area for three main reasons. First, studies focused on detecting forest disturbances or degradation in this country have been conducted primarily at local scales (Kovacs, Wang, and Blanco-Correa 2001; Brower et al. 2002; Vidal, López-García, and Rendón-Salinas 2014; Gao et al. 2015; Romero-Sánchez and Ponce-Hernandez 2017) and rarely at a regional scale (Mildrexler, Zhao, and Running 2009). Second, according to Morales-Barquero et al. (2014), the levels of human disturbance are significantly high in Mexican forest (Morales-Barquero et al. 2014). Third, based on the Land Use and Vegetation Map produced by the *Instituto*

Nacional de Geografía y Estadística (INEGI), more than 14,500 km^2 of the study area were covered by perturbed secondary vegetation in 2014 (INEGI 2017).

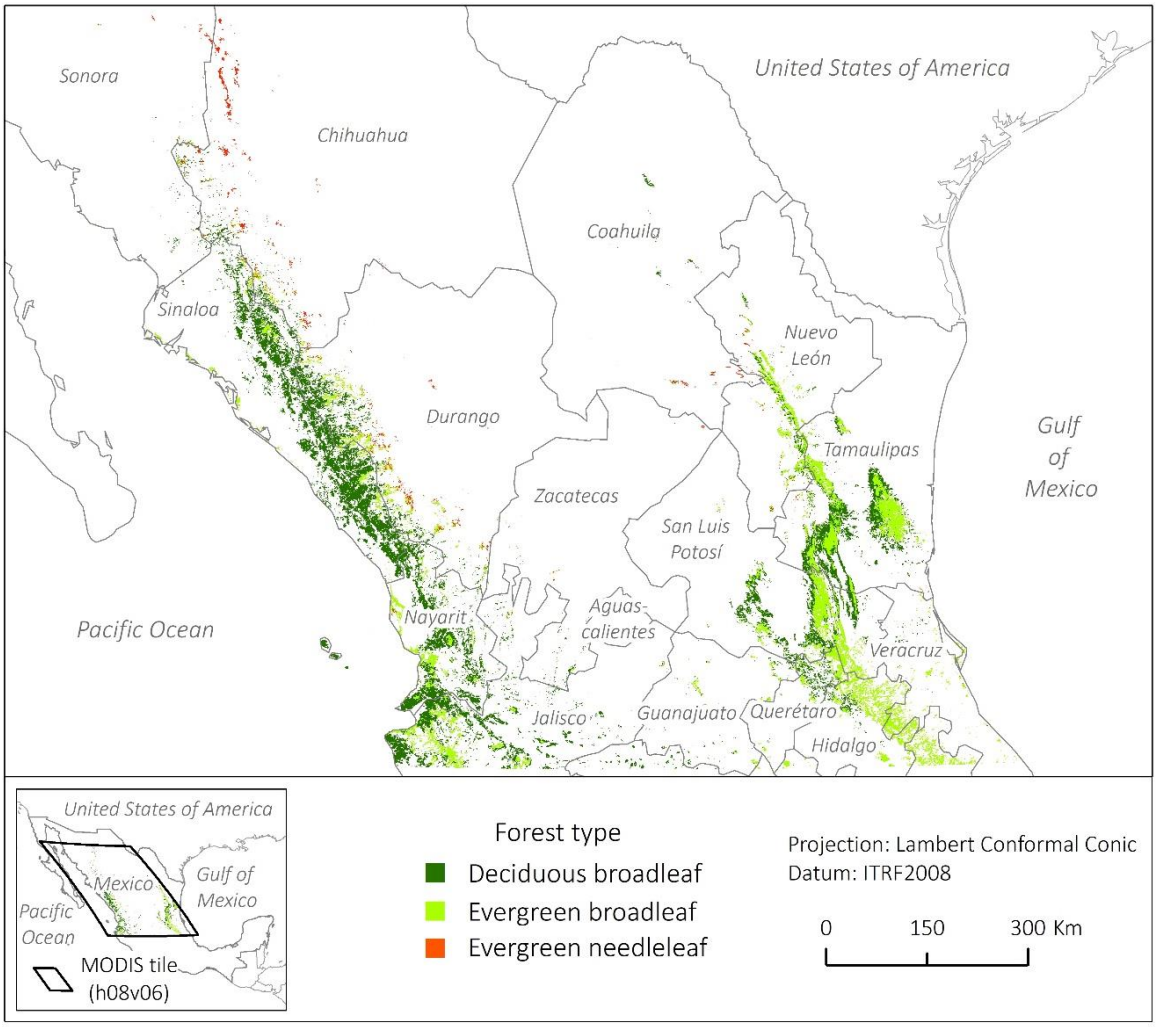

Figure 1.2. Study area: 500-m pixels covered by forest during at least one year between 2002 and 2017

2. ASSESSING THE RELATIONSHIP BETWEEN VEGETATION GREENNESS AND SURFACE TEMPERATURE THROUGH GRANGER CAUSALITY AND IMPULSE-RESPONSE COEFFICIENTS[1]

2.1. Introduction

Many environmental studies have successfully accomplished their objectives, such as detecting ecosystem disturbances (Mildrexler et al. 2007; Coops, Wulder, and Iwanicka 2009; Mildrexler, Zhao, and Running 2009), classifying land covers (Ehrlich and Lambin 1996; Roy, Kennedy, and Folvin et al. 1997), identifying land cover changes (Lambin and Ehrlich 1996, 1997), monitoring drought (Wan, Wang, and Li 2004), or studying urban heat islands (Weng, Lu, and Schubring 2004), by assuming a constant negative relationship between vegetation greenness and surface temperature. This assumption, where vegetation greenness is the cause and surface temperature is the effect, lies on the fact that increased amounts of vegetation augment latent heat losses through transpiration, which provokes a reduction in surface temperature (Goward, Cruickshanks, and Hope 1985). However, some authors have demonstrated that the nature of this relationship is not always negative and that it varies depending on the season, forest type, and spatial scale of analysis (Kaufmann et al. 2003; Zhou et al. 2003; Liu et al. 2006; Notaro, Liu, and Williams 2006; Julien and Sobrino 2009).

Individually, vegetation greenness, commonly measured by multi-spectral sensors

[1] This chapter was accepted for publication with the title "Assessing the relationship between vegetation greenness and surface temperature through Granger causality and Impulse-Response coefficients: a case study in Mexico" in the *International Journal of Remote Sensing*. November 4, 2019.

through spectral indices like the Normalized Difference Vegetation Index (NDVI), reveals the conditions of vegetative covers and responds to regional climatic characteristics (GCOS 2019); while surface temperature, often acquired from thermal infrared satellite measurements, is defined as the skin temperature of the ground and is mostly a result of albedo, vegetation cover, and soil moisture (GCOS 2019; Eagleson 2011). Thus, any fluctuation in climatic variables, including surface temperature, affects vegetation greenness after a certain time lag and, in turn, these vegetation changes cause a modification of surface temperature (Notaro, Liu, and Williams 2006).

This relationship between vegetation greenness and surface temperature has been examined by comparing single-date datasets through correlation analysis (Goward, Cruickshanks, and Hope 1985; Kumar and Shekhar 2015) and regression models where surface temperature is the dependent variable (Yue et al. 2007). These studies have found a significant inverse relationship. However, multitemporal studies have revealed more diverse patterns. By means of regression analysis, Julien and Sobrino (2009) found that in boreal areas the relationship between NDVI and Land Surface Temperature (LST) is clearly positive, while in semi-arid areas is clearly negative. Through correlation analysis that allow for the examination of non-instantaneous effects of one variable over the other, Kaufmann et al. (2003) reported that in North America the effect of vegetation on surface temperature is mostly negative during summer, generally positive during winter and spring, and not statistically significant during fall. Liu et al. (2006) found that vegetation variability is mostly driven by temperature in northern mid and high latitudes; although, vegetation also imposes a positive effect on temperature. Similarly, Zhou et al.

(2003) reported that temperature changes accounted for the largest fraction of NDVI change between the early 1980s and the late 1990s in North America and Eurasia. Notaro, Liu, and Williams (2006) described a significant instantaneous influence of temperature on vegetation over the United States of America, but also a non-instantaneous positive effect of vegetation (leading by one month) on temperature, especially during spring and over northern states.

The Granger causality approach has been used to examine the lagged effects of vegetation greenness on surface temperature or vice versa, but the use of Impulse-Response (IR) coefficients to explore the sign and strength of this relationship is rare in the literature (e.g., Wang et al. 2007). The Granger causality concept is based on the idea of predictability. When the interaction is studied from vegetation greenness to surface temperature, the Granger causality test attempts to predict surface temperature based on past values of surface temperature and vegetation greenness. If the prediction is improved after including the vegetation greenness values, then vegetation greenness is said to Granger-cause surface temperature (Granger 1969; Jiang, Liang, and Yuan 2015; Papagiannopoulou et al. 2017), but the sign and strength of the causality is not specified. IR functions can determine the sign and strength by modelling the over-time response of a variable to an impulse (i.e., change) of another variable based on the Wold Moving Average representation of a Vector Autoregressive (VAR) Model (Lütkepohl, 2005).

Regardless of the methods, most of the studies that have evaluated the relationship between vegetation greenness and surface temperature, or that have

modeled a phenomenon using both variables, have employed NDVI (e.g., Ehrlich and Lambin 1996; Roy et al. 1997; Lambin and Ehrlich 1996,1997; Kaufmann et al. 2003; Zhou et al. 2003; Wan, Wang, and Li 2004; Wang et al. 2006; Wang et al. 2007; Yue et al. 2007; Julien and Sobrino 2009; Jiang, Liang, and Yuan 2015; Papagiannopoulou et al. 2017) or Enhanced Vegetation Index (EVI; e.g., Mildrexler et al. 2007; Coops, Wulder, and Iwanicka 2009; Mildrexler, Zhao, and Running 2009) as the vegetation indicator. However, these indices have some disadvantages. NDVI is very sensitive to background brightness in areas with sparse vegetation and saturates in zones with high biomass, while EVI tends to present relatively low values in all biomes and is sensitive to topographic conditions (Huete et al. 2002; Matsushita et al. 2007). Therefore, this study proposes to explore the performance of Leaf Area Index (LAI) as an alternative vegetation greenness indicator. In coniferous canopies, LAI is defined as the total surface area of just one half of all needles per unit ground area; while in broadleaf canopies, it is described as the total one-sided area of all green leaves per unit ground area (Myneni et al. 2002). LAI is then a measure of the amount of vegetation vertically distributed. It can also be considered a measure of the surface potentially available for photosynthesis and as a proxy of the three-dimensional conditions of vegetation.

Thus, this chapter aims to contribute to the understanding of the relationship between vegetation greenness and surface temperature by evaluating the annual and intraseasonal relationship between LAI and Land Surface Temperature (LST) across forest types of Central Mexico. On a pixel-by-pixel basis, the presence of any relationship is investigated through the notion of Granger causality, while the sign and strength of the

relationship is estimated by means of an IR function. The procedures are performed using monthly anomalies of Moderate Resolution Imaging Spectroradiometer (MODIS) data collected from 2002 to 2017.

2.2. Data and methods

2.2.1. Study area

The study area is comprised of all 1-km pixels of the MODIS tile h08v06 that were covered by forest during at least one year between 2002 and 2017 according to the MODIS Terra + Aqua yearly Land Cover product (MCD12Q1, type 3; Figure 2.1.a). These pixels extend over 88,824 km^2 and are mainly distributed over the *Sierra Madre Occidental* (west mountain range) and *Sierra Madre Oriental* (east mountain range). m with a mean of 1,046 m and a standard deviation of 741 m (Figure 2.1.b). The slopes range from 0 to 35^o with a mean of 6.9^o and a standard deviation of 4.8^o.

Tropical climates dominate the region (Figure 2.1.c). Forty percent of the study area experiences tropical climate and 34% semi-tropical, whose mean annual temperatures exceed 22 and 18 ^{o}C respectively. Temperate climate extends over 13% of the study area and, in comparison with tropical climates, occurs at higher average elevations where the mean annual temperature oscillates between 12 and 18 ^{o}C. Arid climate is generally found towards continental areas and extends over 8% of the study area. Semi-cold climate, whose mean annual temperature oscillates between 5 and 12 ^{o}C, occurs at the highest elevations and covers the remaining 3% of the study area. As for

precipitation regimes, the rainy season (also called “the warm half of the year”) of most of the study area starts in May and ends in October, which coincides with the emergence and senescence of leaves, respectively (García 2004).

The study area is comprised of 61% deciduous broadleaf forest, 35% evergreen broadleaf, and 4% evergreen needleleaf (Figure 2.1.d). These forests are composed of a broad range of species (in the order of hundreds). Some of the most frequently found trees are oaks (e.g., *Quercus magnoliifolia*, *Quercus rugosa*, *Quercus laeta, Quercus sideroxyla*), pines (e.g., *Pinus durangensis, Pinus douglasiana*), firs (e.g., *Abies religiosa, Abies durangensis*), mauto (i.e., *Lysiloma divaricatum*), white mangrove (i.e., *Laguncularia racemose*), nance (i.e., *Byrsonima crassifolia*), and bay cedar (i.e., *Guazuma ulmifolia*; CONAFOR 2019).

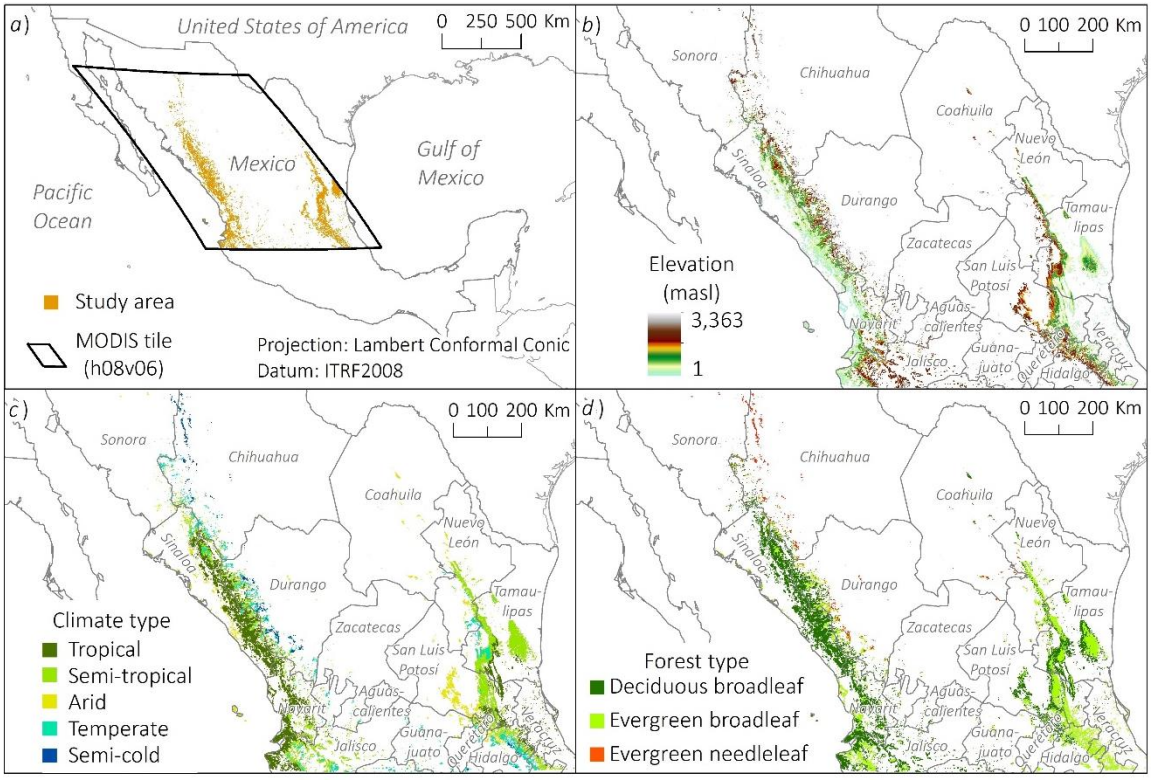

Figure 2.1. Study area: location (a), elevation (b), climate types (c), and forest types (d)

2.2.2. Data and preprocessing

2.2.2.1. MODIS LST product

The MODIS LST data were downloaded from the Land Processes Distributed Active Archive Center (LP DAAC) managed by the NASA Earth Science Data and Information System (ESDIS) project. Specifically, MODIS Aqua 8-day LST composites (MYD11A2, Collection 6) of the MODIS tile h08v06 were acquired from 2002 to 2017 at 1-km spatial resolution. Aqua sensor's overpass time, at approximately 1:30 pm above the equator, allows it to capture temperatures close to the daily peak. LST estimates are retrieved from the generalized split window algorithm (Wan and Dozier 1996) or the day/night algorithm (Wan and Li 1997), which use MODIS Thermal Infrared (TIR) data (Wan et al. 2004) and auxiliary MODIS data, such as geolocation, radiance, cloud masking, atmospheric temperature, water vapor, land cover, and snow (Wan 2013). Because TIR signals are not able to penetrate clouds, the LST retrievals are constrained to cloud-free pixels. Wan (2014) reported that the mean LST error of Collection 6 (i.e., the latest version of the MODIS LST product) is within ± 0.6 Kelvin and the standard deviation of the validation errors is less than 0.5 Kelvin in most validation data sets, which indicates that Collection 6 is an improvement over Collection 5.

All LST composites were projected to Lambert Conformal Conic projection in ITRF2008 datum and clipped to forested areas. To exclude poor quality retrievals, the LST Quality Control (QC) layers were unpacked using the Land Data Operational Product Evaluation (LDOPE) tool. Only LST estimates with an error lower or equal to 2 Kelvin were

selected to perform the analysis. Based on these good quality retrievals, monthly anomalies of LST were calculated on a pixel-by-pixel basis for each month from January 2002 to December 2017. The anomalies were calculated by subtracting the long-term monthly average, often called climatology, from the monthly means (e.g., anomaly= mean of January 2002 - average of all January means of the study period). In order to manipulate the data in an R environment (R Core Team 2018), all LST anomalies were extracted from the raster files and rearranged into a comma-separated values (cvs) file, where each row contains 192 monthly anomalies, which constitute the LST time series of a single pixel.

2.2.2.2. MODIS LAI product

The MODIS LAI data were also downloaded from the LP DAAC. Specifically, MODIS Terra 8-day LAI composites (MOD15A2H, Collection 6) of the MODIS tile h08v06 were acquired from 2002 to 2017 at 500-km spatial resolution. The early Terra sensor's overpass time, at approximately 10:30 am above the equator, allows it to capture more reliable LAI retrievals due to lower cloud presence (King et al. 2013; Yan et al. 2016). MODIS LAI retrievals are acquired from a radiative transfer model (Knyazikhin et al. 1998) that accounts for vegetation structure. This main algorithm selects the best LAI estimates by comparing measured red and near-infrared spectral values with a look-up table composed of observed spectral values of six biome types and their corresponding LAI values. If this algorithm fails, a back-up method based on the biome-specific empirical relationship between NDVI and LAI produces the retrievals (Knyazikhin et al. 1998;

Myneni et al. 2002; Jensen et al. 2011; Yang et al. 2006; Yan et al. 2016); however, in this study only retrievals from the main algorithm were considered for the analysis.

According to Yan et al. (2016), the latest version of the MODIS LAI product, Collection 6, is considerably better than Collection 5. Collection 6 properly captures the interannual variation of LAI and the general seasonality of most biomes, except for evergreen broadleaf forest, for which incorrect seasonal profiles are produced. This issue has been also observed in other satellite products, such as the Carbon cYcle and Change in Land Observational Products from an Ensemble of Satellites (CYCLOPES) and those from the Global Land Surface Satellite (GLASS), and the SPOT-VEGETATION GEOV1 system. Therefore, this shortcoming may be difficult to avoid using remotely sensed data.

All LAI composites were projected to Lambert Conformal Conic projection in ITRF2008 datum, resampled to 1-km spatial resolution to make them compatible with the LST data, and clipped to forested areas. During the resampling process, the geo-location was preserved across data products by snapping the raster environment to the cell alignment of the LST datasets. The geo-location is well conserved because the 500-m LAI pixels are originally aligned with the 1-km LST pixels (i.e., one LST pixel perfectly contains four LAI pixels). The LAI QC layers were also unpacked by means of the LDOPE tool and used to select only LAI values obtained from the main algorithm. Then, similar to the procedure performed on the LST data, monthly anomalies of LAI were calculated on a pixel-by-pixel basis for each month from January 2002 to December 2017 and arranged

into a cvs file, where each row contains 192 monthly anomalies, which constitute the LAI time series of a single pixel.

2.2.3. Assessment of the annual and intraseasonal relationship between LAI and LST

To assess the annual and intraseasonal relationship between LAI and LST, 86,405 multivariate time series of monthly anomalies of LAI and LST were analysed. These multivariate time series consist entirely of good quality estimates (Table 2.1.a). For the annual assessment, all values of the time series were used. For the intraseasonal assessment, the time series were reorganized by season: Winter (December - February), Spring (March-May), Summer (June-August), and Fall (September-November). This means that the three monthly anomalies of a particular season were joined to the three anomalies occurring the following year in the same season. Then, the presence of any relationship between LAI and LST was evaluated in each year-round and season-based multivariate time series through the Granger causality test. If any relationship was encountered, its sign and strength was estimated by means of an IR function.

2.2.3.1. Evaluation of Granger causality

The statistical models of the Granger causality approach rely on linear specifications. However, climate-vegetation interactions are nonlinear in nature. To solve this inconsistency, this analysis is based on anomalies, which represent deviations from the steady state of the variables and, thus, help to linearly approximate relationships (Glendinning 1994; Wang et al. 2006). It should be noted that the time series of monthly LAI and LST anomalies constitute the input data of this analysis; however, to avoid long

repetitions, the terms ‘monthly’ and ‘anomalies’ may be omitted where the reference is clear.

In formal terms, this section describes the methodology implemented to evaluate the causal relationship between time series of monthly LAI anomalies at a specific pixel and time series of monthly LST anomalies at the same pixel. The existence of causality is examined in both directions. When the interaction is studied from LAI to LST, the test attempts to forecast LST, at a given time, based on past values of LST and LAI. If the prediction of LST is improved when the LAI values are included as predictors, then LAI is said to Granger-cause LST. When the interaction is tested from LST to LAI, the logic is inverse. In both cases, if causality is found, the result should be interpreted as ‘predictive causality’ rather than ‘true causality’ (Jiang, Liang, and Yuan 2015; Papagiannopoulou et al. 2017).

A limitation of the Granger causality method is that it cannot be applied to non-stationary time series (i.e., those whose statistical properties, such as mean and variance, do not remain constant over time; Nason 2006) because they are unpredictable and, as a result, cannot be modelled or forecasted (Iordanova 2009). Therefore, prior to examining the causal relationship, a Kwiatkowski-Phillips-Schmidt-Shin (KPSS) test was applied to all LAI and LST time series using the ‘urca’ R package (Pfaff 2008a). The KPSS test examines the null hypothesis of stationarity around a linear trend at 0.05 significance level (Kwiatkowski et al. 1992). Only stationary time series were considered for the analysis (Table 2.1.b).

Vector Autoregressive (VAR) models were used to derive the predictions required to examine the Granger causality. VAR models are an extension of univariate autoregression models useful to explain and forecast the dynamic behaviour of multivariate time series (Zivot and Wang 2006). The pixels containing stationary time series of both LAI and LST (Table 2.1.b) were selected to obtain VAR models, which were computed, as well as the rest of the statistical functions of this section, by means of the 'vars' R package (Pfaff 2008a, 2008b). In a VAR model, each variable is a linear function of its own lagged values and the lagged values of the other variables in the model (Mariano et al. 2018). The general form of the VAR (p) model implemented in this study is as follows:

$$\boldsymbol{y_t} = \boldsymbol{A_1 y_{t-1}} + \ldots + \boldsymbol{A_p y_{t-p}} + u_t, \qquad (1)$$

where $\boldsymbol{y_t}$ represents a $K \times 1$ vector of endogenous variables (i.e., variables that are explained by other variables in the system; often called 'depended variables') at time $\boldsymbol{t}$ and u_t assigns a spherical disturbance term (i.e., white noise process) of the same dimension. $\boldsymbol{A_1, \ldots, A_p}$ are regression coefficient matrices with a dimension of $K \times K$ and p is the lag length (Pfaff 2008b). The *p* parameter determines how much of the previous information of all variables (i.e., lag time) is included in the model to predict future behaviours (Wang et al. 2006). In this analysis, y_t is a $2x1$ vector of LAI and LST monthly anomalies (i.e., a K=2), the regression coefficients are A_1, A_2, A_3 with a dimension of 2×2, and p is measured in months.

The optimal lag lengths at which the time series should be evaluated were identified by first testing the VAR models using the Akaike Information Criterion (AIC), which finds the lag with enough information content on the two variables without over-fitting (i.e., the best goodness of fit; Zivot and Wang 2006). From this preliminary analysis, the most common optimal lag lengths among all time series were 1 and 2-month. Therefore, the VAR models were repeated two times using these two lags. Then, a Portmanteau test was applied to evaluate the existence of serial correlation in the VAR residuals at a specific lag length. This test examines the null hypothesis of no serial correlation at the significance of 0.05 (Pfaff 2008b). The presence of serial correlation implies that some information (e.g., precipitation, solar zenith angle, aerosol optical depth) is missing in the model to explain the relationship. Thus, only time series with absence of serial correlation were considered for the analysis (Table 2.1.c).

After identifying the appropriate VAR models (i.e., without serial correlation), the existence of Granger causality was tested at 1 and 2-month lags in both directions (i.e., from LAI to LST and from LST to LAI). This means that the test was run twice per lag-length. First, considering LAI as cause and LST as response, and then considering LST as cause and LAI as response. To that end, the vector of LAI and LST monthly anomalies, y_t, Equation (1), was split into two subvectors as follows:

$$\begin{bmatrix} \boldsymbol{y_{1t}} \\ \boldsymbol{y_{2t}} \end{bmatrix} = \sum_{i=1}^{p} \begin{bmatrix} \alpha'_{11,i}\ \alpha'_{12,i} \\ \alpha'_{21,i}\ \alpha'_{22,i} \end{bmatrix} \begin{bmatrix} y_{1,t-i} \\ y_{2,t-i} \end{bmatrix} + CD_t + \begin{bmatrix} u_{1t} \\ u_{2t} \end{bmatrix} \quad (2)$$

where $\boldsymbol{y_{1t}}$ and $\boldsymbol{y_{2t}}$ are the subvectors, whose dimensions are $(K_1 \times 1)$ and $(K_2 \times 2)$ with $K = K_1 + K_2$, and α is the coefficient of the model. C is the coefficient matrix of potentially deterministic regressors and D_t is the column vector holding the appropriate deterministic regressors. This Granger causality test is an F-type test and is distributed as $F(pK_1K_2, KT - n)$, n being the total number of parameters in Equation (2) and T the number of observations. The null hypothesis, stated as $\boldsymbol{y_{1t}}$ does not Granger-cause $\boldsymbol{y_{2t}}$, is accepted when $\alpha_{21,i} = 0$ for $i = 1,2, \dots, p$ and rejected when $\exists\ \alpha_{21,i} \neq 0$ for $i = 1,2, \dots, p$ (Pfaff 2008a, 2008b). The test was implemented at 95% confidence level. The rejection of the null hypothesis provides evidence that LAI Granger-causes LST or vice versa, but it does not reveal the sign and strength of the relationship.

Table 2.1. Multivariate time series that meet the following required criteria: a) entirely constituted by good quality estimates, b) stationarity in both variables LAI and LST, and c) absence of serial autocorrelation at the lag length under analysis. These criteria are additive. Thus, a time series that meets the c) criterion also meets the a) and b) criteria

Criteria			Forest type (total of pixels)			
			Deciduous broadleaf (64,136)	Evergreen broadleaf (36,233)	Evergreen needleleaf (4,618)	All (104,987)
a) Good quality			56,561	25,497	4,347	86,405
b) Stationarity	All year		40,231	16,561	2,728	59,520
	Winter		51,026	22,775	3,874	77,675
	Spring		53,773	22,194	3,423	79,390
	Summer		50,710	22,084	3,848	76,642
	Fall		50,104	22,548	4,074	76,726
c) Absence of serial autocorrelation at 1 and 2-month lags	All year	1	37,726	15,297	1,346	54,369
		2	39,428	16,828	2,126	58,382
	Winter	1	50,657	22,646	3,804	77,107
		2	50,869	22,734	3,837	77,440
	Spring	1	53,008	21,449	3,405	77,862
		2	53,659	22,128	3,419	79,206
	Summer	1	50,523	21,987	3,833	76,343
		2	50,655	22,052	3,838	76,545
	Fall	1	49,738	22,328	4,048	76,114
		2	50,031	22,504	4,072	76,607

2.2.3.2. Estimation of Impulse-Response coefficients

To estimate the sign and strength of the relationship between LAI and LST, an IR function was applied to all time series where Granger causality at 1-month lag was found. The IR function measures the over-time response of a variable to an impulse of another variable based on the Wold Moving Average representation of a VAR(p) process (Lütkepohl, 2005), which is defined as follows:

$$y_t = \phi_0 u_t + \phi_1 u_{t-1} + \phi_2 u_{t-2} + \ldots, \qquad (3a)$$

$\phi_0 = I_k$ and ϕ_s ($s = 1,2, \ldots$) can be computed iteratively as indicated below:

$$\phi_s = \sum_{j=1}^{s} \phi_{s-j} A_j, \qquad (3b)$$

where $A_j = 0$ for $j > p$. The $(i,j)th$ coefficients of the matrices ϕ_s are interpreted as the expected response of variable $y_{i,t+s}$ to a change in variable y_{jt}. Hence, the accumulation of these effects over time (s = $1,2, \ldots$) simulates the impact on variable i after a change in variable j at time s (Pfaff 2008b). In this case, the output of the function consists of IR coefficients calculated for 12 months after a single impulse of LAI or LST.

2.3. Results

2.3.1. Annual relationship between LAI and LST

Granger causality was evaluated on 54,369 and 58,382 year-round multivariate time series that met the required criteria at 1 and 2-month lags, respectively. The results, summarized in Table 2.2 and Figure 2.2, indicate that LST Granger-causes LAI in around

80% of the evaluated pixels (grey bar), while LAI Granger-causes LST in no more than 12% of the pixels. In both directions, the presence of causality is slightly higher at 1-month lag. Regarding forest types, causality from LAI to LST occurs in more pixels of evergreen broadleaf forest (8 and 17% at 1 and 2-month lags, respectively), followed by deciduous broadleaf (5 and 10%), and evergreen needleleaf (4 and 7%). In the opposite direction, causality occurs in more pixels of deciduous broadleaf forest (88 and 89%), followed by evergreen needleleaf (71 and 76%), and evergreen broadleaf (65 and 69%).

Table 2.2. Annual Granger causality at 1 and 2-month lags per forest type. Refer to Table 2.1.c to see the number of pixels that meet all the required criteria and, therefore, were used to evaluate Granger causality

Forest type	Percentage of pixels that show Granger causality			
	From LAI to LST		From LST to LAI	
	1	2	1	2
Deciduous Broadleaf	10	5	89	88
Evergreen Broadleaf	17	8	69	65
Evergreen Needleleaf	7	4	76	71
All	12	6	83	81

To examine the nature of the relationship, IR coefficients were calculated for 45,028 and 6,513 pixels that showed Granger causality from LST to LAI and from LAI to LST, respectively, at 1-month lag. The median of those coefficients indicates that Granger causality is primarily negative in both directions (Figure 2.3). The response to an impulse of any of the variables is maximum two months after the impulse and then tends to gradually disappear. This means that, based on the annual behaviour of the variables, an increase in, for example, LAI would produce a decrease in LST, which would be most noticeable two months after the change in LAI. The effect of LST on LAI is generally

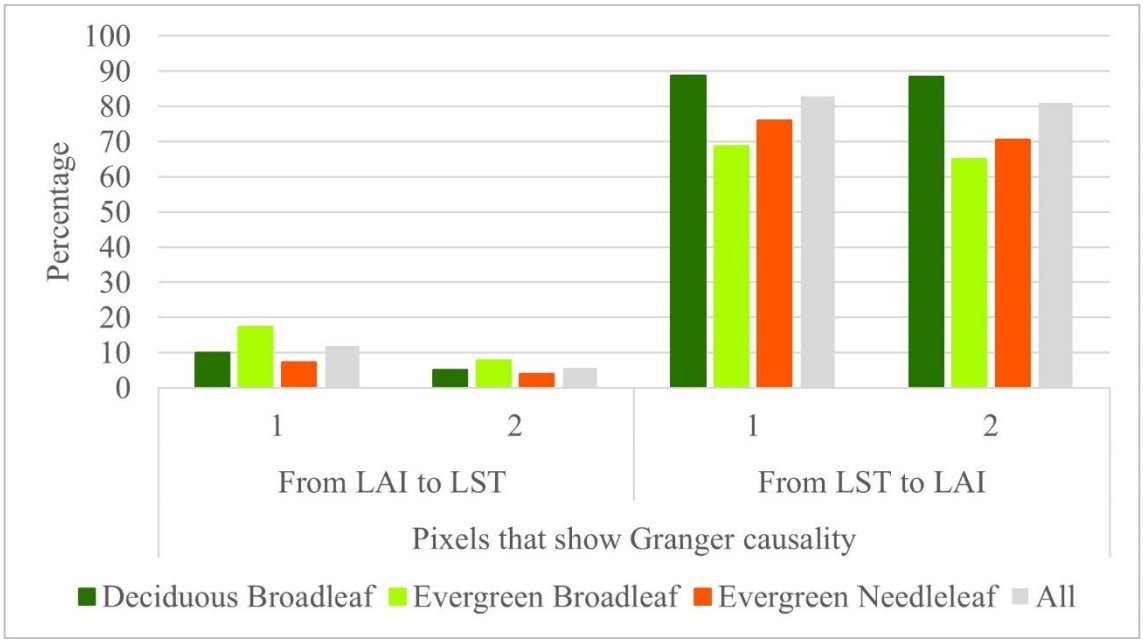

Figure 2.2. Presence of annual Granger causality at 1 and 2-month lags per forest type

stronger than the effect of LAI on LST. The weakest relationship in both directions occurs in evergreen needleleaf forest, while the strongest relationship from LAI to LST is observed in deciduous broadleaf and from LST to LAI in evergreen broadleaf.

Figure 2.4 illustrates the spatial distribution of the IR coefficients calculated for one and two months after a single impulse of LAI (Figure 2.4.a) or LST (Figure 2.4.b). Pixels showing causality from LAI to LST concentrate over the east side of the study area, particularly in the States of *San Luis Potosí* and *Tamaulipas*. The effect of LAI on LST is mainly negative as mentioned before, but there are some pixels in which the relationship is positive. A few coefficients, especially in the east side of the study area, are positive the first month and become negative the second month. A few others, especially in the south-western portion, start being negative and become positive the second month (Figure 2.4.a). Pixels showing causality from LST to LAI are well represented throughout

the study area. The effect of LST on LAI is also predominantly negative, the strongest negative effect occurs in the east region two months after the LST impulse. However, there are few pixels in which the effect is initially positive and becomes negative the

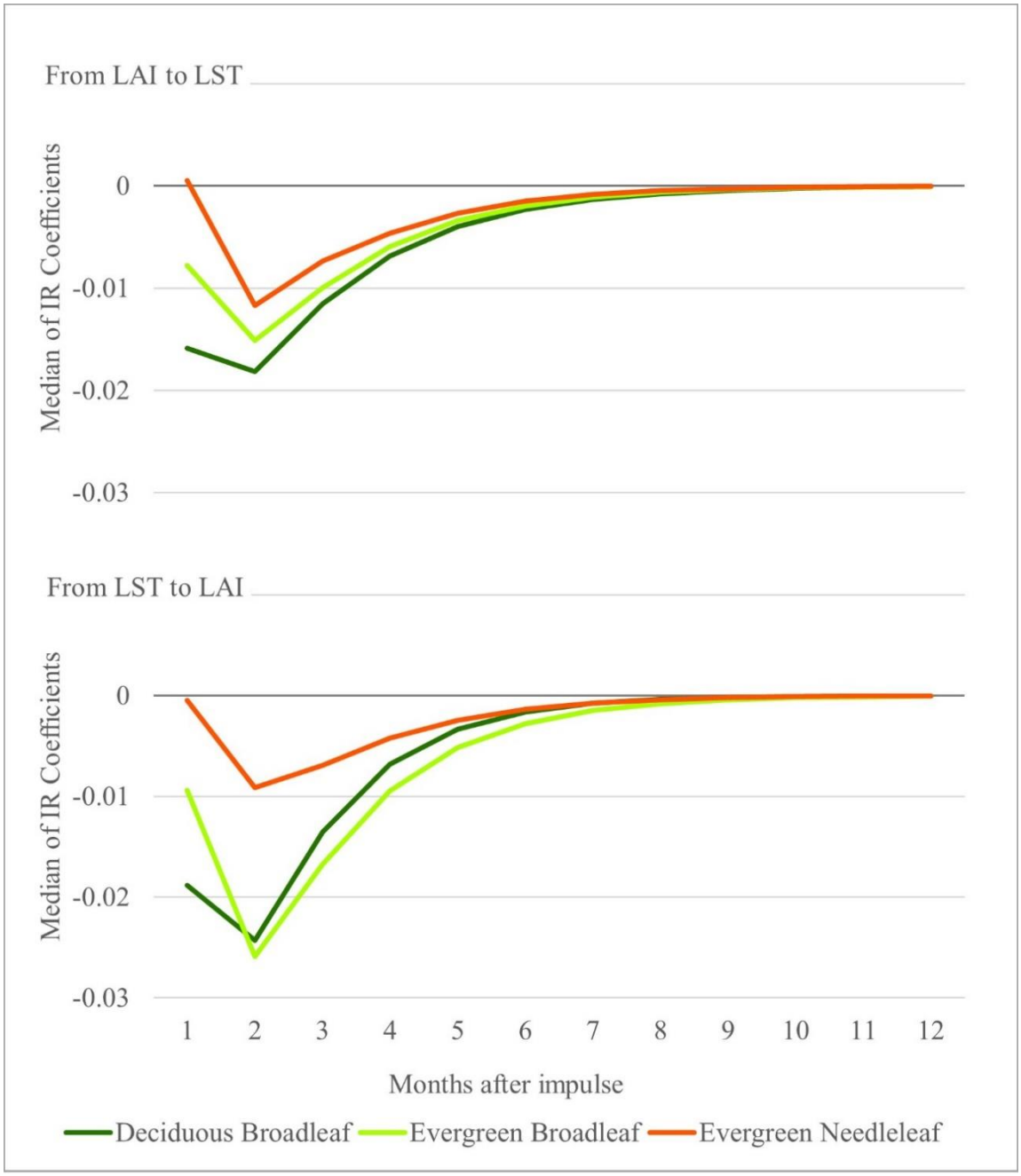

Figure 2.3. Median IR coefficients of pixels that show annual Granger causality at 1-month lag per forest type

second month after the impulse, many of these are located in high elevations of both sides of the study area (Figure 2.4.b).

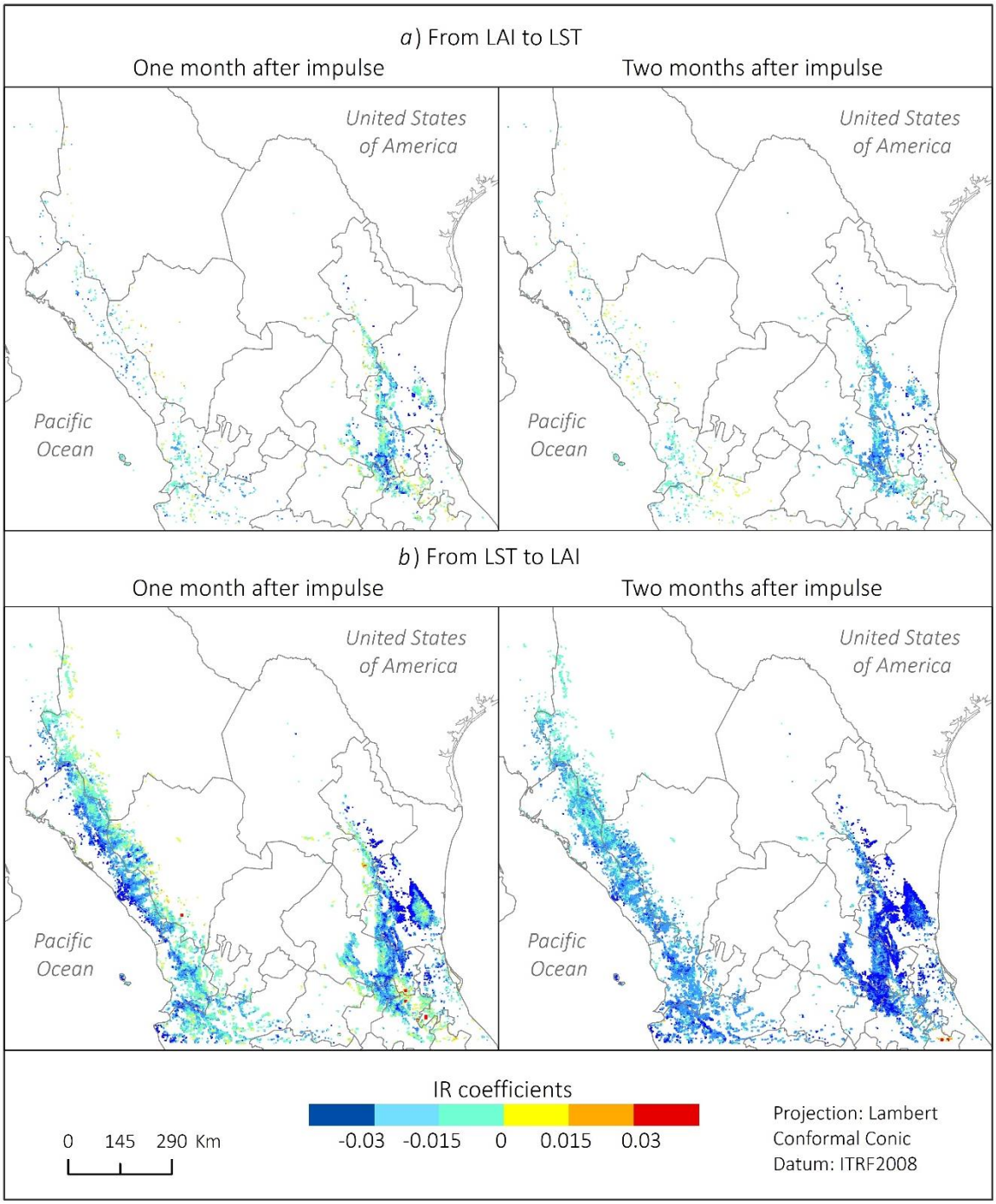

Figure 2.4. IR coefficients of pixels that show annual Granger causality from LAI to LST (a) or from LST to LAT (b) at 1-month lag

2. 3.2. Intraseasonal relationship between LAI and LST

Granger causality was evaluated at 1 and 2-month lags on all season-based multivariate time series that met the required criteria (Table 2.1.c). The results, summarized in Table 2.3 and Figure 2.5, show that Granger causality from LST to LAI occurs more consistently than Granger causality from LAI to LST in all seasons. If all forest types are considered as a whole (grey bar), the presence of LAI to LST causality is higher in spring (18 and 20% at 1 and 2-month lags, respectively) and lower in summer (5 and 6%). LST to LAI causality is also higher in spring (43 and 40%), but lower in winter (11 and 10%). The highest presence of causality in both directions and all seasons occurs in evergreen needleleaf forest, with the exception of spring and summer for LAI to LST, when deciduous broadleaf and evergreen broadleaf show higher occurrence of causality.

Table 2.3. Seasonal Granger causality at 1 and 2-month lags per forest type. Refer to Table 2.1.c to see the number of pixels that meet all the required criteria and, therefore, were used to evaluate Granger causality

Forest type	Percentage of pixels that show Granger causality															
	From LAI to LST								From LST to LAI							
	Winter		Spring		Summer		Fall		Winter		Spring		Summer		Fall	
	1	2	1	2	1	2	1	2	1	2	1	2	1	2	1	2
Deciduous Broadleaf	7	7	23	23	5	6	9	9	10	8	41	37	20	17	17	13
Evergreen Broadleaf	5	7	6	16	6	6	7	9	9	10	46	46	13	11	9	9
Evergreen Needleleaf	11	8	6	5	3	4	10	12	29	28	47	57	21	17	7	14
All	7	7	18	20	5	6	8	9	11	10	43	40	18	16	14	12

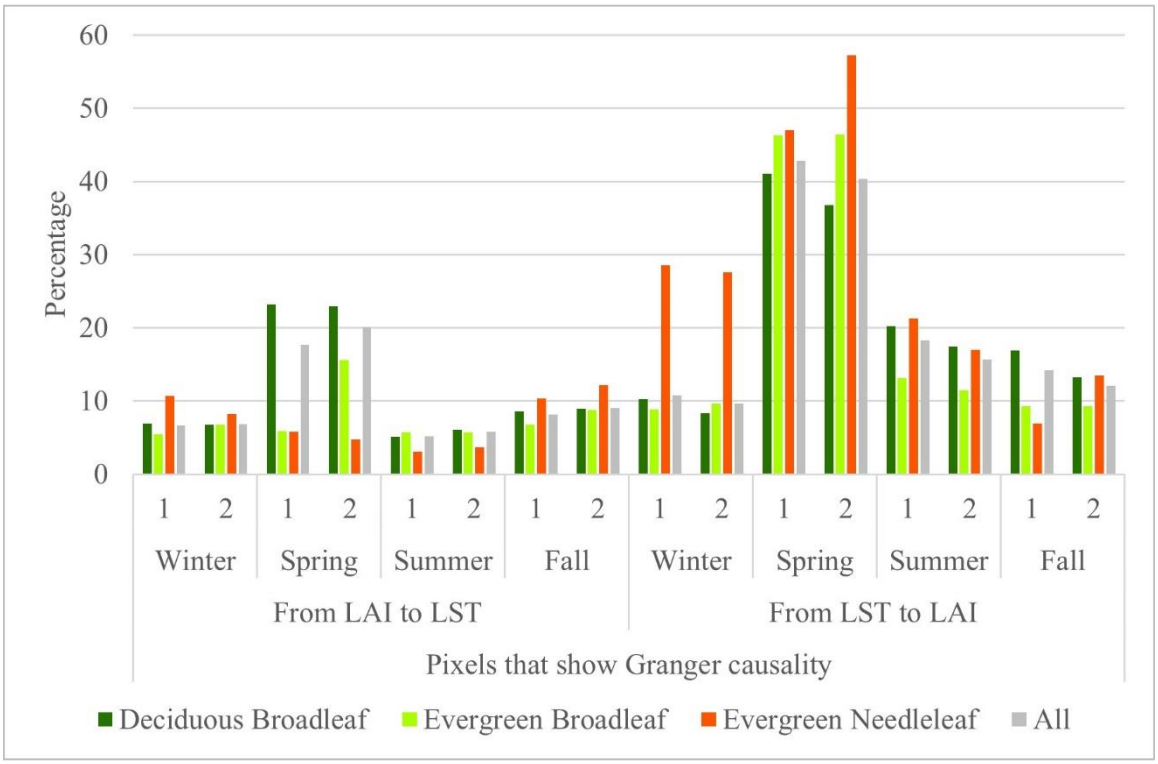

Figure 2.5. Presence of Intraseasonal Granger causality at 1 and 2-month lags per forest type

IR coefficients were calculated for all pixels that showed Granger causality at 1-month lag in each season. The median of those coefficients, plotted in Figure 2.6, revels that the effect of LAI on LST is generally positive in fall and negative in the rest of the seasons, except for evergreen needleleaf forest where the effect is positive in winter and spring (Figure 2.6.a). The effect of LST on LAI is predominantly negative across all season, only a slightly positive impact one month after the LST change occurs in evergreen broadleaf and evergreen needleleaf forests during winter and fall (Figure 2.6.b). In most cases, the response to change in one of the variables is stronger two months after the impulse. In a few cases, such as in summer for deciduous broadleaf (both directions), the strongest impact occurs one month after the impulse. In all cases, the effect tends to gradually disappear after the first or second month. The strongest negative effects of LAI

occur in deciduous broadleaf forest during spring and winter, while the strongest positive occurs in evergreen needleleaf during winter. The strongest effects of LST are all negative and occur in evergreen broadleaf and deciduous broadleaf during spring and summer, respectively.

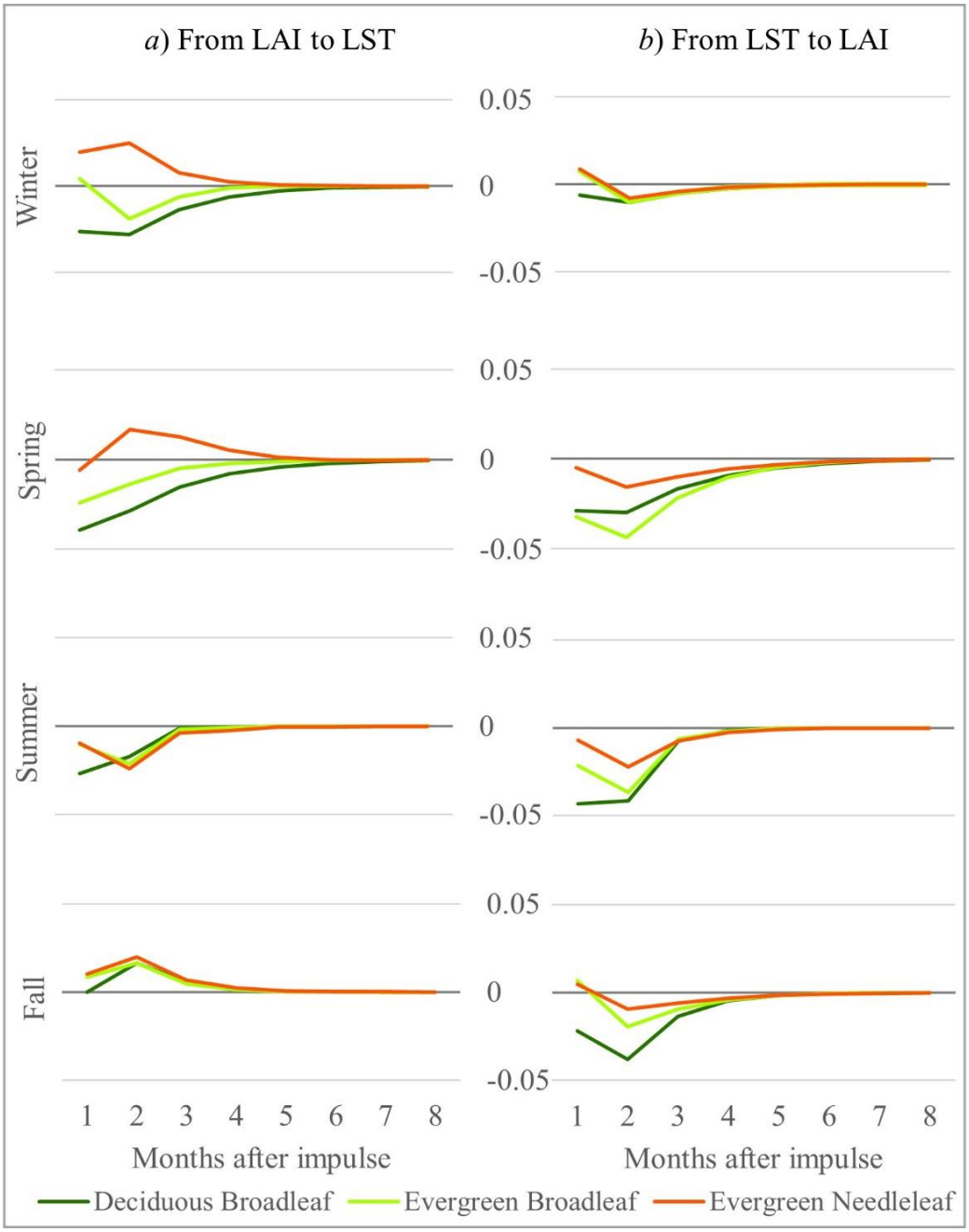

Figure 2.6. Median IR coefficients of pixels that show intraseasonal Granger causality from LAI to LST (a) or from LST to LAT (b) at 1-month lag per forest type

The spatial distribution of the IR coefficients calculated for one and two months after a single impulse of LAI (Figure 2.7) or LST (Figure 2.8) shows the diversity of the interactions between the variables. The effect of LAI on LST during winter is primarily positive over the north-western portion and mainly negative in the remaining area (Figure 2.7.a). In spring, the LAI effect is strongly negative in most pixels, especially one month after the impulse. Only a small group of pixels located south-east and north-west of the study area display positive coefficients (Figure 2.7.b). In summer, the effect of LAI one month after the impulse is predominantly negative. In the following month the effect is positive for many of the pixels located in the west and north-east. There are cases, such as a small area in the south-west portion of the study area, in which the effect is strongly negative the first month and becomes highly positive the second month (Figure 2.7.c). During fall, the effect is weak one month after the impulse and becomes primarily positive in the following month, especially in the west portion of the study area (Figure 2.7.d).

The effect of LST on LAI presents a wider spatial distribution in all seasons (Figure 2.8). During winter, the LST effect is generally weak. One month after the impulse, the coefficients are mainly negative at low elevations and primarily positive at high elevations. After two months, the coefficients are negative in most of the west side and positive in the majority of the east side (Figure 2.8.a). In spring, the effect is predominantly negative and particularly strong in the eastern portion of the study area (Figure 2.8.b). In summer, LST imposes a strongly negative effect on LAI across most of

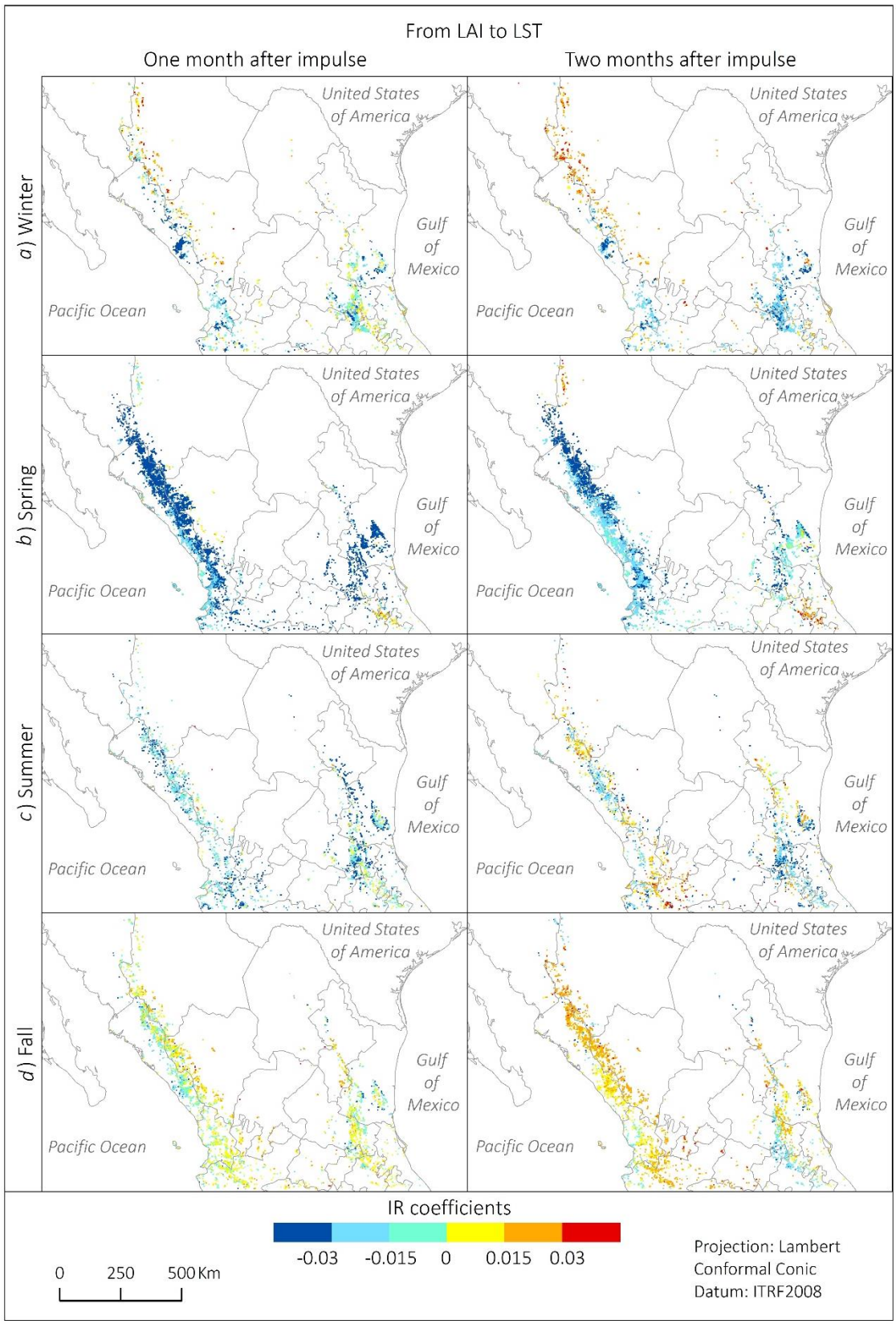

Figure 2.7. IR coefficients of pixels that show LAI to LST Granger causality at 1-month lag in winter (a), spring (b), summer (c), or fall (d)

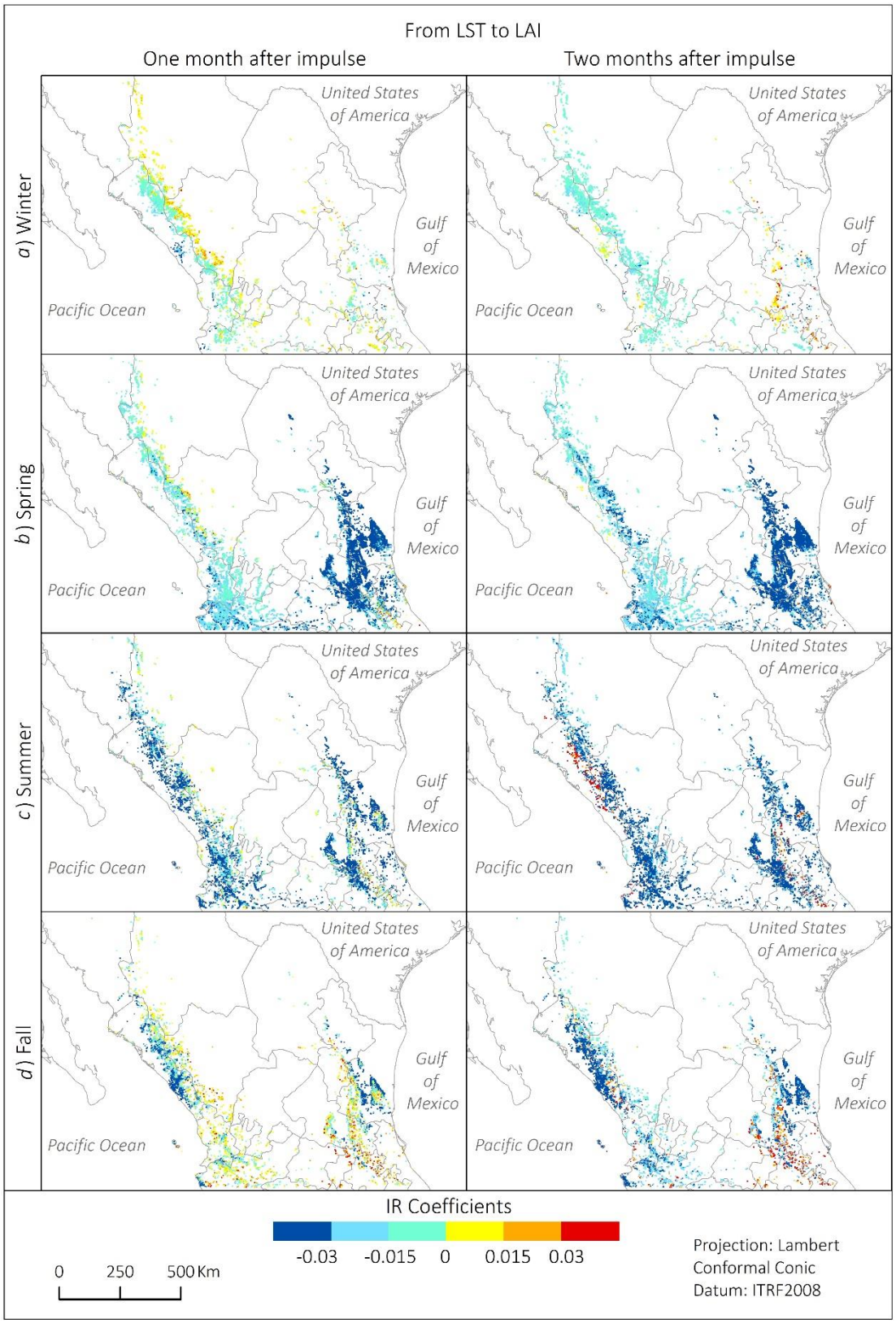

Figure 2.8. IR coefficients of pixels that show LST to LAI Granger causality at 1-month lag in winter (a), spring (b), summer (c), or fall (d)

the study area. A notorious exception occurs in pixels located in the State of *Sinaloa*, where the effect becomes highly positive two months after the LST impulse (Figure 2.8.c). During fall, the effect is heterogenous. The first month is mainly positive, except for the low altitudes of the *Sinaloa* and *Tamaulipas* States. The second month is mostly negative, except for the south-western portion of the study area, where the impact is strongly positive (Figure 2.8.d).

2.4. Discussion

2.4.1. Relationship between LAI and LST

The results of this research demonstrate that the nature of the relationship between LAI and LST varies depending on the temporal scale. The processes responsible for this variation are not the same at different time scales. Vegetation succession and natural disturbances play a more important role at the annual scale, while phenological changes and climate regimes impose a greater influence at the seasonal scale (Liu et al. 2006).

2.4.1.1. Annual relationship

At the annual scale, LST Granger-causes LAI over most of the study area. In contrast, LAI generally does not Granger-causes LST, except for a portion of the east side of the study area and some small isolated areas over the west side (Figure 2.4). The nature of the detected causality is primarily negative in both directions and usually weaker from LAI to LST (Figure 2.3). These findings are in accordance with Liu et al.

(2006), who evaluated feedbacks between Fraction of Photosynthetically Active Radiation (FPAR) and air temperature at a global scale between 1982 and 2000. Using led-lag regression/correlations to identify the presence of interactions and the Frankignoul, Czaja, and L'Heveder (1998) method to estimate the strength of those interactions, they observed a year-round strong negative correlation from temperature to FPAR over most of the Mexican territory at 1-month lag, but a general absence of correlation from FPAR to temperature. The only area where they detected correlation from FPAR to temperature also exhibits weaker negative coefficients and coincides with the eastern portion where this study found presence of LAI to LST causality (Figure 2.4).

The existence of a significant effect of surface temperature on vegetation has been similarly addressed by other authors. Zhou et al. (2003) found that fluctuations in temperature accounted for the largest fraction of NDVI change in northern high latitudes between 1982 and 1999. Liu et al. (2006) detected that FPAR variability is predominantly driven by temperature, not only in Mexico, but also in northern mid and high latitudes. Notaro, Liu, and Williams (2006) declared that temperature imposes a significant instantaneous forcing on FPAR over the United States. These results reflect some of the physical process taking place at the land-surface. At global and regional scale, surface temperature is a product of several physical drivers (e.g., albedo, soil moisture), of which vegetation is only a moderating factor (Liu et al. 2006; Eagleson 2011). In contrast, vegetation greenness is purely influenced by regional climatic conditions, where temperature is a primary element (Liu et al. 2006; GCOS 2019).

As for forest types (Figure 2.2), a higher proportion of deciduous broadleaf showed causality from LST to LAI, which demonstrates the general influence of temperature on leaves phenology. LAI to LST causality was observed in more pixels of evergreen broadleaf forest, where fluctuations in temperature are less variable year-round and, therefore, a change in vegetation density may have a more significant impact on the naturally stable surface temperature.

The eastern portion of the study area is characterized by a relatively higher occurrence of LAI to LST causality (Figure 2.4.a) and a negatively stronger effect of LST on LAI (Figure 2.4.b), which can be indicators of more dynamic forest ecosystems. More specifically, these characteristics may suggest vegetation disturbances. According to the Mexico's National Forest and Soils Inventory collected by the *Comisión Nacional Forestal* (CONAFOR), the most common disturbances recorded between 2004 and 2017 on the eastern side are presence of epiphytes, drought, and defoliating insects (in order of importance), while for the western side are fire, logging and drought (CONAFOR 2019). Among these disturbances, drought has been highlighted as an important diver of forest change. Indeed, in 2009 and 2011, Central Mexico suffered the most severe droughts in seven decades (Domínguez 2016) and, according to CONAFOR (2019), the effects of these droughts have been most severe on the eastern region. Although this study suggests that the distinct behaviour of the LAI and LST variables over the east side of the study area may be associated with vegetation disturbances, more research must be performed to elaborate on a definitive conclusion.

2.4.1.2. Intraseasonal relationship

In all season, Granger causality from LST to LAI occurs more consistently than causality in the opposite direction. The highest and lowest presence of this causality occur in spring and winter, respectively (Figure 2.5). The effect of LST on LAI is predominantly negative, generally stronger in summer and weaker in winter (Figure 2.6). As mentioned in section 2.2.1, the rainy period (May to October) is also called the "warm half of the year" and coincides with the growing season. Therefore, a higher presence of LST to LAI causality in spring suggests that the effect of surface temperature on vegetation greenness is greater during the emergence of leaves than during the senescence. Although the occurrence of causality is lower in summer than in spring, the strongest coefficients are observed in deciduous broadleaf forest during summer, when leaves typically reach maturity. On the other hand, the dry season (November to April), which is also referred to as the "cold half of the year", is characterized by a lower presence of LST to LAI causality. Thus, colder temperatures are associated with a lower occurrence of causality, which is particularly weak in winter, when the lowest temperatures are reached. These findings are overall in line with what the global scale study of Liu et al. (2006) estimated for Mexico.

Regardless of the season, Granger causality from LAI to LST occurs less commonly than causality in the opposite direction (Figure 2.5). The effect of LAI on LST is mainly positive in fall and negative in the remaining seasons, except for evergreen needleleaf forest where the effect is negative only in summer (Figure 2.6). Despite the low presence

of this causality, there is a relatively higher occurrence in spring over deciduous broadleaf forest, where LAI imposes a particularly strong negative effect on LST, which suggests that leaf emergence has a cooling effect on land surface. Kaufmann et al. (2003) also estimated a negative effect of NDVI on surface temperature for this forest type during spring in Eurasia. Another aspect to highlight is that the strongest positive effect of LAI on LST occurs in winter over evergreen needleleaf. This interaction is also consistent with Kaufmann et al. (2003), who found a strong positive relationship from NDVI to surface temperature in winter over evergreen needleleaf forests of North America and Eurasia. According to these authors, NDVI is not a good indicator of vegetation greenness in winter. Instead, it can be a useful proxy of snow cover extent as these variables are negatively correlated during this season. Thus, a reduction in the extent of snow cover (i.e., an increase in vegetation greenness) increases the absorption of solar radiation and, consequently, raises surface temperature. This process creates a positive correlation from vegetation greenness to surface temperature.

2.4.2. Challenges and opportunities

This research has a few limitations that can be addressed in future research. First, Granger causality and IR coefficients were estimated using only LAI and LST. However, other variables (e.g., precipitation, solar zenith angle, aerosol optical depth, latitude) may also help to explain the behaviour between vegetation greenness and surface temperature (Kaufmann et al. 2003; Papagiannopoulou et al. 2017). Therefore, the inclusion of additional variables is considered as future step to improve these models.

Second, only pixels with stationary time series were considered for the analysis (Table 2.1.b). However, the exclusion of non-stationary time series may be avoided by detrending those trajectories or by implementing the Toda and Yamamoto (1995) procedure, which allows for the examination of Granger causality in the context of non-stationary data.

Third, there is a false continuity in the season-based time series. For example, the three monthly anomalies of a particular winter were joined to the three monthly anomalies of the following winter. This false seasonal continuity (e.g., winter 2002 and winter 2003) provokes the model to estimate not only relationships occurring among anomalies of the same season, but also between anomalies of a given season and anomalies of the following season. Although, several authors do not discard an interaction between anomalies of different seasons (e.g., Kaufmann et al. 2003; Wang et al. 2006; Kaufmann et al. 2007; Jiang, Liang, and Yuan 2015) and there should not be a reason to discard it *a priori*, this research may be extended to explore an alternative methodology that better handles this false continuity on the season-based time series.

2.5. Conclusion

On a pixel-by-pixel basis of MODIS imagery, this research evaluated the annual and intraseasonal relationship between LAI and LST collected from 2002 to 2017 across the forest vegetation of Central Mexico. The Granger causality approach was used detect the presence of any relationship and an IR function was implemented to estimate the sign and strength of the relationship. The main results indicate that, at any temporal

scale, Granger causality from LST to LAI occurs more consistently than causality in the opposite direction. At the annual scale, the nature of the relationship is primarily negative in both directions and usually weaker from LAI to LST. At the seasonal scale, the occurrence of LST to LAI causality is higher in spring and lower in winter. The effect of LST on LAI is predominantly negative and particularly strong in deciduous broadleaf forest during summer, when leaves typically reach maturity. On the other hand, the effect of LAI on LST is mainly positive in fall and negative in the remaining seasons, except for evergreen needleleaf forest where the effect is negative only in summer. The highest presence of LAI to LST causality occurs in spring over deciduous broadleaf forest, where LAI imposes a particularly strong negative effect on LST, which suggests that leaf emergence has a cooling effect on land surface.

These results support general conclusions presented in other studies (e.g., Zhou et al. 2003; Liu et al. 2006; Notaro, Liu, and Williams 2006) and reveal novel spatio-temporal patterns of the relationships between vegetation greenness and surface temperature in Central Mexico. As for the input data and methods, this research proposed LAI as an alternative index to overcome the shortcomings of other widely used vegetation greenness indicators (i.e., NDV and EVI). Unlike traditional regression and correlation analysis, the Granger causality approach enabled the examination of lagged effects of LAI on LST, and vice versa. IR coefficients, which have been rarely used in the related literature, helped to model the over-time response of a variable to a change of another variable.

The findings of this research suggest that the relationship between vegetation greenness and surface temperature varies depending on the temporal scale, forest type, and causal variable. Therefore, caution has to be exercised when assuming a consistent inverse relationship driven by vegetation, which seems to be the general consensus in much of the literature that makes use of these two variables to study an environmental phenomenon (Lambin and Ehrlich 1996, 1997; Wan, Wang, and Li 2004; Mildrexler et al. 2007; Coops, Wulder, and Iwanicka 2009; Mildrexler, Zhao, and Running 2009). Finally, this study is expected to be a contribution to the understanding of vegetation dynamics in Mexico. Based on the results, surface temperature is a significant driver of vegetation greenness in Mexican forests. Therefore, LST products can be considered a potential proxy of vegetation greenness trajectories, especially in the context of a warming climate.

3. FOREST DEGRADATION ASSESSMENT BASED ON TREND ANALYSIS OF MODIS-LEAF AREA INDEX[2]

3.1. Introduction

Forest ecosystems play an essential role maintaining the carbon cycle balance because they are able to store carbon (Brown et al. 1996). However, when these ecosystems are perturbed, stored carbon is released as carbon dioxide (CO2) into the atmosphere, where it contributes to global warming by absorbing heat and impeding transmission to space. The assessment of forest degradation depends on how "forest" and "forest degradation" are defined. Both concepts, which have been subject of extensive debates (Schoene et al. 2007; Chazdon et al. 2016), have been defined by many institutions based on particular perspectives and purposes. In this research, forests are "lands dominated by woody vegetation with a percent cover of more than 60 percent and height exceeding 2 meters"(Strahler et al. 1999), which is in agreement with the definition used by the Moderate Resolution Imaging Spectroradiometer (MODIS) land cover product (MCD12Q1). Regarding forest degradation, this work adopts a simple but comprehensive approach for which context needs to be provided.

Definitions from international organizations, such as the Intergovernmental Panel on Climate Change (IPCC) and the United Nations Food and Agriculture Organization (FAO), share a set of basic notions, which describe forest degradation as a process that

[2] This chapter was published with the title "Forest Degradation Assessment Based on Trend Analysis of MODIS-Leaf Area Index: A Case Study in Mexico" in *Remote Sensing*. 2019. 11(21): 2503. doi:10.3390/rs11212503

involves a long-term observation period in which negative changes affect the forest's structure, function, and capacity to provide services and goods (UNEP-CBD 2001; Penman et al. 2003; ITTO 2005; FAO 2006; Schoene et al. 2007; Sasaki and Putz 2009; Shoch, Eaton, and Settelmyer 2013). Within the literature on remote sensing of forest dynamics, forest degradation is frequently embedded in the context of forest disturbances, which are described as drivers of a forest's state and function that range from high-impact events (e.g., caused by fires, windstorms, deforestation) to subtle and gradual processes (e.g., caused by insects, diseases, droughts, acid rain; Cohen et al. 2017). As far as we are aware, the scientific literature lacks an explicit explanation of the relationship between forest degradation and forest disturbances. However, according to the forest disturbances definition, forest degradation is a type of disturbance and other disturbances can eventually lead to forest degradation. Therefore, this research considers forest degradation as any negative monotonic (i.e., single-direction), not necessarily linear, trend in vegetation greenness. This includes any disturbances that are not associated with a recovery process during the period of observation. Special attention is given to changes that are very subtle and become apparent gradually as they have traditionally been hard to monitor.

Although not used as frequently as Landsat (see Cohen et al. 2017 for examples of Landsat-based algorithms), MODIS has been employed to detect forest disturbances, including forest degradation. MODIS-based algorithms make use of surface reflectance (Jin and Sader 2005; Xin et al. 2013; de Beurs, Owsley, and Julian 2016; Tran, de Beurs, and Julian 2016), Percent Tree Cover (PTC; Gao et al. 2015), fires and thermal anomalies

(Hammer, Kraft, and Wheeler 2014), and a variety of spectral indexes, such as the Normalized Difference Vegetation Index (NDVI; Vandecar et al. 2011; Hammer, Kraft, and Wheeler 2014), the Normalized Burned Ratio (NBR; Sulla-Menashe et al. 2014), the Modified Soil Adjusted Vegetation Index (MSAVI; Hashim, Beiranvand, and Wei 2014), and the Enhanced Vegetation Index (EVI) together with Land Surface Temperature (LST; Mildrexler et al. 2007; Coops, Wulder, and Iwanicka 2009; Mildrexler, Zhao, and Running 2009). Some authors combine a broad range of MODIS products into a single algorithm. For example, Pouliot et al. (2009) used surface reflectance, NDVI, the Wide Dynamic Range Vegetation Index (WDVI), the Soil Adjusted Vegetation Index (SAVI), the Global Environment Monitoring Index (GEMI), the Reduced Simple Ratio (RSR), and the Normalized Difference Moisture index (NDMI) to train a decision tree classifier. Unlike other vegetation greenness indicators, such as NDVI and EVI, Leaf Area Index (LAI) has not been tested to assess forest disturbances. LAI is a measure of the amount of vegetation vertically distributed and is formally defined as the total one-sided area of all green leaves per unit ground area in broadleaf canopies, and as the total surface area of just one half of all needles per unit ground area in coniferous canopies (Myneni et al. 2002). In theory, the higher the LAI values, the denser the vegetation vertical structure and, therefore, the greater the surface potentially available for photosynthesis. Therefore, this research proposes to use time series of LAI, which may provide a good description of forest conditions through time.

MODIS-based algorithms have identified forest disturbances through linear trend analysis (Hammer, Kraft, and Wheeler 2014), temporal segmentation (Sulla-Menashe et

al. 2014), regression and decision trees (Pouliot et al. 2009; Loboda et al. 2012; Guindon et al. 2014), unsupervised classifications (Jin and Sader 2005), linear combinations of the pixel components (Hashim et al. 2014), Tasseled Cap transformations (Hilker et al. 2009; Tran, de Beurs, and Julian 2016; de Beurs, Owsley, and Julian 2016), and multitemporal analysis of surface temperature and vegetation greenness ratios (Mildrexler et al. 2007; Coops, Wulder, and Iwanicka 2009; Mildrexler, Zhao, and Running 2009). A considerable number of algorithms have fused MODIS with Landsat data to improve the detection of forest disturbances (Hilker et al. 2009; Xin et al. 2013; Schmidt et al. 2015; Tran, de Beurs, and Julian 2016). To the best of our knowledge, no MODIS-based algorithms have decomposed LAI time series to extract and analyze the trend component. Time series decomposition procedures were developed within the field of econometrics; however, environmental sciences have adopted these techniques to study different processes, including ecosystem changes (Verbesselt et al.2010) and vegetation dynamics (Jacquin, Sheeren, and Lacombe 2010; Schucknecht et al. 2013). Often, time series are assumed to be comprised of three basic components; “trend”, “seasonal”, and “remainder”. The trend component improves the identification of very subtle and gradual changes because it extracts low frequency changes that occur throughout the time series (Dokumentov and Hyndman 2015).

Therefore, this study aims to assess forest degradation by analyzing, on a pixel-by-pixel basis, the trend component of MODIS LAI time series collected over Central Mexico from 2002 to 2017. To achieve this objective, a time series decomposition procedure based on regression is applied to extract the trend component, whose strength and

magnitude are calculated through a modified Mann-Kendall non-parametric test and the Theil-Sen´s slope test, respectively. The product of the strength and magnitude is proposed as a measure of forest degradation. The validation is performed by comparing the overall trend analysis with an analogous trend analysis of a health index, which was developed for the specific purposes of this research and is calculated using reference data from the Mexico's National Forest and Soils Inventory (NFSI).

3.2. Data and methods

3.2.1. Study area

Due to the multitemporal nature of this work, the study area encompasses all 500-m pixels contained in the MODIS tile h08v06 that were covered by forest during at least one year between 2002 and 2017 (Figure 3.1). According to the MODIS Land Cover product (MCD12Q1, type 3), these pixels comprise 63,964 square kilometers, 60% of which correspond to deciduous broadleaf forest, 36% to evergreen broadleaf, and 4% to evergreen needleleaf. These forests are home of a wide variety of species (in the order of hundreds), some of the most commonly found include *Quercus magnoliifolia*, *Quercus rugosa*, *Quercus laeta*, *Quercus sideroxyla*, *Pinus durangensis*, *Abies sp*., *Lysiloma divaricatum*, *Laguncularia racemosa*, *Byrsonima crassifolia*, *Beilschmiedia mexicana*, and *Guazuma ulmifolia* (CONAFOR 2019).

This vegetation is primarily distributed across the *Sierra Madre Occidental* (west mountain range) and *Sierra Madre Oriental* (east mountain range). In the western region, elevation ranges from sea level to 3,104 m with a mean of 972 m and a standard

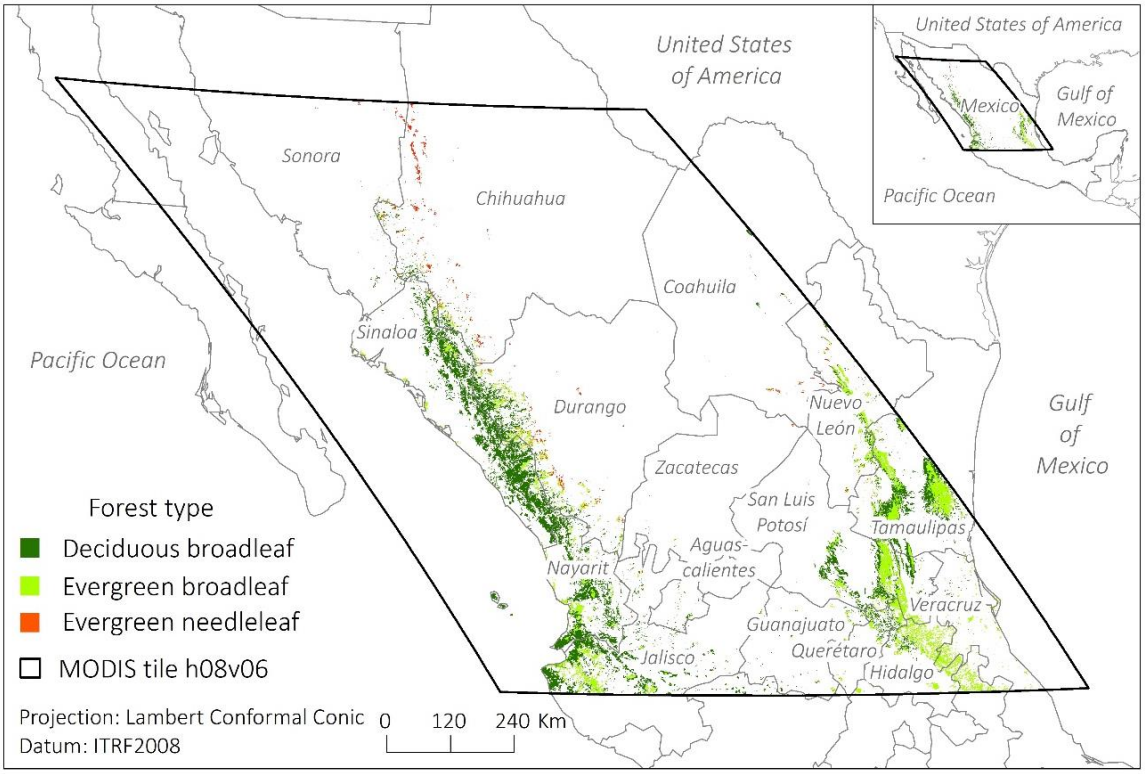

Figure 3.1. Study area: pixels covered by forest during at least one year between 2002 and 2017

deviation of 742 m, while slopes range from 0 to 30° with a mean of 6.9° and a standard deviation of 4.5°. In the eastern region, the altitudinal range is wider, it goes from sea level to 3,300 m with a mean of 1,067 m and a standard deviation of 684 m, while slopes range from 0 to 35° with a mean of 6.9° and a standard deviation of 5°.

The climatic conditions range from tropical to semi-cold. Tropical and semi-tropical climates, whose mean annual temperature exceeds 18 °C, extend over most of the areas facing the coastal plains and cover 41 and 35% of the study area, respectively. Temperate climate, whose mean annual temperature oscillates between 12 and 18 °C, extends over higher elevations and covers 13% of the study area. Arid climates are generally found towards continental areas and represent 8% of the study area. The

highest elevations are occupied by semi-cold climates, which cover the remaining 3% of the study area.

In Mexico, nearly 60% of the forest lands are owned by *ejidos* (i.e., a tenurial system in which land is managed collectively) or agrarian communities (Skutsch et al. 2013), where forests are often managed for timber production. The remaining forested areas are managed by private property owners and, in a smaller proportion, by the government in the form of natural protected areas (Klooster and Masera 2000; Morales-Barquero et al. 2014). In the study area, about 50% of the land is managed by *ejidos*. Although this proportion is lower than at national level, *ejidos* are the dominant land tenure units.

Central Mexico was chosen as the study area for three reasons. First, studies focused on detecting forest disturbances or degradation in Mexico have been conducted primarily at local scales (Kovacs, Wang, and Blanco-Correa 2001; Brower et al. 2002; Vidal, López-García, and Rendón-Salinas 2014; Gao et al. 2015; Romero-Sánchez and Ponce-Hernandez 2017) and rarely at a regional scale (Mildrexler, Zhao, and Running 2009) like this study. Second, according to Morales-Barquero et al. (2014), the levels of human disturbance in Mexican forest are significantly high. Third, according to the Land Use and Vegetation Map produced by the *Instituto Nacional de Geografía y Estadística* (INEGI), 14,900 km^2 (23%) of the study area were covered by perturbed secondary vegetation in 2014 (INEGI 2017).

3.2.2. Data and preprocessing

LAI, the ratio of half of the total leaf surface area per unit ground area, is a dimensionless measure that ranges from 0 (e.g., bare ground) to over 10 (e.g., dense forest; GCOS 2010). In this research, LAI estimates were acquired from the MODIS sensor onboard the Terra satellite. The morning overpass time of Terra (at approximately 10:30 am at the equator) provides more reliable LAI estimates than the afternoon overpass time of Aqua (at approximately 1:30 pm) due to lower cloud presence (Yan et al 2016). King et al. (2013) performed a visual comparison of the Terra and Aqua cloud fractions and found a generally cloudier pattern over land in the Aqua products.

MODIS LAI is released in conjunction with Fraction of Photosynthetically Active Radiation (FPAR) in a single product. Both variables are estimated from an algorithm based on a tridimensional (i.e., it accounts for vegetation structure) radiative transfer model that selects the best LAI and FPAR estimates by comparing measured spectral values (from the red and near-infrared regions) with a look-up table that contains observed spectral values of six biome types and their corresponding LAI/FPAR values. This main algorithm may fail to obtain a solution due to large uncertainties in the input spectral values, cloud effects, or too low sun/view zenith angles. In this case, the retrievals, with relatively poor quality, are produced from a back-up algorithm based on the biome-specific empirical relationship between NDVI and LAI/FPAR (Knyazikhin et al. 1998; Myneni et al. 2002; Jensen et al. 2011; Yang et al. 2006; Yan et al. 2016). According to Yan et al. (2016), Collection 6 (C6) of the MODIS LAI/FPAR product is considerably

better than Collection 5 (C5). C6 properly captures the interannual variation of LAI, as well as the general seasonality of all biomes, except for evergreen broadleaf forests, where poor quality retrievals are produced. However, this shortcoming is also observed in other satellite products, such as the Carbon cYcle and Change in Land Observational Products from an Ensemble of Satellites (CYCLOPES) and those from the Global Land Surface Satellite (GLASS), and the SPOT-VEGETATION GEOV1 system.

MODIS data were acquired through the Land Processes Distributed Active Archive Center (LP DAAC) managed by the NASA Earth Science Data and Information System (ESDIS) project. Based on the characteristics mentioned, MODIS Terra 8-day LAI/FPAR composites (MOD15A2H, C6) of the tile h08v06 were downloaded from 2002 to 2017 at 500 meters spatial resolution. To extract forest land covers, MODIS Terra + Aqua yearly Land Cover composites (MCD12Q1, C6) were also obtained for the same area and time period, and at the same spatial resolution. The preprocessing steps that are described below were conducted by means of ArcPy, a site package that allows for the use of ArcGIS functionalities through Python programming language.

All datasets were projected to Lambert Conformal Conic projection in ITRF2008 datum and clipped to forested areas, which were delimited by identifying all pixels covered by forest during at least one year between 2002 and 2017. In the few cases for which the type of forest changed between years, the most frequent forest type was assigned. Only good quality LAI retrievals (i.e., obtained from the main algorithm) were selected to perform the analysis. The Land Data Operational Product Evaluation (LDOPE) tool was used to unpack the LAI Quality Control layers, which specify the type of

algorithm used to derive the retrievals. Once the good quality values were extracted, monthly LAI means were calculated on a pixel-by-pixel basis for each month from January 2002 to December 2017. Finally, in order to manipulate the data in an R environment, all LAI means were extracted from the raster files and rearranged into a comma-separated values (cvs) file, where each row contained the monthly LAI time series of a single pixel. Due to the exclusion of poor-quality retrievals, 0.5% of the pixels (1,505) were discarded from the analysis.

3.2.3. Algorithm to analyze LAI trends

A seasonal-trend decomposition procedure based on regression (STR; see Dokumentov and Hyndman 2015 for a complete description of the procedure) was used to break down the time series (y_t, where t is time) into trend (μ_t), seasonal (γ_t), and remainder (ϵ_t) components. In a given time series (Figure 3.2.a), the simplest STR model considers these components to be additive:

$$y_t = \mu_t + \gamma_{sn(t),t} + \epsilon_t, \qquad t = 1, \dots, T. \tag{4}$$

The trend component (Figure 3.2.b) describes low frequency non-stationary long-term changes. The seasonal component (Figure 3.2.c) shows a stable repeating pattern of change; thus, γ_t represents only one element of the seasonal pattern, while $\gamma_{sn(t),t}$ represents a *k* x *n* matrix of seasonal shapes, where *k* is the number of seasons and *n* is the length of the time series. The remainder (Figure 3.2.d) depicts variations considered as a normally distributed white noise process with mean zero and variance σ_ϵ^2 (Harvey

and Tood 1983; Harvey 1985; Harvey and Peters 1990; Cleveland 1990; Dokumentov and Hyndman 2015).

The trend (Figure 3.2.b), which is the component of interest in this research, can be modeled as a local approximation to a linear trend:

$$\mu_t = \mu_{t-1} + \beta_{t-1} + \eta_t, \quad (5a)$$

$$\beta_t = \beta_{t-1} + \zeta_t, \quad (5b)$$

where η_t and ζ_t are normally distributed independent white noise processes with mean zero and variance σ_η^2 and σ_ζ^2, respectively. The level and slope change slowly over time

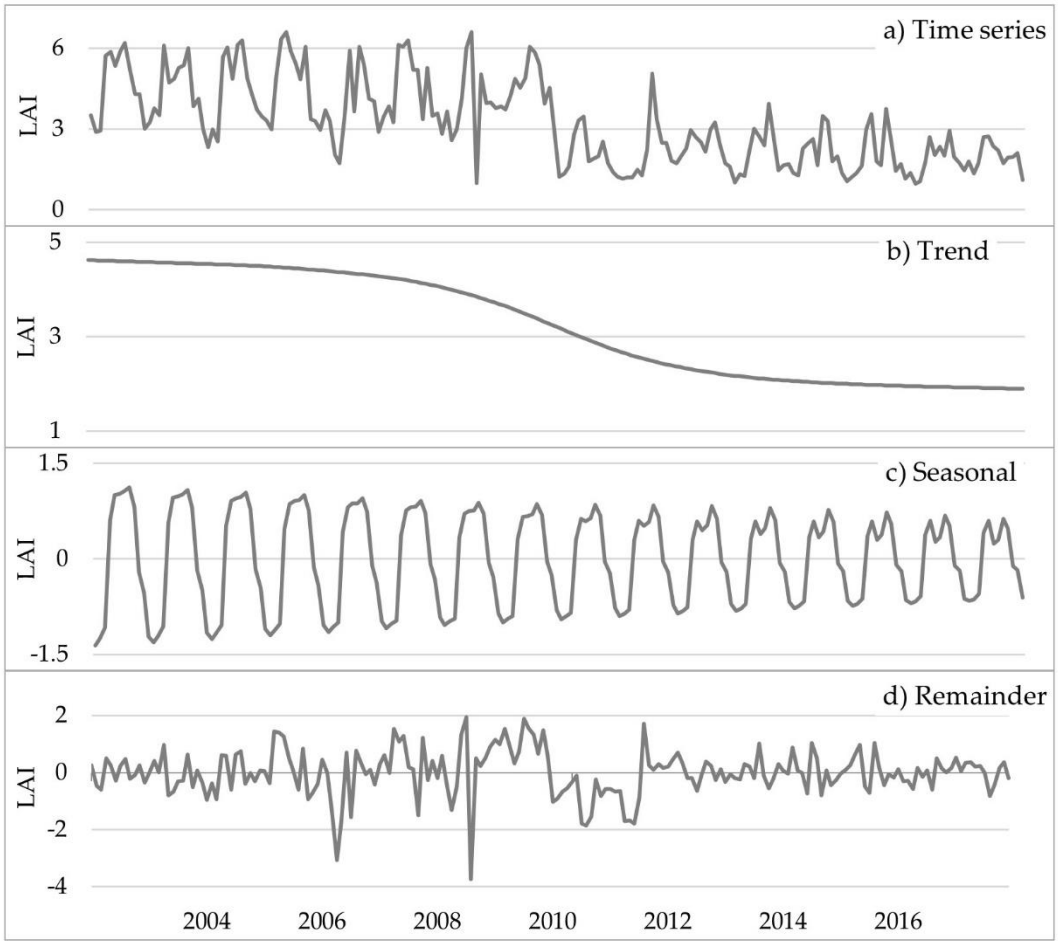

Figure 3.2. Example of the decomposition of a time series (a) into trend (b), seasonal (c), and reminder (d) components

based on a random walk mechanism (Harvey and Tood 1983). The reason behind analyzing the trend lies on the nature of the component. Its low frequency, non-stationary behavior, and small rate of change in a long-term basis allows for the identification of very subtle and gradual changes that may otherwise be obscured.

Using the "stR" package (Dokumentov and Hyndman 2018) in an R environment (R Core Team 2018), trend components were extracted in the form of a new time series with as many values as the original time series. These new sets of values may or may not exhibit a general increase or decrease. This means that, in some cases, the trend component may actually show that the time series does not exhibit a trend. Therefore, to evaluate the presence of a monotonic trend in the trend component, a modified Mann-Kendall test for serially-correlated data (Mann 1945; Kendall 1955; Hamed and Rao 1998) was applied. This non-parametric test evaluates the null hypothesis of independent and randomly ordered observations (i.e., no trend).

The original Mann-Kendall (Mann 1945; Kendall 1955) test determines if the *Y* variable (in this case LAI) tends to increase or decrease as the *X* variable (time) increases. To achieve this, data are ordered chronologically and a Kendall's τ correlation coefficient is computed as follows:

$$\tau = \frac{S}{n(n-1)/2}, \tag{6a}$$

$$S = C - D, \tag{6b}$$

where n is the number of observations and S is the test statistic, which is calculated by subtracting D, the number of "discordant pairs of observations", from C, the number of

"concordant pairs of observations". In D, the later-in-time observation has a smaller value than the previous observation (i.e., *Y* decreases as *X* increases); while in C, the later-in-time observation has a larger value that the previous observation (i.e., *Y* increases as *X* increases). A total of $n(n-1)/2$ pairs of observations are possible. If half of the pairs are concordant and half discordant, so that $S = 0$, τ will equal 0 (i.e., no trend). If all pairs are concordant, so that $S = n(n-1)/2$, τ will equal 1 (i.e., strong increasing trend). In contrast, if all pairs are discordant, so that $S = -(n(n-1)/2)$, τ will equal -1 (i.e., strong decreasing trend). Therefore, τ produces values, from -1 to 1, that show the strength of the monotonic association between the variable of interest (*Y*) and time (*X*; Helsel and Frans 2006).

The significance of the trends is evaluated by comparing the standardized S statistic, $Z = S/[var(S)]^{0.5}$, with the standard normal variate at the desired level or significance. Under the null hypothesis of trend absence, the S statistic tends to show zero mean and variance $n(n-1)(2n+5)/18$. However, the variance of S and, as a consequence, the p values are affected when serial correlation is detected. A positive serial correlation increases the probability of detecting a significant trend when it actually does not exist, while a negative serial correlation decreases the probability of detecting a significant trend when it actually exists (Hamed and Rao 1998). A rank von Neumann ratio test (Bartels 1982), which assesses the null hypothesis of randomness, corroborated the presence of serial correlation in the extracted trend components of this study. Therefore, a S variance correction approach, proposed by Hammed and Rao (1998), was

implemented to address the issue of serial correlation and, consequently, generate the correct p values.

As explained, the modified Mann-Kendall test detects significant monotonic trends and provides a measure of their strength (i.e., how consistently-decreasing or consistently-increasing they are) through the Kendall's τ correlation coefficient. However, it does not specify their magnitude (i.e., how much they change). To account for the magnitude, a Theil-Sen's slope (Theil 1950; Sen 1968), which estimates a monthly rate of change that can be used to calculate the absolute change over the study period, was obtained by computing a set of $N = n(n-1)/2$ slope values (Hollander, Wolfe, and Chicken 2013):

$$b_{ij} = \frac{Y_j - Y_i}{X_j - X_i}, \quad 1 \le i < j \le n, \; X_i \ne X_j, \tag{7a}$$

median of those slopes:

$$\hat{\beta} = median\{b_{ij}, 1 \le i < j \le n\}. \tag{7b}$$

The "modifiedmk" R package (Patakamuri and O'Brien 2019) was used to calculate the Mann-Kendall p value, the Kendall's τ correlation coefficient, and the Theil-Sen's slope for each of the trend components. After exploring the overall results and computing the occurrence of positive versus negative significant trends, a subset of negative trends was created for a deeper analysis. Negative trends are potential indicators of forest degradation. However, consistently-decreasing trends alone (i.e., negative Kendall's τ correlation coefficients) cannot be considered processes of forest degradation because their magnitude of change may be insignificant. Similarly, negative

magnitudes alone (i.e., Theil-Sen's slopes) cannot be considered processes of forest degradation because their rate of change may be weakly monotonic and, therefore, not representative of a typical process of forest degradation. Therefore, the product of negative Kendall's τ correlation coefficients and negative Theil-Sen's slopes is here proposed as a measure of forest degradation. This measure facilitates the identification of consistently-decreasing trends with high magnitudes of change, which can be interpreted as severe processes of forest degradation. As a rule, the higher the product, the greater the degradation severity. The outcomes of the multiplication were reclassified into three categories of severity (i.e., high, moderate, and low) based on a geometrical interval classification method, which performs well with non-normally distributed data.

3.2.4. Validation of the algorithm

To validate the results, the health conditions of 52,807 trees collected in 177 conglomerates were used as reference data (CONAFOR 2019). This information was gathered between 2004 and 2017 by the *Comisión Nacional Forestal* (CONAFOR) as part of Mexico's National Forest and Soils Inventory (NFSI). A simple trend analysis of the tree conditions was performed and compared with the proposed measure of forest degradation. The Mexico's NFSI is completely updated every five years by re-visiting 20% of the sampling conglomerates every year. Within the study area, there are approximately 1,540 conglomerates separated from each other by roughly 5 km. These conglomerates have been measured two or, in a few cases, three times during the study

period. Based on these spatio-temporal characteristics, only conglomerates that have been visited three times and whose centroids fall within a buffer of 150 m around the center of the MODIS pixels were considered for the analysis. The first criterion responds to the necessity of at least three observations to perform a trend analysis. The second criterion ensures that the conglomerates are representative of what the Instantaneous Field of View (IFOV) of the MODIS pixels captures. In other words, it warrants spatial coincidence.

The 177 conglomerates that meet the two aforementioned criteria mimic the distribution of the original systematically collected NFSI data. Therefore, they are representative of the overall characteristics of the area (i.e., forest type, altitude, slope, climate). Each conglomerate contains four sampling sites that are distributed in an inverted "Y" shape and whose centroids are separated by 45.14 m. Each site has an area of 400 m^2 and a radius of 11.28 m. The health conditions of all trees falling within this area and having diameter greater than 7.5 cm were recorded. As a result, 13,905 trees were measured during the NFSI 2004-2009 in the 177 conglomerates, 15,730 during the NFSI 2009-2014, and 23,172 during the first 3 years of the NFSI 2014-2019. Two classification systems were used to record the tree conditions. The first system, employed for the NFSI 2004-2009 and the NFSI 2009-2014, comprises the six following classes: stump, dead-standing, very poor vigor, poor vigor, good vigor, and maximum vigor. The second system, used for the NFSI 2014-2019, comprises the five following classes: stump, dead-standing, low vigor, moderate vigor, and high vigor. This incompatibility between classification schemes implies a limitation that is addressed in

section 3.4.3. For the purposes of this validation, the conditions from the two classification schemes were unified as follows: stump, dead-standing, very poor or low, poor, moderate, good, and maximum or high.

To obtain a single measure representative of all trees within each conglomerate, a health index was developed. First, the number and proportion of trees within each class was calculated. Then, the proportion was multiplied by the weight of the class (i.e., stump = 1, dead-standing = 2, very poor or low vigor = 3, poor vigor = 4, moderate vigor = 4.5, good vigor = 5, and maximum or high vigor= 6). The resulting values were summed to obtain an overall index that ranges from 1 to 6, where 6 is the optimum vigor condition (Table 3.1).

Table 3.1. Example of health index calculation in a selected conglomerate (conglomerate ID 39373, NFSI 2004-2009)

Condition	Trees		Weight	Proportion × Weight	Health index (addition)
	No.	Proportion			
Stump	0	0.00	1	0.00	5.07
Dead-standing	4	0.03	2	0.06	
Very poor or low vigor	4	0.03	3	0.09	
Poor vigor	9	0.07	4	0.27	
Moderate vigor	0	0.00	4 .5	0.00	
Good vigor	78	0.59	5	2.93	
Maximum or high vigor	38	0.29	6	1.71	

Once three index values were computed per conglomerate (i.e., one per observation date), the presence of trends was evaluated by looking at the sign of the differences between two consecutive index values (later date minus earlier date). As there are three observations, two differences were calculated. When these differences share the same sign, a given location exhibits a trend, which is negative if both signs are negative and positive otherwise. The magnitude of change of all negative trends was

calculated by subtracting the last observation from the first one and dividing the outcome by two. The resulting values were reclassified into three categories of severity (i.e., low, moderate, and high) based on a geometrical interval classification method. According to this methodology, each conglomerate can take one of the following classes: no trend, positive trend, low degradation, moderate degradation, or high degradation (Table 3.2). By means of a confusion matrix, these results were compared with the results of the trend analysis proposed in this research.

Table 3.2. Examples of trend analysis in selected conglomerates based on the calculated health index values

Conglo-merate ID	Health index per NFSI			Sign of the difference		Trend	Magnitude	Trend analysis classification
	A) 2004-2009	B) 2009-2014	C) 2014-2019	B - A	C - B			
35110	3.80	4.50	3.60	+	-	None	----	No trend
44140	3.30	4.30	5.50	+	+	Positive	----	Positive trend
38822	4.70	4.60	4.40	-	-	Negative	- 0.15	Low degradation
54050	5.50	4.50	2.00	-	-		- 1.75	Moderate degradation
53937	5.00	3.00	1.20	-	-		- 1.90	High degradation

3.3. Results

3.3.1. LAI trends

To achieve the objective of detecting forest degradation in Mexican forested areas, the STR procedure was used to decompose 295,298 monthly LAI pixel-based time series comprised of 192 values into trend, seasonal, and remainder components. Only the trend component was extracted from each of the time series to evaluate the

presence and strength of significant monotonic trends through a modified Mann-Kendall test proposed by Hammed and Rao (1998). Additionally, a Theil-Sen's slope was calculated to estimate the magnitude of change of the significant trends.

The trend analysis results in 63% of the time series (187,414 pixels) exhibiting trends at a significance level of 0.05 or higher. Fifty two percent are positive trends (i.e., they show a positive Kendall's τ correlation coefficient), while only 11% are negative (Figure 3.3). Particularly, evergreen broadleaf forest presents the highest proportion of negative trends (18%), followed by evergreen needleleaf (12%), and deciduous broadleaf (7%). Significant trends do not cluster in a specific area, their distribution is regular across all the study area (Figure 3.4.a). The majority of negative trends are located over the eastern portion of the study area (Figure 3.4.b). The overall magnitude of change, measured by the Theil-Sen's slope, ranges from -0.026 to 0.021 LAI/month and presents

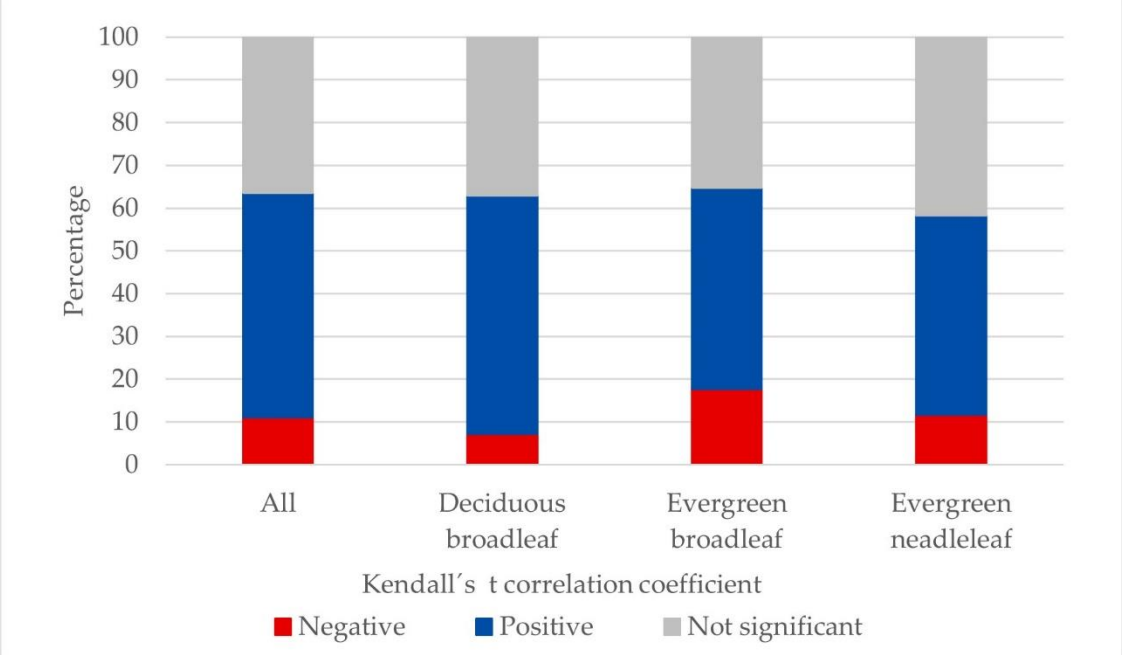

Figure 3.3. Direction of trends at 95% confidence level per forest type, 2002-2017

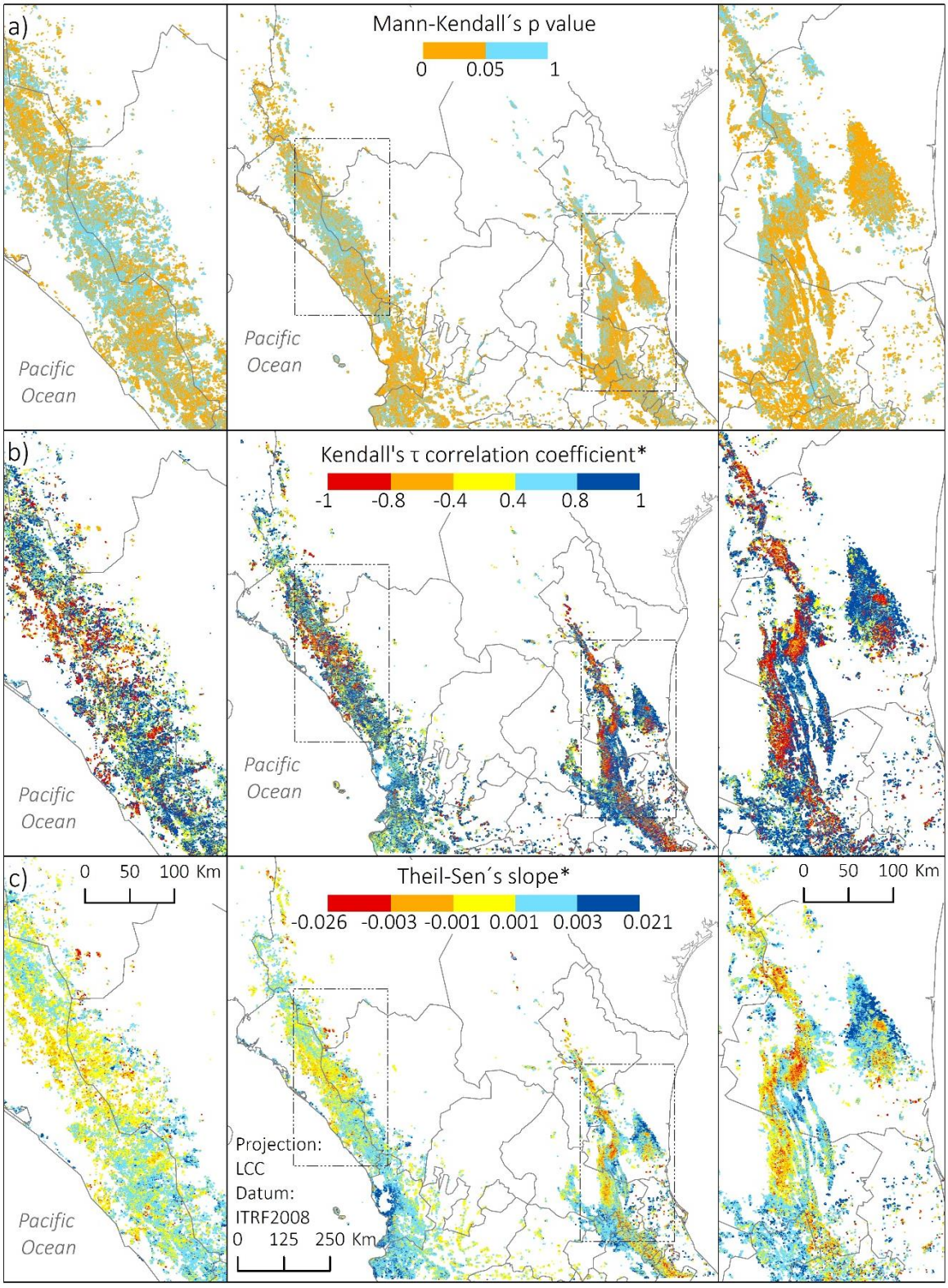

Figure 3.4. Significance of all trends (a), as well as strength (b) and magnitude (c) of trends at 95% confidence level or higher, 2002-2017

a median of 0.001 LAI/month. The steepest negative slopes are predominantly located in the state of *Tamaulipas* (eastern region), which, together with the state of *Nayarit* (western region), is also scenario of the steepest positive slopes. Lower magnitudes are located along the highest elevations of the *Sierra Madre Oriental* (east mountain range), as well as over the western states of *Sinaloa* and *Durango* (Figure 3.4.c).

Figures 3.3 and 3.4 provide context of the occurrence of negative trends (potential indicators of forest degradation), which extend over 7,036 km^2 and represent 11.1% of the study area. Two thirds of the negative trends present a strength of -1, which means that most of them display consistently-decreasing trajectories; these trends are evenly distributed across the 7,036 km^2 (Figure 3.5.a). The maximum negative magnitude is -0.0256 LAI/month and the median -0.0012 LAI/month, which are equivalent to an absolute change of -4.92 and -0.23 LAI units, respectively, between 2002 and 2017. Magnitudes are generally high in the east portion and generally low in the west (Figure 3.5.b).

Forest degradation is presented as the dimensionless product of the strength and magnitude of negative trends (Figure 3.6). In this study area, the product ranges from 0 to 0.02 and was reclassified into three categories of severity (i.e., high, moderate, and low) based on a geometrical interval classification method. This classification method indicates that 385 km^2 (0.6% of the study area) are highly degraded, while 3,406 km^2 (5.4%) and 3,245 km^2 (5.1%) are moderately and slightly degraded, respectively. Forest degradation is mostly low in the west and generally higher in the eastern region of Mexico, which is characterized by consistently-decreasing trends with high magnitudes of change. Although the western portion also displays consistently-decreasing trends

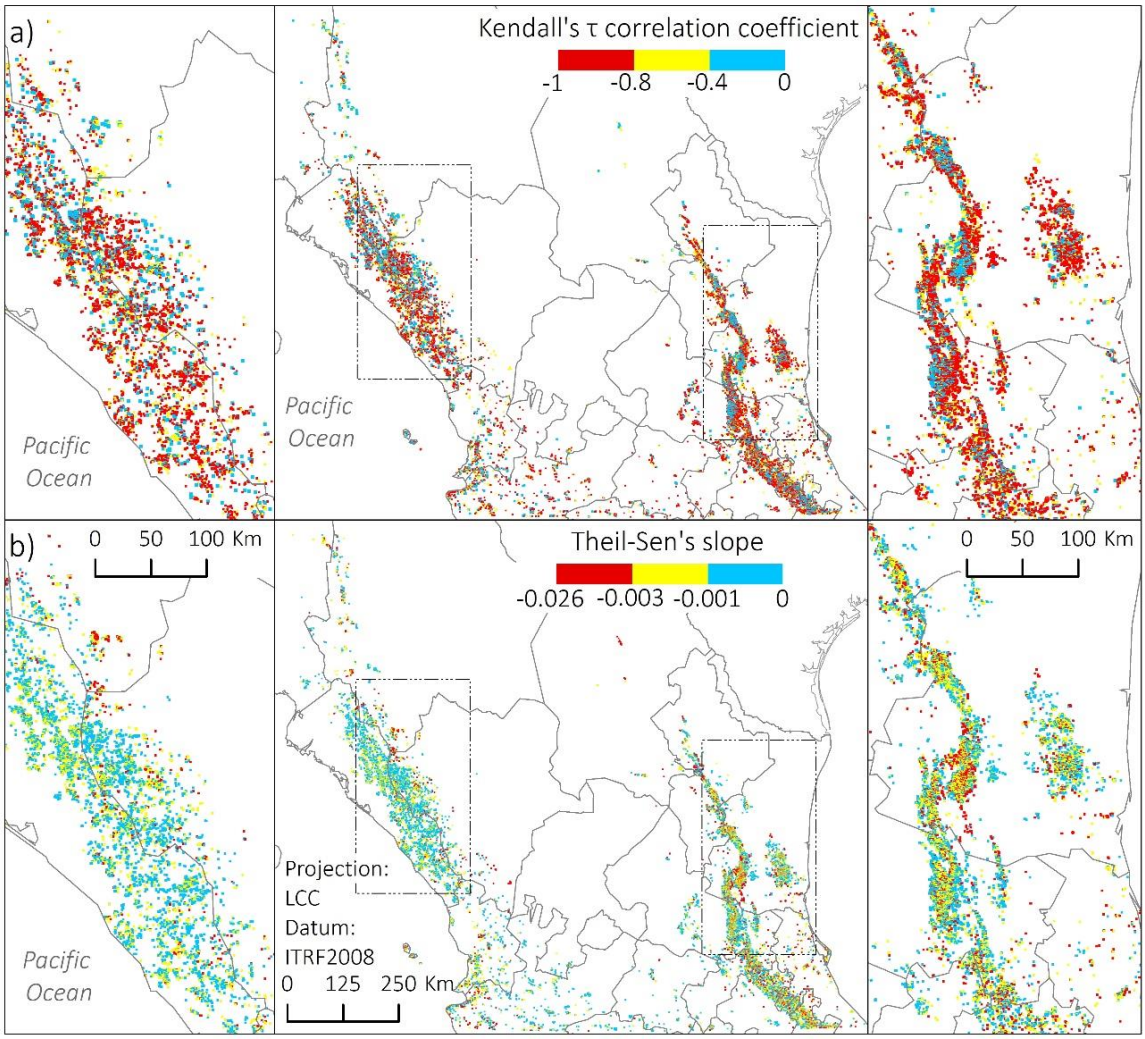

Figure 3.5. Strength (a) and magnitude (b) of negative trends at 95% confidence level, 2002-2017 -The pixels size has been exaggerated for visualization proposes-

(Figure 3.5.a), the magnitudes of change are generally not high (Figure 3.5.b). The most degraded areas are irregularly distributed along the *Sierra Madre Oriental* and, to a lesser extent, over southwest *Chihuahua*, the western fringe of *Durango* and *Jalisco*, and some isolated areas of *Nayarit*.

Regarding forest types, evergreen broadleaf has the highest median severity score of forest degradation (0.0011), followed by evergreen needleleaf (0.0008), and deciduous broadleaf (0.0006). In general, evergreen broadleaf forest is characterized by a

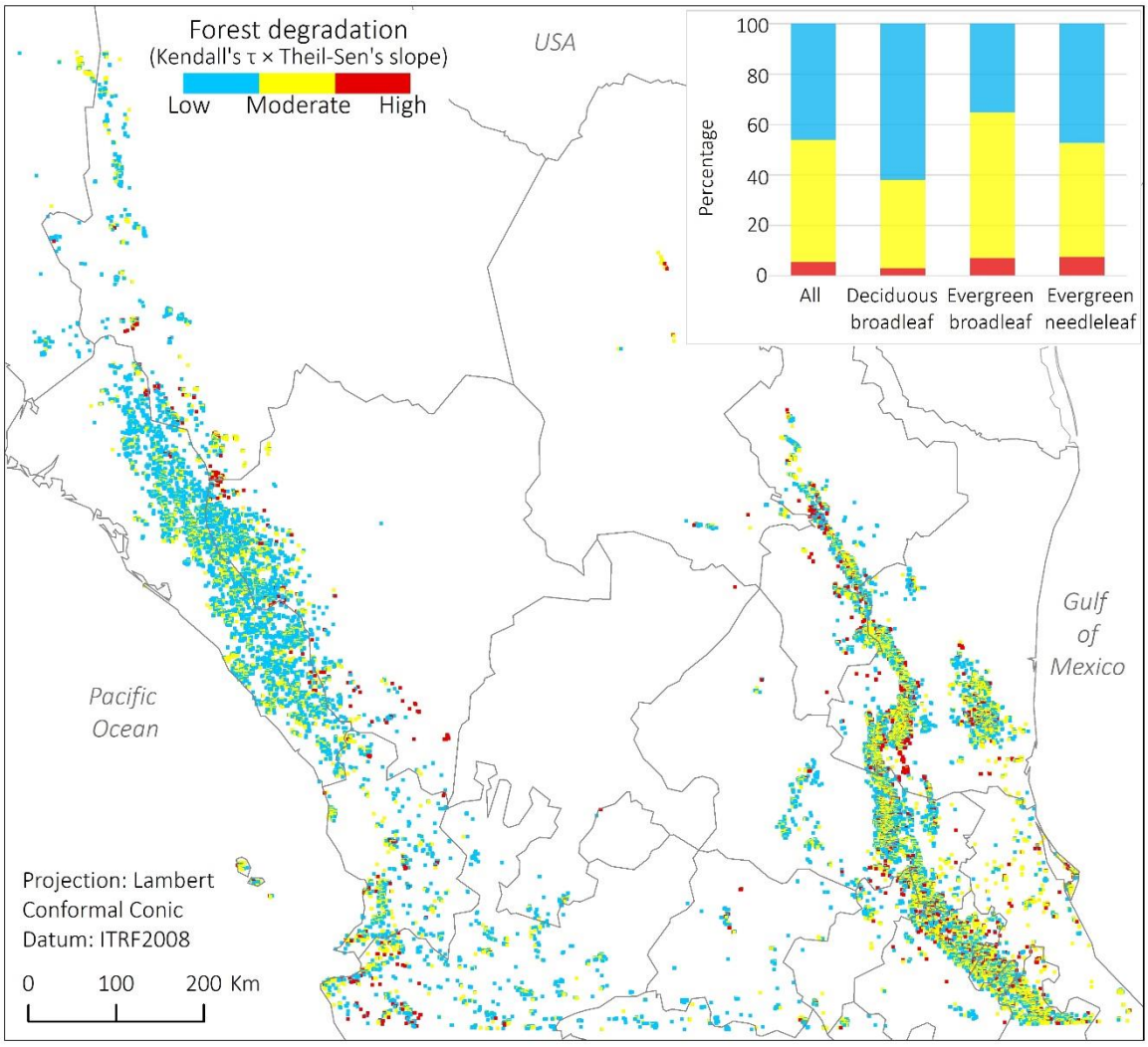

Figure 3.6. Forest degradation based on the strength and magnitude of negative trends at 95% confidence level, 2002-2017 -The pixels size has been exaggerated for visualization proposes-

combination of consistently-decreasing trends with high magnitudes of change, evergreen needleleaf by a combination of irregularly decreasing trends with high magnitudes of change, and deciduous broadleaf by a combination of consistently-decreasing trends with low magnitudes of change.

Evergreen needleleaf shows the highest proportion of highly degraded areas (8%), followed by evergreen broadleaf (7%), and deciduous broadleaf (3%; Figure 3.6). Deciduous broadleaf (Figure 3.7.a) is almost free of highly degraded areas in the west

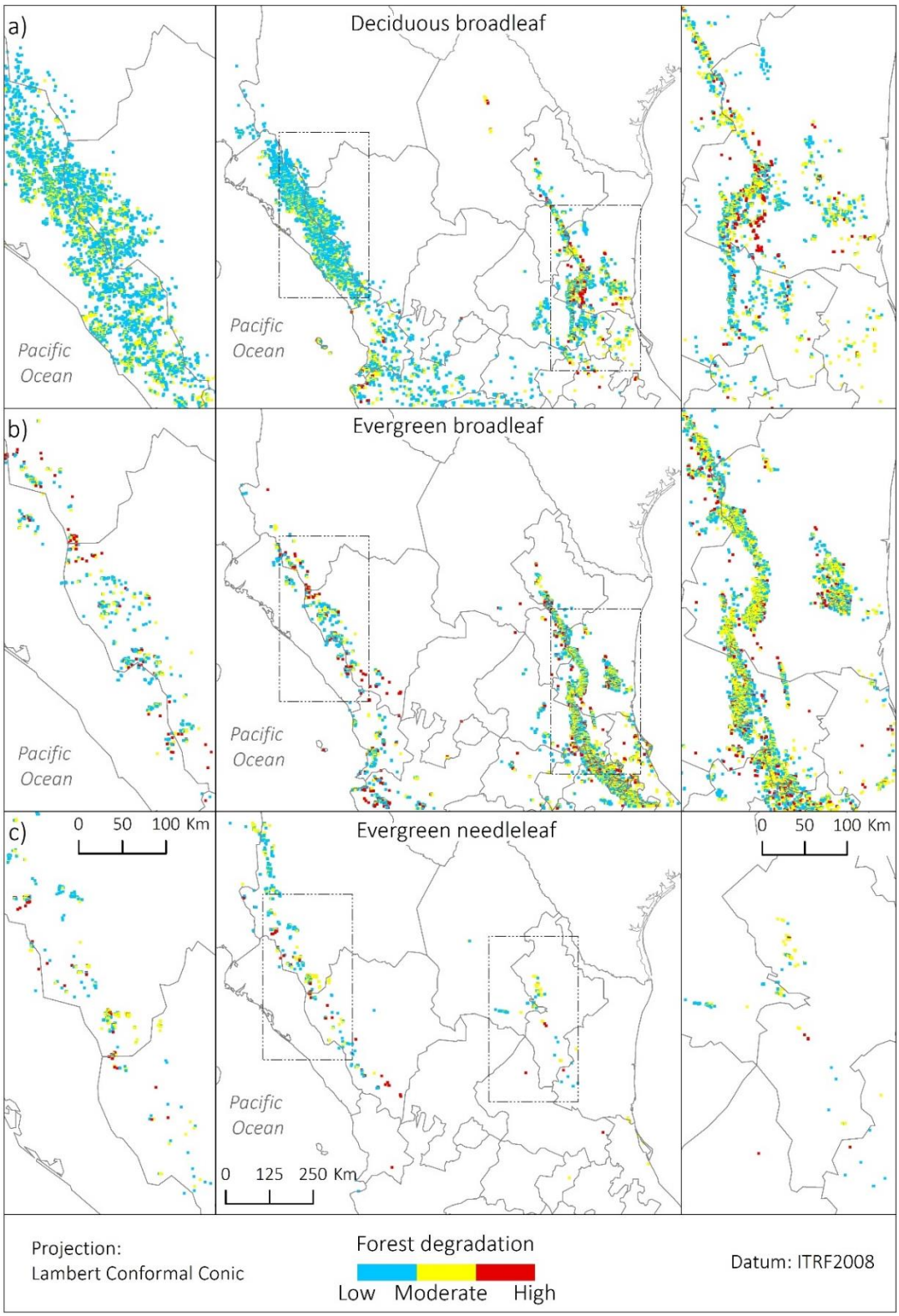

Figure 3.7. Degradation of deciduous broadleaf forest (a), evergreen broadleaf forest (b), and evergreen needleleaf forest (c) based on the strength and magnitude of negative trends at 95% confidence level, 2002-2017 -The pixel size has been exaggerated for visualization proposes-

part of the study area, but it presents a concentration of highly degraded pixels in the west portion, specifically over the state of *Tamaulipas*. Evergreen broadleaf (Figure 3.7.b) exhibits highly degraded pixels distributed throughout its range as well as a high proportion of moderately degraded pixels. Unlike the other forest types, evergreen needleleaf (Figure 3.7.c) displays more degraded areas in the east portion of the study area.

3.3.2. Validation

The comparison between the trend analysis of the MODIS LAI data and the reference data shows an overall agreement of 63%. This agreement between the remotely sensed products and the field observations is slightly better in the west side (69%) than in the east side (56%) of the study area (Figure 3.8). According to the confusion matrix (Table 3.3), the "high degradation" and "no trend" classes have the highest accuracy. All of the MODIS pixels classified as "high degradation" are actually highly degraded, while 81% of the MODIS pixels classified as "no trend" do not actually exhibit a significant trend. On the other hand, half of the reference data identified as highly degraded were correctly classified as "high degradation", whereas 72% of the reference data without any trend were correctly classified as "no trend".

In contrast, the "moderate degradation" class exhibits the poorest accuracy. Forty five percent of the MODIS pixels classified as "moderate degradation" are actually moderately degraded and only 19% of the reference data identified as moderately degraded were correctly classified as "moderate degradation". These pixels were

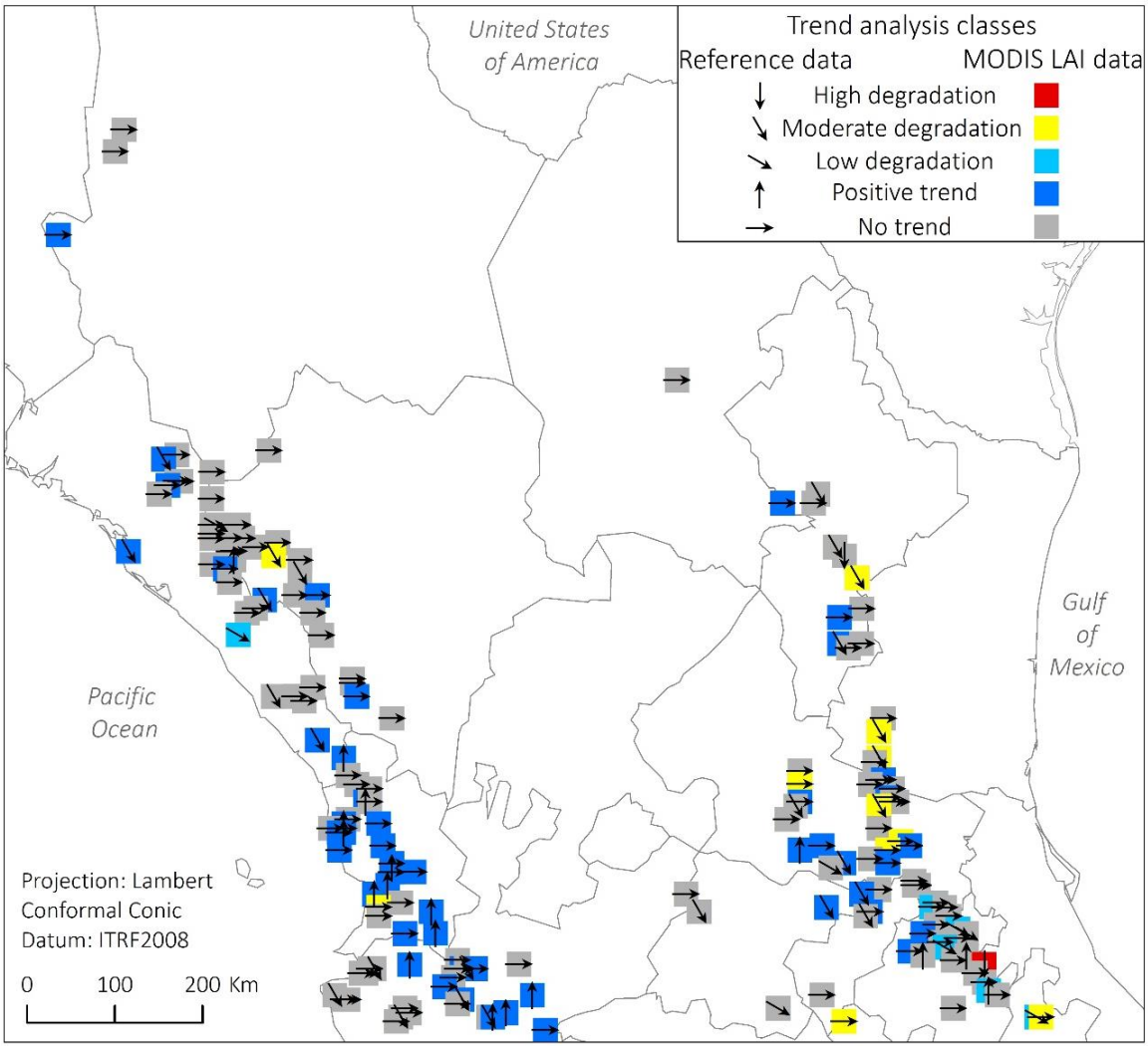

Figure 3.8. Spatial comparison between the trend analysis of MODIS LAI data and the reference data

Table 3.3. Confusion matrix of the trend analysis of the MODIS LAI data and the reference data

Trend analysis classes			Reference data						
			Degradation			Positive trend	No trend	Total	User's accuracy
			High	Moderate	Low				
MODIS LAI data	Degradation	High	1	0	0	0	0	1	1
		Moderate	0	5	0	0	6	11	0.45
		Low	0	0	4	1	1	6	0.67
	Positive trend		0	9	0	14	28	51	0.27
	No trend		1	12	4	3	88	108	0.81
	Total		2	26	8	18	123	177	
	Producer's accuracy		0.50	0.19	0.50	0.78	0.72		**0.63**

erroneously classified as “no trend” and “positive trend”. Finally, the class with the highest contrast between accuracy types is “positive trend”. Although 78% of the reference positive trends were correctly classified as “positive trend”, only 27% of the MODIS pixels classified as “positive trend” exhibited positive trends.

Although the “high degradation” MODIS sample is comprised of only one pixel, that pixel is representative of the actual size of the highly degraded class. Indeed, the MODIS sampling sizes of all classes are representative of the actual class sizes. This is because the distribution of the 177 conglomerates used to perform the validation mimic the spatial distribution of the original systematically collected NFSI data.

3.4. Discussion

3.4.1. Potential drivers of forest degradation

The objective of this research was to detect forest degradation through a trend analysis of monthly MODIS LAI collected over Central Mexico from 2002 to 2017. The overall results indicate that about half of the study area (52%, Figure 3.3) has exhibited positive trends of forest change, while the other half has either remained unchanged (37%) or experienced negative trends (11%). Of the 7,036 km^2 exhibiting negative trends, the proposed measure of forest degradation estimates that 385 km^2 are highly degraded, 3,406 km^2 moderately degraded, and 3,245 km^2 slightly degraded. Most of the moderate and highly degraded areas are distributed over the east side of the study area (Figure 3.6) and evergreen broadleaf seems to be the most affected forest type (Figure 3.7).

The authors are not aware of other studies that examine vegetation trends at the regional scale in Mexico, which precludes a direct comparison of the results of this research. However, the set of INEGI's Land Use and Vegetation Maps provides points of comparison. For example, this research reveals that 7,036 km^2 (11%) of the study area have experienced forest degradation between 2002 and 2017. According to the most recent INEGI's cartography, 14,900 km^2 (23%) were covered by perturbed secondary vegetation in 2014. Of that area, 12,787 km^2 were already perturbed in 2002. As the level of disturbance of these areas is unknown for both dates, they could have experienced no changes, or slight negative or positive trends. In contrast, 1,686 km^2 were covered by undisturbed primary vegetation in 2002, which clearly translates into negative trends since in 2014 were classified as perturbed. The remaining 427 km^2 were agriculture or water (INEGI 2005, 2017). Thus, although this research and the INEGI's cartography are not directly comparable, both show that important processes of forest degradation are of the order of a few thousands of km^2.

In terms of spatial distribution, this research shows more severe levels of forest degradation in the eastern portion. The most common disturbance recorded by the Mexico´s NFSI on this side of the study area is presence of epiphytes, followed by drought and defoliating insects. On the western portion, the most frequent disturbance is fire, followed by logging and drought (CONAFOR 2019). Although not all forest degradation can be attributed to these disturbances, they provide an indication of the factors affecting forest health in Central Mexico. For instance, changes in microclimate or vegetation structure may affect the abundance and distribution of epiphytes (Hietz,

Buchberger, and Winkler 2006). This seems to be a major problem because, although epiphytes do not obtain nutrients from their host as parasitic plants do, they use the host as support, which suffocates the branches and eventually kills the trees (SEMARNAT 2007). Drought has also been recorded as an important driver of forest disturbance. Indeed, in 2009 and 2011, Central Mexico suffered the most severe droughts in seven decades (Domínguez 2016). The effects of these droughts continue to affect the region and, according to CONAFOR (2019), the impacts on forest vegetation have been most pronounced on the east side of the study area, where higher levels of forest degradation are encountered based on this research.

3.4.2. Methodological approach

Assessing forest degradation has been a challenging task due to the generally slow-changing nature of the process, which demands long periods of observation with high frequency of records. In this research, the analysis of the trend component of monthly LAI time series helped to overcome the challenge of identifying subtle and gradual changes. This component extracts low frequency changes that occur throughout the time series. Figure 3.9 demonstrates how the proposed algorithm successfully classifies the trend components based on their strength and magnitude of change.

Figure 3.9.a is a good example of a very subtle consistently-decreasing change that may pass unnoticed if only the original time series is analyzed. This was confirmed by a Seasonal Kendall test (Helsel and Frans 2006), which did not detect a significant trend in the raw time series. Figure 3.9.b shows a pixel that, although it is classified as highly

degraded, does not exhibit one of the highest scores because its trajectory is not typical of a forest degradation process (e.g., caused by a disease). Along this line, highly degraded pixels with weak Kendall's τ correlation coefficients and steep slopes can be used to identify potential events of deforestation. Pixels with those characteristics are representative of a major non-consistently decreasing change in LAI, which may indicate an abrupt vegetation change provoked by a high-impact event, such as deforestation. Figure 3.9.c shows a clear example of forest degradation, where LAI changed substantially during the study period following a consistently-decreasing trajectory. The Seasonal Kendal test and the Theil-Sen´s slope test applied to the raw time series of

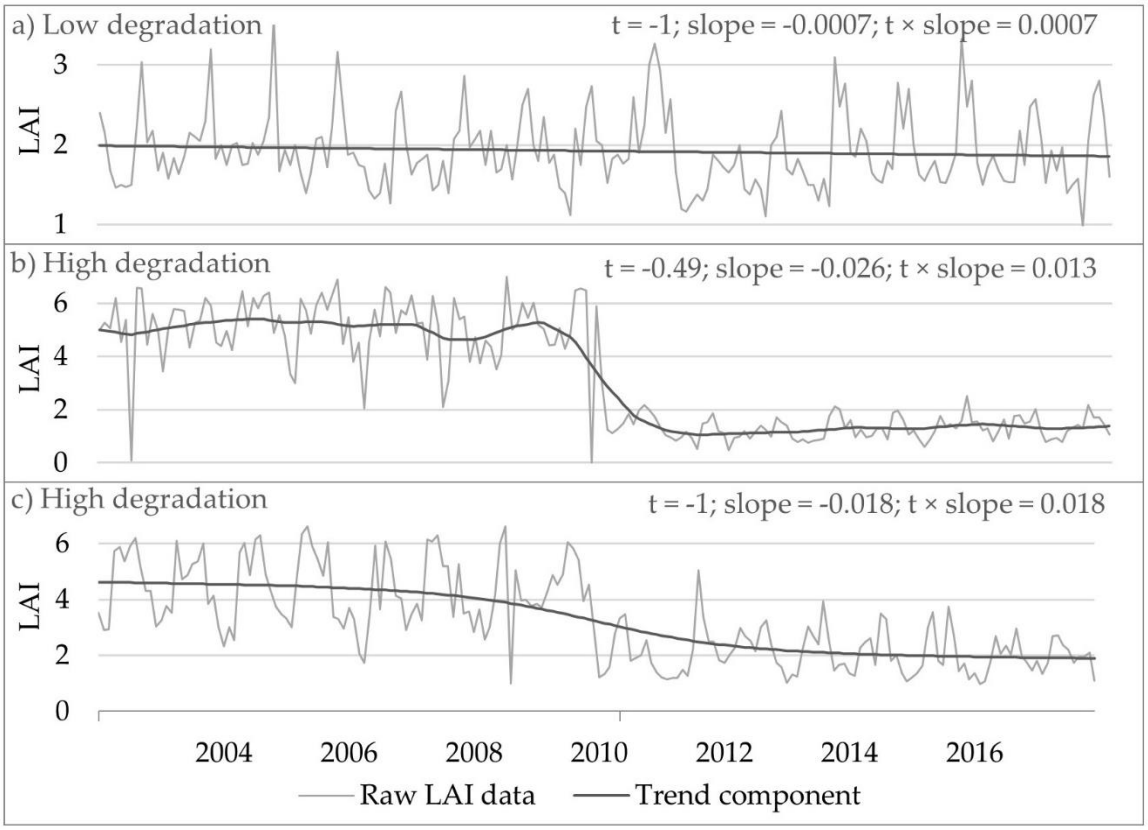

Figure 3.9. Examples of slightly degraded (a) and highly degraded (b and c) pixels based on the strength (t) and magnitude (slope) of the extracted trend component

examples 11b and 11c detected negative trends with a strength of -0.53 and -0.52 and a magnitude of -0.34 and -0.20, respectively. The product of these measures is higher for Figure 3.9.b (0.18) than for Figure 3.9.c (0.10), which would have assigned a higher score to a trajectory less representative of a typical process of forest degradation.

3.4.3. Potential sources of validation uncertainty

The difficulty of validating degradation models has been recognized and attributed to the considerable amount of economic and human resources needed to collect reference data during long periods of study (Metternicht et al. 2010). This research made use of reference data that were not collected for the specific purpose of validating this study. Therefore, although these data are considered the best possible information available, they present some limitations. In this context, there are at least four reasons that may be associated with the moderate agreement (i.e., 63%) between the remotely sensed LAI and the field observations of tree conditions.

First, the spatial extent of the reference data is not ideally compatible with the spatial resolution of the MODIS pixels. Each sampling conglomerate extends over 1,600 m^2, while each MODIS pixel covers 216,516 m^2. This means that the reference data are representative of less than 1% of the MODIS pixel with which they are compared. Second, the classification schemes of tree conditions are slightly different between forest inventories. The NFSI 2004-2009 and the NFIS 2009-2014 recognize four vigor conditions (i.e., very poor, poor, good, and maximum), while the NFSI 2014-2019 recognizes only three (i.e., low, moderate, and high). This incompatibility hindered an appropriate

comparison of the vigor conditions through time. Third, the number of field observation dates within the study period is limited for the purposes of a trend analysis. Fourth, the collection of tree conditions may be subjective since it depends on the criterion and expertise of the data collector.

The accuracy of future validation efforts may be improved by including all field observations regardless of the position within a pixel, by establishing a unique classification scheme of tree conditions, by considering a longer study period that allows for the incorporation of more field observation dates, and by testing other reference data such as crown density or proportion of live crown. The latter two variables were not considered in this work due the high proportion of missing records in the study area and period of interest. On the other hand, forest degradation studies may need an entirely different validation approach. Although an index that aimed to identify the general condition of the forest in each conglomerate was created (see section 3.2.4 for details), forest degradation studies may need field observations that evaluate forest as a whole in a given area rather than as single individuals (i.e., trees) or plots. Collecting data to properly validate forest degradation studies at a regional scale represents an area of opportunity for future research.

3.5. Conclusion

This research detected forest degradation over Central Mexico through a trend analysis of monthly MODIS LAI collected from 2002 to 2017. The results indicate that 52% of the study area has experienced positive trends of vegetation change, 37% has

remained unchanged, and 11% has suffered some level of forest degradation. The proposed algorithm estimated that 385 km^2 are highly degraded, 3,406 km^2 moderately degraded, and 3,245 km^2 slightly degraded. Most of the moderate and highly degraded areas are distributed over the east side of the study area and evergreen broadleaf appears to be the most affected forest type.

This research overcame the problem of detecting very slow and gradual changes associated with forest degradation by measuring the strength and magnitude of the trend component of pixel-based LAI time series. None of the algorithms cited in this document have made use of LAI as vegetation greenness indicator, nor have performed this type of trend analysis to detect forest degradation. The main limitation of this study is the moderate accuracy of the validation effort (i.e., 63%). Some suggestions to improve this accuracy are expressed in section 3.4.3, but also a different approach to validate this type of studies is suggested as an area of opportunity for future research.

This study is expected to be a contribution to the regional efforts to measuring and monitoring forest degradation in Mexico. It could serve as one of the first steps towards the mitigation of the serious impacts that forest degradation has on the environmental services that these ecosystems provide. Thus, this work suggests that this methodology can be applied at the national level and be used as a first look into hot spots of forest degradation.

4. RESPONSE OF LEAF AREA INDEX TO PRECIPITATION IN THE CONTEXT OF FOREST DEGRADATION CONDITIONS

4.1. Introduction

When forest ecosystems are disturbed, the carbon they store is released as carbon dioxide (CO_2) into the atmosphere, where it contributes to global warming by absorbing heat and impeding energy transmission to space. There is evidence that the frequency and intensity of some of the hydrometeorological events (e.g., drought, heavy storms or snowfall, heat waves, frost, hurricanes, fires) that disturb forest ecosystems and frequently lead to degradation processes have increased as climate change becomes more evident (IPCC 2014). As a consequence, there has been growing interest in understanding the effects of climate variability on a variety of vegetated ecosystems aspects, such as carbon storage (Tian et al. 1998; Chen et al. 1999; Bachelet et al. 2001; Falloon et al. 2007; Frank et al. 2015), vegetation greenness (Brendel, Bohn, and Piccolo 2017; Na-U-Dom, Mo, and García 2017), plant growth (Myneni et al. 1997), growing season length (Menzel and Fabian 1999), and net primary production (Nemani et al. 2003). These aspects may respond differently to variations in climate elements, such as temperature or precipitation, depending on the ecosystem conditions.

According to Scheffer et al. (2009), ecosystems close to critical transitions are more sensitive to disturbances. Seddon et al. (2016) assessed the relative sensitivity of global terrestrial ecosystems to climate variability through a vegetation sensitivity index (VSI) based on an autoregressive model, whose input data are vegetation greenness

(Enhanced Vegetation Index) and climatic driving variables (air temperature, water availability and cloud cover). Their study estimated high VSI values for several regions with critical ecological thresholds (e.g., boreal and wet tropical forests), as well as for areas without critical thresholds (e.g., steppe and prairies). To continue to understand the effect of climate variability on vegetation associated with different contexts of environmental disturbances, this chapter takes into consideration the forest degradation conditions of Central Mexico, which were estimated in Chapter 3 based on a trend analysis of Moderate Resolution Imaging Spectroradiometer (MODIS)-Leaf Area Index (LAI).

Therefore, the objective of this chapter is to evaluate the response of LAI to precipitation in Central Mexico in the context of forest degradation conditions. The study uses monthly anomalies of MODIS LAI and monthly anomalies of Climate Hazards Group InfraRed Precipitation with Station (CHIRPS) data calculated for the period 2002-2017. The presence/absence of any LAI response is determined through the Granger causality notion, which enables the examination of lagged effects of precipitation over LAI based on past values of both variables (Granger 1969). The sign and strength of the LAI response (if any) is estimated by means of an Impulse-Response (IR) function, which allows for the modelling of the temporal response of LAI to changes in precipitation according to the Wold Moving Average representation of a vector autoregressive process (Lütkepohl, 2005). The outputs from these methods are grouped and analyzed by forest degradation condition, which results in a novel approach to investigate the effect of precipitation on vegetation greenness and structure.

4.2. Data and methods

4.2.1. Study area

The study area extends over 63,964 km^2 and comprises all 500-m pixels of the MODIS tile h08v06 that were covered by forest during at least one year between 2002 and 2017. The MODIS Land Cover product (MCD12Q1, type 3) estimates that 60% of these pixels corresponds to deciduous broadleaf forest, 36% to evergreen broadleaf, and 4% to evergreen needleleaf. According to the trend analysis of LAI performed in Chapter 3, 52% of the study area has experienced positive trends of vegetation change (i.e., increased biomass accumulation), 37% has remained almost unaltered, and 11% has suffered negative trends. These findings can be also grouped as non-degraded (89%) and degraded (11%) forest (Figure 4.1). Of the 7,036 km^2 covered by degraded forest, the proposed measure of forest degradation (see sections 3.2.3 and 3.3.1) estimates that 385 km^2 are highly degraded, 3,406 km^2 moderately degraded, and 3,245 km^2 slightly degraded. Most of the moderate and highly degraded areas are distributed over the eastern section of the study area and evergreen broadleaf is the most affected forest type.

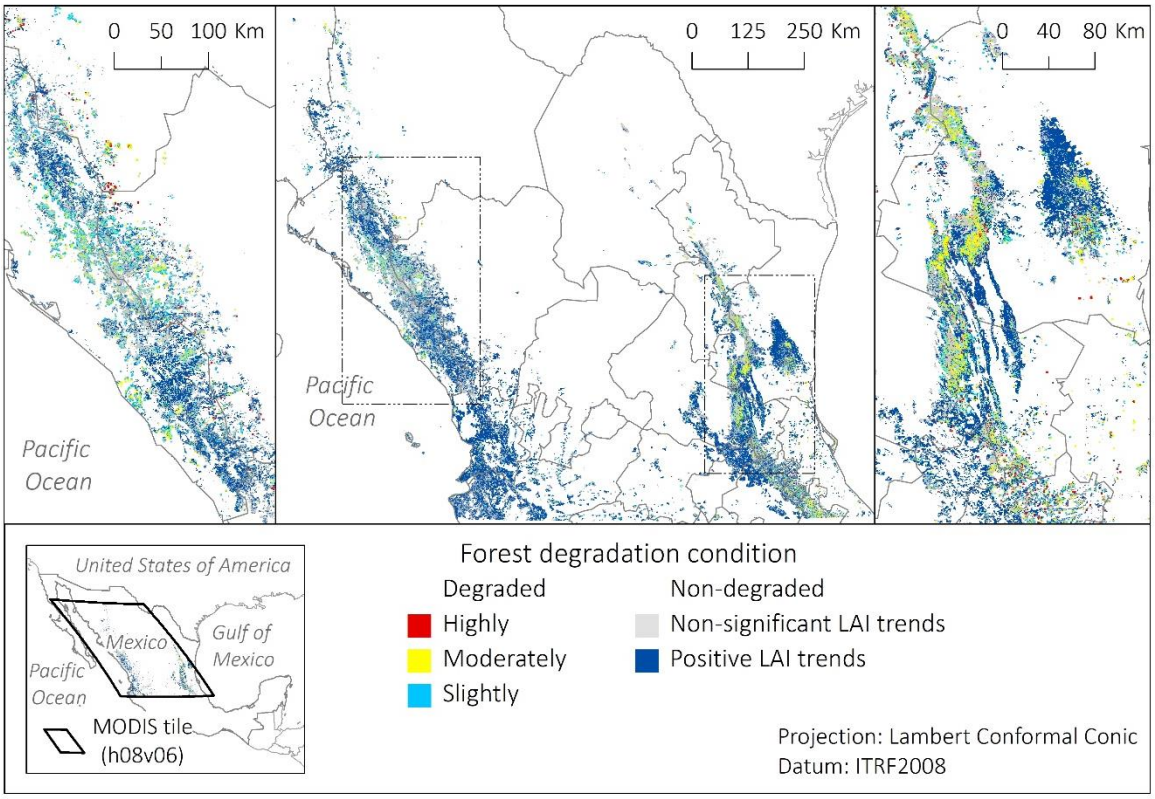

Figure 4.1. Study area: forest conditions based on a trend analysis of MODIS LAI, 2002-2017

4.2.2. Data and preprocessing

4.2.2.1. LAI

MODIS Terra 8-day LAI composites (MOD15A2H, Collection 6) of the MODIS tile h08v06 were acquired from 2002 to 2017 at 500-km spatial resolution. These data were downloaded though the Land Processes Distributed Active Archive Center (LP DAAC) managed by the NASA Earth Science Data and Information System (ESDIS) project. LAI retrievals estimated from the back-up algorithm, which is based on the biome-specific empirical relationship between Normalized Difference Vegetation Index (NDVI) and LAI, were discarded. Therefore, only LAI retrievals from the main algorithm were considered from the analysis. The main algorithm consists of a radiative transfer model (Knyazikhin

et al. 1998) accounts for vegetation structure by comparing the measured values from the red and near-infrared spectral regions with previously observed spectral values of six biome types and their corresponding LAI values, which are stored in a look-up table (Knyazikhin et al. 1998; Myneni et al. 2002; Yang et al. 2006; Jensen et al. 2011; Yan et al. 2016).

All LAI datasets were projected to Lambert Conformal Conic projection in ITRF2008 datum and clipped to the study area. The Land Data Operational Product Evaluation (LDOPE) tool was used to unpack the LAI Quality Control layers, which helped to discriminate retrievals from the back-up algorithm. On a pixel-by-pixel basis, monthly anomalies were calculated for each month as the following example: anomaly of January 2002 = mean of January 2002 - average of all January means of the 2002-2017 period (often called climatology). All anomalies were extracted from the raster files and stored in a comma-separated values (cvs) file, where each row contains 192 monthly anomalies of LAI, which compose the time series of a single pixel.

4.2.2.2. Precipitation

Monthly precipitation anomalies from January 2002 to December 2017 were acquired at 0.05^{o} (5.42 km) spatial resolution from the Climate Hazards Group InfraRed Precipitation with Station (CHIRPS) dataset, which was developed by the United States Geological Survey (USGS) and the Climate Hazards Center (CHC). The CHIRPS dataset combines precipitation climatologies (composed of station normals, a variety of satellite means, elevation, latitude, and longitude), thermal infrared (TIR) satellite observations

produced by the NOAA´s National Climatic Data Center (1981–2008) and the Climate Prediction Center (2000-present), Tropical Rainfall Measuring Mission (TRMM) data, atmospheric model rainfall fields from the NOAA Climate Forecast System (CFSv2), and *in situ* precipitation observations. The CHIRPS estimation process is based on steps of 5-day (pentad) rainfall accumulations. Initially, the algorithm calculates the percentage of time in which TIR observations indicate cold cloud tops (<235 ^{o}K) during a pentad. This percentage is converted into millimeters based on a local regression with TRMM data. The resulting TIR precipitation pentads are divided by their long term means to identify variations from average conditions. Then, these variations, called percent of normal TIR precipitation pentads, are multiplied by the corresponding precipitation climatology pentad to generate unbiased gridded estimates reported as millimeters per pentad. Finally, the unbiased estimates are blended with stations to produce the CHIRPS product (Funk et al. 2014; Funk et al. 2015).

Once the downloaded CHIRPS data were projected to Lambert Conformal Conic projection in ITRF2008 datum and clipped to the study area, all precipitation anomalies were extracted from the raster files and rearranged into a cvs file. Similar to the LAI file, each row contains 192 monthly anomalies of precipitation, which constitute the time series of a single pixel.

4.2.3. Estimation of the LAI response to precipitation

This section describes the methodology to evaluate the presence, sign, and strength of any causal relationship from time series of monthly precipitation anomalies to

time series of monthly LAI anomalies. This relationship is assessed by associating each 500 m-based LAI time series with the corresponding 5.4 km-based precipitation time series. Thus, 207,775 multivariate time series entirely constituted by good quality estimates of LAI and precipitation were analysed (table 4.1.a) in an R environment (R Core Team 2018). The presence of any response was evaluated through the Granger causality test, which has been successfully used for similar purposes (e.g., Kaufmann et al. 2003; Wang et al. 2006, 2007; Jiang, Liang, and Yuan 2015; Papagiannopoulou et al. 2017). The sign and strength of the response (if any) was estimated by means of an IR function, which, although not as frequently used for environmental studies as Granger causality, has also been implemented for similar objectives (e.g., Wang et al. 2007; Mariano et al. 2018).

4.2.3.1. Presence of any response

In this research, the Granger causality test aims to forecast LAI based on past information of LAI and precipitation. If the prediction of LAI is improved after including precipitation values as predictors, precipitation is considered to Granger-cause LAI. This causality should be interpreted as 'predictive causality' rather than 'true causality' (Jiang, Liang, and Yuan 2015; Papagiannopoulou et al. 2017). Prior to evaluating the presence of Granger causality, non-stationary time series (i.e., those whose statistical properties do not remain constant over time and, therefore, cannot be forecasted; Nason 2006) were discarded (Table 4.1.b) by means of a Kwiatkowski-Phillips-Schmidt-Shin (KPSS) test,

which examines the null hypothesis of stationarity around a linear trend (Kwiatkowski et al. 1992).

To derive the predictions required to examine Granger causality, Vector Autoregressive (VAR) models, extensions of univariate autoregression models used to analyze multivariate time series (Zivot and Wang 2006), were calculated on pixels containing stationary time series of both LAI and precipitation (Table 4.1.b). In this study, the implemented VAR model, in which each variable is a linear function of its own lagged values and the lagged values of the other variable, is defined as follows:

$$\boldsymbol{y_t} = \boldsymbol{A_1 y_{t-1}} + \ldots + \boldsymbol{A_p y_{t-p}} + u_t, \quad (1)$$

where $\boldsymbol{y_t}$ is a $2x1$ vector of LAI and precipitation monthly anomalies at time t, u_t assigns a white noise process of the same dimension, and $\boldsymbol{A_1, \ldots, A_p}$ are regression coefficient matrices with a dimension of 2×2. The *p* parameter is a 4-month lag, which determines how much of the previous information of both variables is included in the model to predict LAI (Wang et al. 2006; Pfaff 2008b). The lag length was selected by first testing the VAR models using the Akaike Information Criterion (AIC), which finds the lag with enough information content on the two variables without over-fitting (Zivot and Wang 2006). This preliminary analysis showed that the most common optimal lag length among all time series was four months. The existence of serial correlation in the VAR residuals indicates that some information (e.g., temperature, solar zenith angle, aerosol optical depth) is missing in the model to explain the behavior of the variables. Therefore, time series with serial correlation at 4-month lag were identified by means of the Portmanteau

test, which examines the null hypothesis of no serial correlation (Pfaff 2008b). Those pixels were discarded from the analysis (Table 4.1.c).

Table 4.1. Multivariate time series that meet the following required criteria: a) entirely constituted by good quality estimates, b) stationarity in both variables precipitation and LAI, and c) absence of serial autocorrelation at the lag length under analysis. These criteria are additive. Thus, a time series that meets the c) criterion also meets the a) and b) criteria

Criteria	Forest conditions (total of pixels)					
	Degraded			Non-degraded		All (295,298)
	Highly (1,792)	Moderately (15,869)	Slightly (15,114)	Non-significant LAI trend (107,884)	Positive LAI trend (154,639)	
a) Good quality	1,023	5,918	9,002	75,022	116,810	207,775
b) Stationarity	101	4,182	7,384	48,722	96,054	156,443
c) Absence of serial autocorrelation at 4-month lag	62	3,434	6,283	42,713	80,341	132,833

The presence of Granger causality from precipitation to LAI was finally tested at 95% confidence level by splitting the vector of LAI and precipitation monthly anomalies (y_t in equation 1) as follows:

$$\begin{bmatrix} \boldsymbol{y_{1t}} \\ \boldsymbol{y_{2t}} \end{bmatrix} = \sum_{i=1}^{p} \begin{bmatrix} \alpha'_{11,i} & \alpha'_{12,i} \\ \alpha'_{21,i} & \alpha'_{22,i} \end{bmatrix} \begin{bmatrix} y_{1,t-i} \\ y_{2,t-i} \end{bmatrix} + CD_t + \begin{bmatrix} u_{1t} \\ u_{2t} \end{bmatrix} \quad (2)$$

where $\boldsymbol{y_{1t}}$ and $\boldsymbol{y_{2t}}$ are the subvectors of precipitation and LAI, whose dimensions are $(K_1 \times 1)$ and $(K_2 \times 2)$ with $K = K_1 + K_2$, and α is the coefficient of the model. C is the coefficient matrix of potentially deterministic regressors and D_t is the column vector holding the appropriate deterministic regressors. This Granger causality test is an F-type test and is distributed as $F(pK_1K_2, KT - n)$, where n is the number of parameters in equation 2 and T is the total number of observations. The null hypothesis, stated as

precipitation ($\boldsymbol{y_{1t}}$) does not Granger-cause LAI ($\boldsymbol{y_{2t}}$), is accepted when $\alpha_{21,i} = 0$ for $i = 1,2,\ldots,p$ and rejected when $\exists\ \alpha_{21,i} \neq 0$ for $i = 1,2,\ldots,p$ (Pfaff 2008a, 2008b).

4.2.3.2. Sign and strength of the response

The sign and strength of the LAI response to precipitation was estimated by applying an IR function to all time series where Granger causality was confirmed. The IR function implemented in this study measures the over-time response of LAI to an impulse of precipitation based on the Wold Moving Average representation of a VAR(p) process (Lütkepohl, 2005), which is expressed as follows:

$$y_t = \phi_0 u_t + \phi_1 u_{t-1} + \phi_2\, u_{t-2} + \ldots, \qquad (3a)$$

$\phi_0 = I_k$ and ϕ_s ($s = 1,\ldots,12$) can be computed recursively based on the following equation:

$$\phi_s = \sum_{j=1}^{s} \phi_{s-j} A_j, \qquad (3b)$$

where $A_j = 0$ for $j > p$. The $(i,j)th$ coefficients of the matrices ϕ_s are interpreted as the expected response of variable $y_{i,t+s}$ to a change in variable y_{jt} . Thus, the accumulation of these effects over time (s = $1,\ldots,12$) simulates the impact on variable i (LAI) after a change in variable j (precipitation) at time s (Pfaff 2008b).

4.3. Results

The presence of any response of LAI to precipitation was found in 42% of the 132, 833 multivariate time series in which Granger causality was evaluated (Figure 4.2). Overall, the occurrence of causality is higher in non-degraded pixels (43% on average)

than in degraded pixels, for which only 28% of the pixels showed causality. The lowest presence of causality occurs in highly degraded pixels (23%), while the highest presence of causality occurs in pixels with non-significant LAI trends (44%).

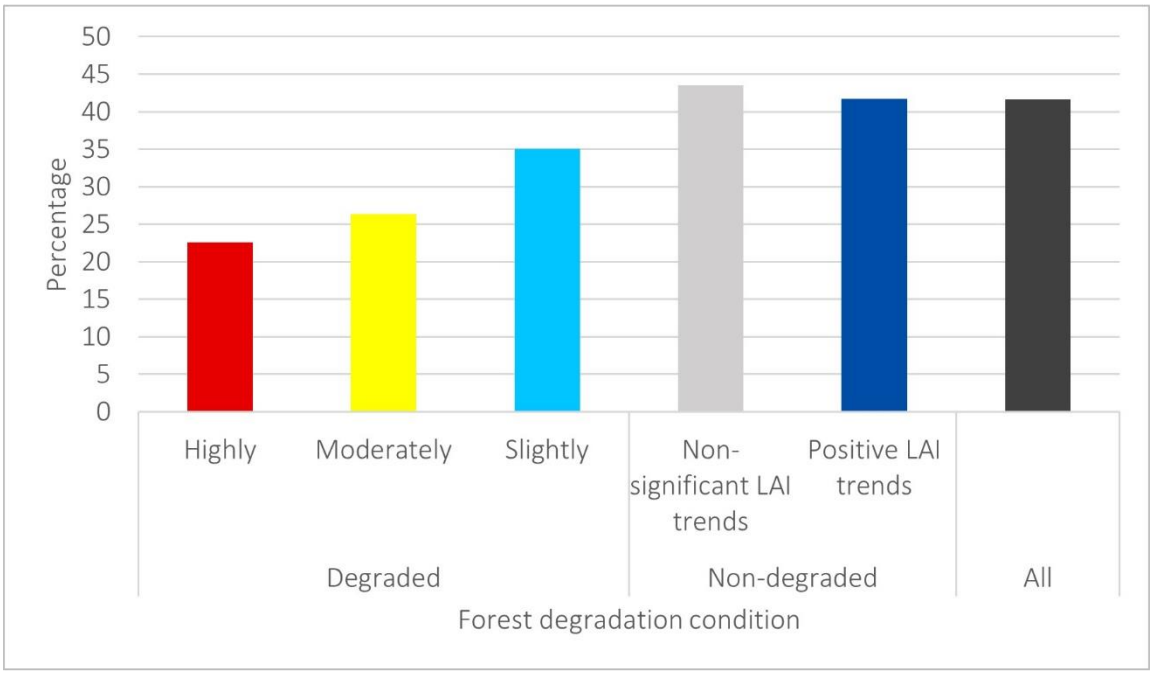

Figure 4.2. Presence of Granger causality from precipitation to LAI at 4-month lag per forest degradation condition

According to the median of the IR coefficients calculated, the LAI response to precipitation is predominantly positive (i.e., LAI increases if precipitation increases and decreases if precipitation decreases). It generally reaches its maximum strength three months after the precipitation impulse and then tends to gradually disappear (Figure 4.3). This means that a precipitation decrease produces a LAI decrease, which is most noticeable three months after the change in precipitation. Similarly, an increase in precipitation results in an increase in LAI. Highly degraded forest tends to deviate from the aforementioned behavior by initially exhibiting a negative response (i.e., LAI increases if precipitation decreases and decreases if precipitation increases), which becomes

positive in the third month and gradually decreases after the fourth month. Additionally, highly degraded forest, together with forests with non-significant LAI trends, show the weakest LAI responses.

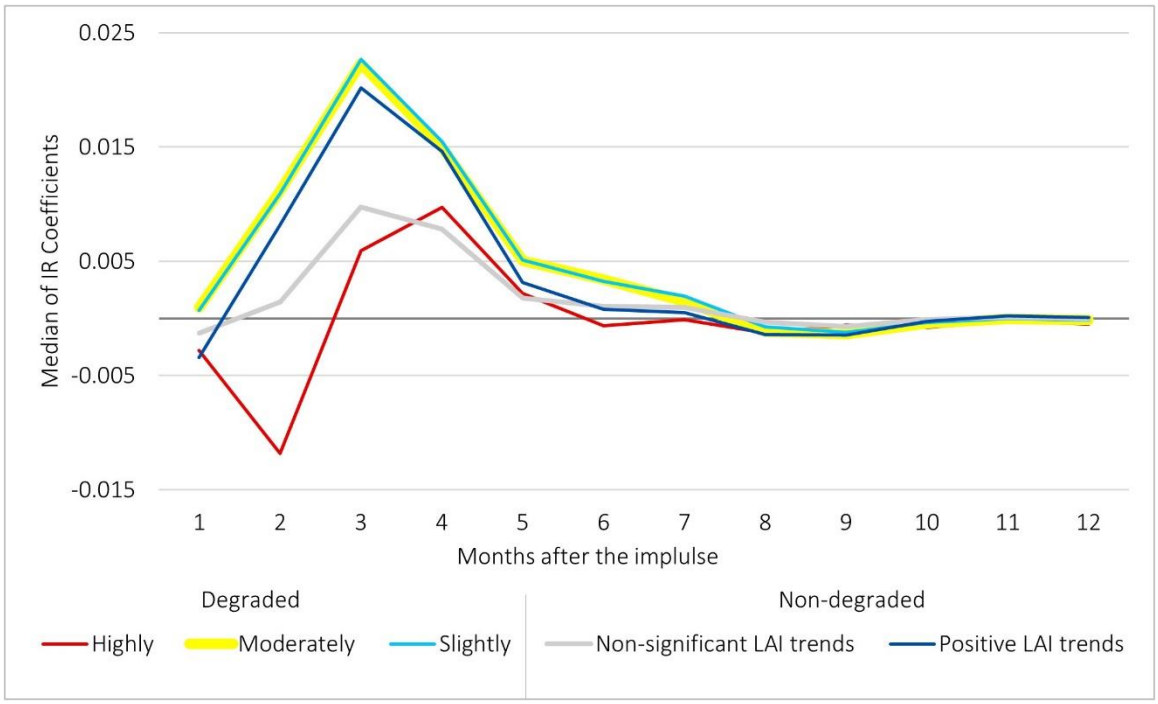

Figure 4.3. Median of IR Coefficients of pixels that show Granger causality from precipitation to LAI (at 4-month lag) per forest degradation condition

Figure 4.4 shows the spatial distribution of the IR coefficients estimated for the second month and the third month after a given impulse of precipitation. The presence of causality occurs in a higher proportion in the analyzed pixels that are located in the western side of the study area. The eastern side is characterized by a lower presence of causality and generally stronger IR coefficients. Negative responses are more common two months after the change in precipitation, especially in the eastern portion of the study area, while stronger positive responses dominate three months after the impulse.

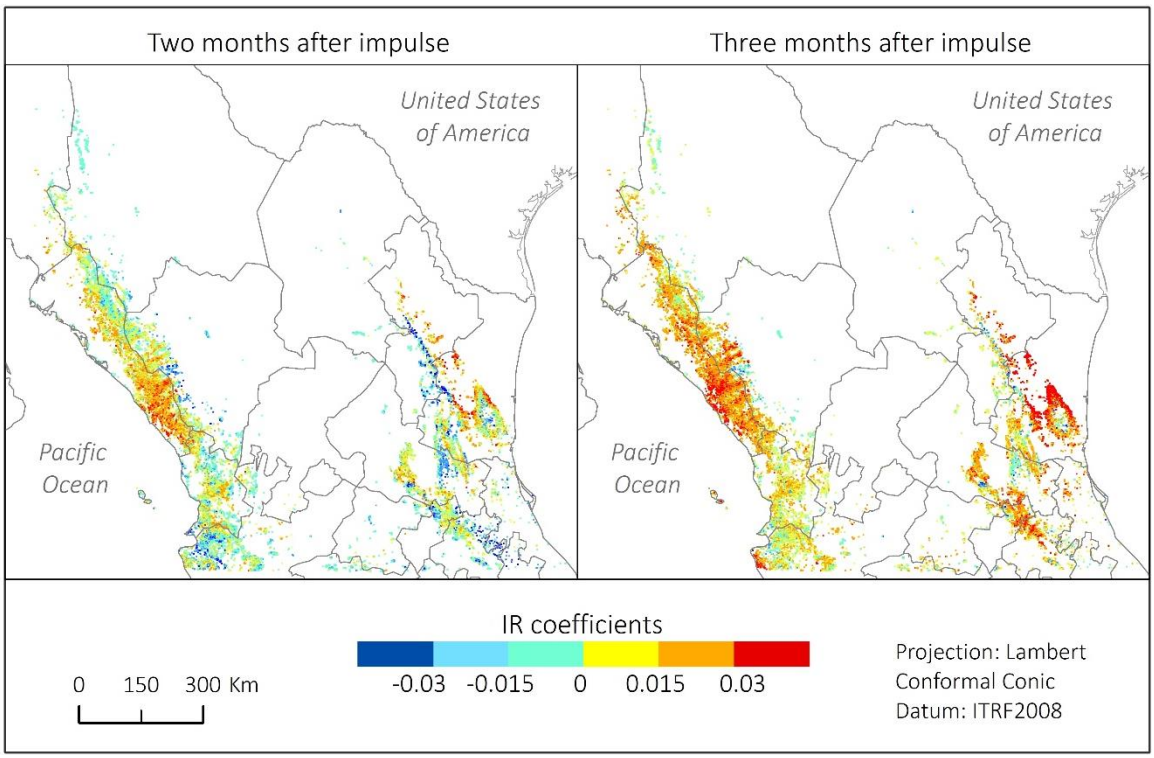

Figure 4.4. IR coefficients of pixels that show Granger causality from precipitation to LAI at 4-month lag

4.4. Discussion

4.4.1. Response of LAI to precipitation

The occurrence of a generally positive response of LAI to precipitation was found in about 42% of the analyzed pixels. This positive response means that greater precipitation produces increased vegetation greenness by enhancing water availability, higher stomatal conductance and, therefore, higher photosynthetic rates (Gimenez, Gallardo, and Thompson 2005). This is in agreement with the global scale study conducted by Liu et al. (2006), who detected a highly significant positive effect of precipitation on Fraction of Photosynthetically Active Radiation (FPAR) at 1-month lag over Central Mexico between 1982 and 2000.

According to the results obtained in Chapter 2 (section 2.3.1), the presence of Granger causality from temperature to LAI (around 80%) is higher than from precipitation to LAI. This lower occurrence of precipitation to LAI causality does not necessarily suggest that precipitation is not an important driver of vegetation dynamics. It may only indicate that changes in precipitation are not significant between 2002 and 2017 as confirmed by a trend analysis performed on time series of monthly precipitation acquired from the CHIRPS dataset (Figure 4.5). Zhou et al. (2003) found a similar pattern in northern forests of North America and Eurasia (i.e., evergreen needleleaf, deciduous needleleaf, deciduous broadleaf, mixed, and woodlands) between 1982 and 1999. These authors reported that temperature imposed the greatest effect on NDVI during this period, while precipitation showed a smaller effect.

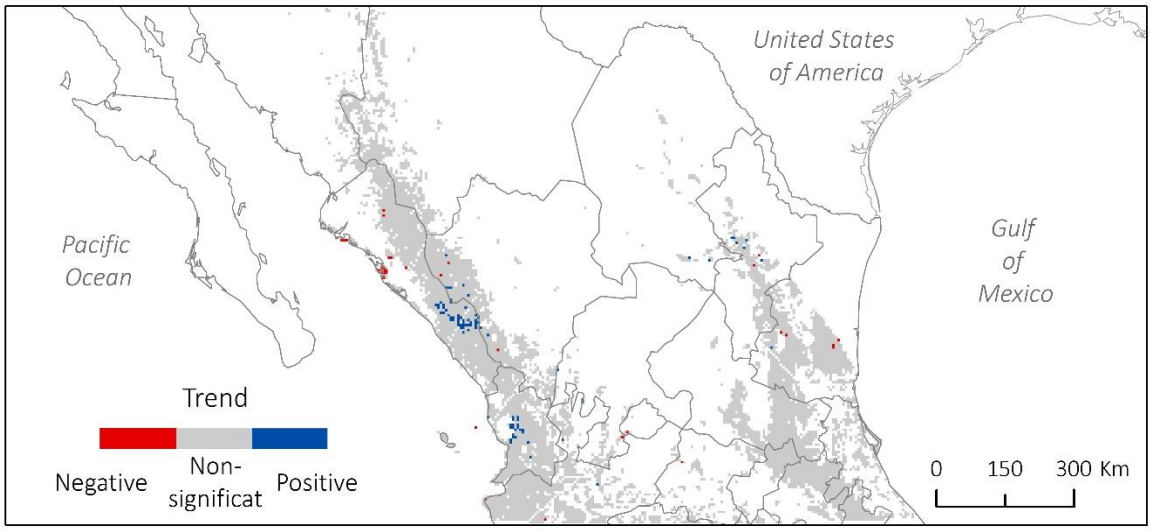

Figure 4.5. Precipitation trends, 2002-2017. The direction and significance of these trends was calculated trough a Mann-Kendall test (Hamed and Rao 1998) applied to trend components, which were extracted from pixel-based time series of monthly CHIRPS precipitation by means of a seasonal-trend decomposition procedure based on regression (Dokumentov and Hyndman 2015)

Regarding forest degradation conditions, the highest presence of any response of LAI to precipitation occurs in non-degraded forests with non-significant LAI trends, while the lowest presence occurs in highly degraded forests (Figure 4.2). However, both forest conditions exhibit weak LAI responses (Figure 4.3). In forests with non-significant LAI trends, this is not surprising due to the state of stability associated with ecosystems that remain relatively unchanged during a given period. In other words, these forests may be less sensitive to extraordinary rainfall events or droughts. In highly degraded forests, these characteristics, together with an unusual behavior observed in the response, may be indicators of weak (sometimes nonexistent) recovery responses and an unstable ecological state. However, this suggestion should be taken with caution as the theory indicates that ecosystems close to critical thresholds respond more sensitively to disturbances (Scheffer et al. 2009).

Another reason behind this behavior in highly degraded pixels may relate to the low capacity of forests in this state to intercept and infiltrate water, which leads to erosion processes and, therefore, to an initially negative response of LAI to increased precipitation. To better support this statement, this discussion suggests extending this research to explore how forest types and the underlying geology may act as a factor in this response of LAI to precipitation.

Figure 4.6 illustrates the response of LAI to precipitation in pixels located in degraded and non-degraded forests. Although there is a statistically significant Granger causality in all cases (a-d), only for some pixels (a and c) does the LAI response seem to

be clearly associated with precipitation variability. In other pixels (b and d), there appears to be other factors (climatic or anthropogenic) influencing this response. While the investigation of how LAI is affected specifically by precipitation is crucial, these results

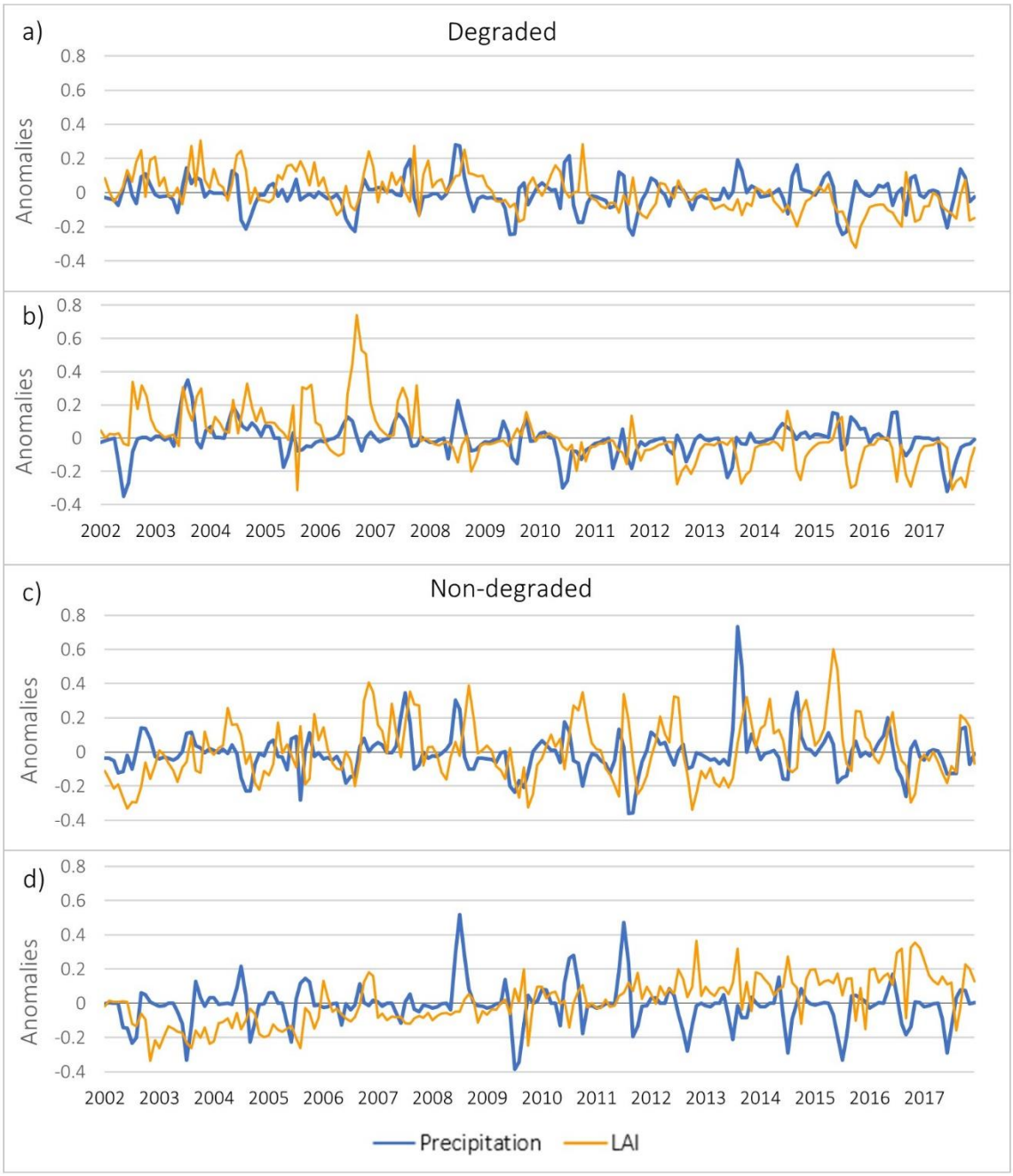

Figure 4.6. Normalized (from -1 to 1) LAI and precipitation anomalies in selected pixels located in degraded (a and b) and non-degraded (c and d) forests

have to be interpreted together with other driving variables in order to understand how forest ecosystems with different degrees of degradation respond to climate variability.

4.4.2. Limitations and opportunities

This study has three main limitations, two are associated with the data availability at specific spatio-temporal scales and one with the methodological approach. First, the spatial resolution of the CHIRPS dataset (5.42 km) is not ideally compatible with that of the MODIS LAI (500 m) product. However, CHIRPS is considered one of the best possible datasets available for regional studies. Second, the climatologies used to estimate anomalies of LAI and precipitation were not calculated based on the same period (2002-2017 for LAI; 1980-2009 for precipitation). LAI anomalies were computed as part of the methodology of this research using all temporally available MODIS data, while precipitation anomalies were previously calculated by the CHIRPS team according to a very detailed protocol (see section 4.2.2.2 and Funck et al. 2015). Third, pixels with non-stationary time series were discarded, which considerably reduced the number of pixels analyzed (Table 4.1.b).

The data-related limitations are difficult to avoid as those products are the best available at present and the generation of new data is beyond the scope of this research. Resampling LAI data to 5.4-km spatial resolution or calculating precipitation anomalies based on the 2002-2017 period to create compatibility would bring more uncertainty rather than improve the analysis. In contrast, the methodological-related limitation can be addressed in future research by detrending non-stationary time series or by

implementing the Toda and Yamamoto (1995) procedure, which allows for the examination of Granger causality in the context of non-stationary data.

4.5. Conclusion

This work evaluated the response of MODIS-LAI to CHIRPS-precipitation in Central Mexico between 2002 and 2017 based on forest degradation conditions, which were previously estimated in Chapter 3. The presence/absence of any LAI response was determined by means of the Granger causality notion, while the sign and strength of the LAI response (if any) was estimated through an IR function. The results indicate that the LAI response to precipitation is predominantly positive and occurs in a higher proportion in non-degraded pixels (43% in average) than in degraded pixels (28%). Highly degraded forests as well as non-degraded forests with non-significant LAI trends show the weakest LAI responses, which may be associated with weak recovery responses in the first case and with stable ecosystems that are inherently less sensitive to external changes in the second. The investigation of the LAI response to precipitation from a forest degradation perspective is a novel approach, which contributes to the efforts to understand how ecosystems in different ecological states respond to climate variability.

5. CONCLUSIONS

5.1. Forest degradation and climate-vegetation feedbacks in Mexico

The general objective of this dissertation was to develop an algorithm to detect forest degradation using MODIS images collected over Central Mexico (tile h08v06) between 2002 and 2017. The literature on which this research is based reveled that the underlying assumption of a constant negative relationship between vegetation greenness and surface temperature has guided some studies that aim to identify ecosystem disturbances. In this context, the first specific objective evaluated the relationship between these two variables to determine the potential of their coupling to assess forest degradation. The results of this objective showed that the relationship is not constant and its nature (i.e., sign) varies depending on the temporal scale and forest type under analysis. Because the premise of a constant negative relationship between vegetation greenness and surface temperature was discarded as a foundation on which to build the algorithm, the second objective focused only on vegetation greenness by developing a forest degradation algorithm that relies on a trend analysis of MODIS-LAI. The use of LAI was proposed to facilitate consideration of the structural changes evident from degradation though not necessarily observable through widely used vegetation spectral indices, such as NDVI and EVI. The degraded and non-degraded areas detected by the developed algorithm served as a scenario for the third objective, which evaluated the MODIS-LAI response to precipitation in the context of forest degradation conditions. The specific conclusions derived from each of the objectives can be summarized as follows:

- Objective 1 contributed to the understanding of relationship between vegetation greenness and surface temperature by evaluating the annual and intraseasonal relationship between monthly anomalies of MODIS-LAI and monthly anomalies of MODIS-LST. The presence/absence of any relationship was investigated through the notion of Granger causality, while the sign and strength of the relationship was estimated by means of an IR function. Unlike traditional regression and correlation analysis, the Granger causality approach enabled the examination of lagged effects of one variable over the other based on past values of both variables. IR coefficients, which have been rarely used in the related literature, helped to model the over-time response of a variable to the change of another variable. The results showed that, at any temporal scale, Granger causality from LST to LAI occurs more consistently than causality in the opposite direction. At the annual scale, the relationship is primarily negative in both directions and usually weaker from LAI to LST. At the seasonal scale, the occurrence of LST to LAI causality is higher in spring (it occurs in about 40% of all the evaluated pixels) and lower in winter (10%). The effect of LST on LAI is predominantly negative and particularly strong (median coefficient one month after impulse -0.043) in deciduous broadleaf forest during summer. On the other hand, the effect of LAI on LST is mainly positive in fall and negative in the remaining seasons, except for evergreen needleleaf forest where the effect is negative only in summer. The highest presence (23%) and strength (-0.039) of LAI to LST causality occurs in spring over deciduous broadleaf forest. Based on these findings, caution has to be

exercised when assuming a consistent strong negative relationship between vegetation greenness and surface temperature, which seems to be the general consensus in much of the literature that makes use of these two variables to study an environmental phenomenon.

- Objective 2 overcame the challenge of detecting subtle and gradual vegetation changes associated with forest degradation by analyzing the trend component of MODIS-LAI time series. A STR model was used to extract the trend component, whose strength and magnitude were calculated through a modified Mann-Kendall non-parametric test and the Theil-Sen´s slope test, respectively. The product of the strength and magnitude was proposed as a measure of forest degradation. The analysis found that 52% of the study area has experienced increasing LAI trends, 37% has remained unchanged, and 11% has exhibits decreasing LAI trends. Of the total area where negative trends were detected, the algorithm estimated that 385 km^2 are highly degraded, 3,406 km^2 moderately degraded, and 3,245 km^2 slightly degraded. Most of the moderate and highly degraded areas are distributed over the east side of the study area and evergreen broadleaf seems to be the most affected forest type. The algorithm showed 63% of accuracy. The validation was performed by comparing the trend analysis with an analogous trend analysis of a health index calculated using reference data from the Mexico's NFSI. Some actions to improve the accuracy were recommended, but also a different validation approach was suggested as an area of opportunity for future research.

- Objective 3 evaluated the response of LAI to precipitation based on the forest degradation conditions estimated in objective 2. The study used monthly anomalies of MODIS-LAI and monthly anomalies CHIRPS-precipitation. The presence/absence of any LAI response was determined by means of the Granger causality notion, while the sign and strength of the LAI response was estimated trough an IR function. The results demonstrated that the occurrence of LAI to precipitation causality is predominantly positive and higher in non-degraded pixels (43% in average) than in degraded pixels (28%). Non-degraded forests with non-significant LAI trends as well as highly degraded forests exhibit the weakest LAI responses, which may be associated with stable ecosystems less sensitive to external changes and with weak recovery responses, respectively. The forest degradation perspective adopted by this objective is a novel approach to investigate the effect of precipitation on vegetation greenness.

Overall, this dissertation suggests the application of the proposed methodology at national level in Mexico as a first step towards the mitigation of the forest degradation impacts on environmental services, especially those related to climate regulation through carbon sequestration. Moreover, the results of the first and third objective are expected to contribute to the body of knowledge that aims to comprehend the feedbacks between the climate and vegetation. Specifically, the third objective is expected to contribute to the understanding of how ecosystems in different ecological states respond to climate variability.

5.2. Limitations and future directions

The limitations and future directions of this research can be divided into the two following categories:

- Data-related. Although the data selected to carry out this dissertation are considered the best possible information available, they present some limitations. The Mexico's NFSI tree conditions used to validate the forest degradation algorithm have the following disadvantages: the spatial extent of the collected data is not ideally compatible with the spatial resolution of the MODIS pixels, the classification schemes are slightly different between forest inventories, the number of field observation dates within the study period is limited for the purposes of a trend analysis, and the collection of tree conditions may be subjective since it is a qualitative variable. These shortcomings hindered an appropriate validation. Therefore, future validation efforts may be improved by establishing a unique classification scheme, by considering a longer study period that allows for the incorporation of more field observation dates, and by testing the performance of reference data derived from quantitative variables. The exploration of different approaches to validate degradation studies and evaluating forest degradation directly from the Mexico's NFSI data are suggestions for future research. Regarding the remotely sensed data, the spatial resolution of the CHIRPS-precipitation (5.42 km) dataset is not ideally compatible with that of the MODIS-LAI (500 m) product. Moreover, the climatologies used to

estimate anomalies of LAI and precipitation were not calculated based on the same period (2002-2017 for LAI; 1980-2009 for precipitation). These two limitations are difficult to avoid as these datasets are the best available at this spatio-temporal scale. However, future research may explore the possibility of applying a downscaling procedure to current precipitation datasets, as well as the possibility of calculating equivalent anomalies.

- Methodology-related. The main methodological limitation of this research is associated with the reduced number of pixels on which Granger causality was tested. Only pixels with stationary time series were considered for analysis. Future studies may investigate the possibility of detrending the trajectories of non-stationary time series or implementing the Toda and Yamamoto (1995) procedure, which allows for the examination of Granger causality in the context of non-stationary data. Another limitation that can be addressed in future research deals with the false continuity on the season-based time series that were used to evaluate the intraseasonal relationship between LAI and LST. This false continuity was originated when the three monthly anomalies of a particular season were joined to the three monthly anomalies occurring the following year during the same season. This provokes the model to estimate not only intraseasonal relationships but also interannual relationships of a given season.

By addressing these limitations, future research can better estimate forest degradation and evaluate vegetation-climate feedbacks at regional scale.

REFERENCES

Bachelet, D., R. P. Neilson, J. M. Lenihan, and R. J. Drapek. 2001. Climate change effects on vegetation distribution and carbon budget in the United States. *Ecosystems* 4 (3):164–185.

Bartels, R. 1982. The Rank Version of von Neumann's Ratio Test for Randomness. *Journal of the American Statistical Association* 77(377): 40–46.

Belward, A.S., J. E. Estes, and K. D. Kline. 1999. The IGBP-DIS Global 1-km Land-Cover Data Set DISCover: A Project Overview. *Photogrammetric Engineering & Remote Sensing* 65(9): 103-1020.

Brendel, A. S., V. Y. Bohn, and M. C. Piccolo. 2017. Climatic Variability Effects on the Vegetation State and Water Coverage in a Watershed of Temperate Climate (Argentina). *Anuário do Instituto de Geociências* 40(2): 05-16.

Brooks, E. B., R. H. Wynne, V. A. Thomas, C. E. Blinn, and J. W. Coulston. 2014. On-the-fly massively multitemporal change detection using statistical quality control charts and Landsat data. *IEEE Transactions on Geoscience and Remote Sensing 52*(6): 3316-3332.

Brower, L. P., G. Castilleja, A. Peralta, J. Lopez-Garcia, L. Bojorquez-Tapia, S. Díaz, D. Melgarejo, and M. Missrie. 2002. Quantitative changes in forest quality in a principal overwintering area of the monarch butterfly in Mexico, 1971–1999. *Conservation Biology* 16(2): 346-359.

Brown, S., J. Sathaye, M. Cannell, and P. E. Kauppi. 1996. Mitigation of carbon emissions to the atmosphere by forest management. *The Commonwealth Forestry Review* 75(1) 80-91.

CBD. 2001. Forest Biological Diversity. Review of the status and trends of, and major threats to, the forest biological diversity, prepared by the Ad Hoc Technical Expert Group on Forest Biological Diversity. Convention on Biological Diversity. Subsidiary Body on Scientific, Technical and Technological Advice. Seventh meeting. Montreal, 12-16 November 2001.

Chazdon, R. L., P. H. S. Brancalion, L. Laestadius, A. Bennett-Curry, K. Buckingham, C. Kumar, J. Moll-Rocek, I. C. G. Vieira, S. J. Wilson. 2016. When is a forest a forest? Forest concepts and definitions in the era of forest and landscape restoration. *Ambio* 45(5): 538.

Chen, W. J., T. A. Black, P. C. Yang, A. G. Barr, H. H. Neumann, Z. Nesic, P. D. Blanken, M. D. Novak, J. Eley, R. J. Ketler, and R. Cuenca. 1999. Effects of climatic variability on the annual carbon sequestration by a boreal aspen forest. *Global Change Biology* 5 (1):41–53.

Cleveland, R. B., W. S. Cleveland, J. E. McRae, and I. Terpenning. 1990. STL: A seasonal-trend decomposition. *Journal of official statistics* 6(1): 3-73.

Cohen, W. B., A. Yang, and R. Kennedy. 2010. Detecting trends in forest disturbance and recovery using yearly Landsat time series: 2. TimeSync — Tools for calibration and validation. *Remote Sensing of Environment* 114: 2911–2924.

Cohen, W. B., S. P. Healey, Z. Yang, S.V. Stehman, C.K. Brewer, E.B. Brooks, N. Gorelick, C. Huang, M.J. Hughes, R.E. Kennedy, T.R. Loveland, G. G. Moisen, T. A. Schroeder, J. E. Vogelmann, C. E. Woodcock, L. Yang and Z. Zhu. 2017. How Similar Are Forest Disturbance Maps Derived from Different Landsat Time Series Algorithms?. *Forests* 8(4): 98.

Cohen, W. B., Z. Yang, S. V. Stehman, T. A. Schroeder, D. M. Bell, J. G. Masek, C. Huang, and G. W. Meigs. 2016. Forest disturbance across the conterminous United States from 1985–2012: the emerging dominance of forest decline. *Forest Ecology and Management* 360: 242-252.

CONAFOR. 2019. *National Forest and Soils Inventory Dataset, 2004-2017*. Zapopan, Mexico.

Coops, N. C., M. A. Wulder, and D. Iwanicka. 2009. Large area monitoring with a MODIS-based Disturbance Index (DI) sensitive to annual and seasonal variations. *Remote Sensing of Environment 113* (6): 1250-1261.

de Beurs, K. M., B. C. Owsley, and J. P. Julian. 2016. Disturbance analyses of forests and grasslands with MODIS and Landsat in New Zealand. *International journal of applied earth observation and geoinformation* 4: 42-54.

DOF. 2005. *Regulation of the General Law of Sustainable Forest Development*. Article 121, regulation published in the Federal Official Journal, February 21, 2005. Chamber of Deputies of the Congress of the Union, Mexico D.F., 44.

Dons, K., C. Smith-Hall, H. Meilby, and R. Fensholt. 2015. Operationalizing measurement of forest degradation: Identification and quantification of charcoal production in tropical dry forests using very high resolution satellite imagery. *International Journal of Applied Earth Observation and Geoinformation* 39: 18–27.

Dokumentov, A., and R. J. Hyndman. 2015. STR: A seasonal-trend decomposition procedure based on regression (No. 13/15). Monash University, Department of Econometrics and Business Statistics.

----------. 2018. stR: STR Decomposition. R package version 0.4. https://cran.r-project.org/web/packages/stR/stR.pdf (last accessed 11 November 2019)

Domínguez, J. 2016. Revisión histórica de las sequías en México: de la explicación divina a la incorporación de la ciencia. *Tecnología y ciencias del agua 7*(5): 77-93.

Eagleson, P.S. 2011. *Land surface processes in atmospheric general circulation models*. Cambridge University Press.

Eckert, S., F. Hüsler, H. Liniger, and E. Hodel. 2015. Trend analysis of MODIS NDVI time series for detecting land degradation and regeneration in Mongolia. *Journal of Arid Environments* 113: 16-28.

Eckert, S., H.R. Ratsimba, L.O. Rakotondrasoa, L.G. Rajoelison, and A. Ehrensperger. 2011. Deforestation and forest degradation monitoring and assessment of biomass and carbon stock of lowland rainforest in the Analanjirofo region, Madagascar. *Forest Ecology Management* 262(11): 1996-2007.

Ehrlich, D., and E. F. Lambin. 1996. Broad scale land-cover classification and interannual climatic variability. *International Journal of Remote Sensing* 17 (5):845–862.

Erb, K. H., T. Kastner, C. Plutzar, A. L. S. Bais, N. Carvalhais, T. Fetzel, S. Gingrich, H. Haberl, C. Lauk, M. Niedertscheider, J. Pongratz, M. Thurner, and S. Luyssaert. 2018. Unexpectedly large impact of forest management and grazing on global vegetation biomass. *Nature* 553(7686): 73.

Falloon, P., C. D. Jones, C. E. Cerri, R. Al-Adamat, P. Kamoni, T. Bhattacharyya, M. Easter, K. Paustian, K. Killian, K. Coleman, and E. Milne. 2007. Climate change and its impact on soil and vegetation carbon storage in Kenya, Jordan, India and Brazil. *Agriculture, Ecosystems and Environment* 122 (1):114–124.

Fang, J., Z. Guo, S. Piao, and A. Chen. 2007. Terrestrial vegetation carbon sinks in China, 1981–2000. *Science in China Series D: Earth Sciences* 50(9): 1341-1350.

FAO. 2001. Global forest resources assessment 2000. Main Report. Food and Agriculture Organization of the United Nations. *FAO Forestry Paper* 140.

-----. 2006. Global forest resources assessment 2005. Main Report. Food and Agriculture Organization of the United Nations. *FAO Forestry Paper* 147.

FAO, UNDP, and UNEP. 2015. *UN-REDD Programme Strategic Framework 2016-20*. Food and Agriculture Organization of the United Nations, United Nations Development Programme and United Nations Environment Programme. United States.

Frank, Dorothea, M. Reichstein, M. Bahn, K. Thonicke, David Frank, M. D. Mahecha, P. Smith, M. van der Velde, S. Vicca, F. Babst, C. Beer, N. Buchmann, J. G. Canadell, P. Ciais, W. Cramer, A. Ibrom, F. Miglietta, B. Poulter, A. Rammig, S. I. Seneviratne, A. Walz, M. Wattenbach, M. A. Zavala, and J. Zscheischler. 2015. Effects of climate extremes on the terrestrial carbon cycle: Concepts, processes and potential future impacts. *Global Change Biology* 21 (8):2861–2880.

Frankignoul, C., A. Czaja, and B. L'Heveder. 1998. Air–sea feedback in the North Atlantic and surface boundary conditions for ocean models. *Journal of Climate* 11: 2310–2324.

Funk, C. C., P. J. Peterson, M. F. Landsfeld, D. H. Pedreros, J. P. Verdin, J. D. Rowland, B. E, Romero, G. J. Husak, J. C. Michaelsen, and A. P. Verdin 2014. A quasi-global precipitation time series for drought monitoring. *US Geological Survey Data Series*, *832*(4), 1-12.

Funk, C. C., P.J. Peterson, M. F. Landsfeld, D. H.Pedreros, J. P. Verdin, S. Shukla, G. Husak, J. Rowland, L. Harrison, A. Hoell, and J. Michaelsen. 2015. The climate hazards infrared precipitation with stations - A new environmental record for monitoring extremes. *Scientific Data* 2:1–21.

Gao, Y., A. Ghilardi, J. Paneque-Galvez, M. Skutsch and J. F. Mas. 2015. Validation of MODIS Vegetation Continuous Fields for monitoring deforestation and forest degradation: two cases in Mexico. *Geocarto International* 31(9): 1019-1031.

Gao, Y., J.F. Mas, J. Paneque, M. Skutsch, A. Navarrete, and A. Ghilardi. 2013. Analysis of deforestation hot-spots in Mexico over 2000-2010 using time-series MODIS Vegetation Continuous Fields (VCF) data*. Conference paper*.

García, E. 2004. *Modified Koppen climatic classification (adaptation for Mexican conditions)*. 5th edition. 551.59 G37.

GCOS. 2010. Global Observing System for Climate Essential Climate Variables Data Access Matrix. National Centers for Environmental Information, NOAA. https://www.ncdc.noaa.gov/gosic/gcos-essential-climate-variable-ecv-data-access-matrix (last accessed 4 April 2019).

Gimenez, C., M. Gallardo, and R. B. Thompson. 2005. Plant-Water Relations. In *Encyclopedia of Soils in the Environment* 231–238. Elsevier.

Glendinning, P. 1994. *Stability, instability and chaos: an introduction to the theory of nonlinear differential equations* Vol. 11. Cambridge University Press.

GOFC-GOLD. 2009. *Reducing greenhouse gas emissions from deforestation and degradation in developing countries: a sourcebook of methods and procedures for monitoring, measuring and reportin*g. GOFC-GOLD Report version COP14-2. Natural Resources Canada, Alberta, Canada.

Goward, S. N., G. D. Cruickshanks, and A. S. Hope. 1985. Observed relation between thermal emission and reflected spectral radiance of a complex vegetated landscape. *Remote Sensing of Environment* 18 (2):137–146.

Granger, C. W. J. 1969. Investigating Causal Relations by Econometric Models and Cross-spectral Methods Author(s): C. W. J. Granger Source: *Econometrica* 37 (3):424–438.

Griffiths, P., T. Kuemmerle, M. Baumann, V. C. Radeloff, I. V. Abrudan, J. Lieskovsky, C. Munteanu, K. Ostapowicz, and P. Hostert. 2014. Forest disturbances, forest recovery, and changes in forest types across the Carpathian ecoregion from 1985 to 2010 based on Landsat image composites. *Remote Sensing of Environment* 151: 72–88.

Guindon, L., P. Y. Bernier, A. Beaudoin, D. Pouliot, P. Villemaire, R. J. Hall, R. Latifovic, and R. St-Amant. 2014. Annual mapping of large forest disturbances across Canada's forests using 250 m MODIS imagery from 2000 to 2011. *Canadian Journal of Forest Research* 44(12): 1545-1554.

Hamed, K. H., and A. R. Rao. 1998. A modified Mann-Kendall trend test for autocorrelated data. *Journal of Hydrology* 204(1–4): 182–196.

Hammer, D., R. Kraft, and D. Wheeler. 2014. Alerts of forest disturbance from MODIS imagery. *International Journal of Applied Earth Observation and Geoinformation* 33: 1-9.

Harvey, A. C. 1985. Trends and cycles in macroeconomic time series. *Journal of Business & Economic Statistics* 3(3): 216-227.

Harvey, A. C., and S. Peters. 1990. Estimation procedures for structural time series models. *Journal of Forecasting* 9(2): 89-108.

Harvey, A. C., and Tood P. H. J. 1983. Forecasting economic time series with structural and Box-Jenkins models: A case study. *Journal of Business & Economic Statistics* 1(4): 299-307.

Hashim, M., A. Beiranvand, and C. K. Wei. 2014. Comparison of ETM+ and MODIS Data for Tropical Forest Degradation Monitoring in the Peninsular Malaysia. *Indian Society of Remote Sensing* 1-14.

Healey, S.P., W. B. Cohen, Y. Zhiqiang, and O. N. Krankina. 2005. Comparison of Tasseled Cap-based Landsat data structures for use in forest disturbance detection. *Remote Sensing of Environment* 97: 301–310.

Helsel, D. R., and L. M. Frans. 2006. Regional Kendall test for trend. *Environmental Science & Technology* 40(13): 4066-4073.

Hilker, T., M. A. Wulder, N. C. Coops, J. Linke, G. McDermid, J. G. Masek, F. Gao, and J. C. White. 2009. A new data fusion model for high spatial-and temporal-resolution mapping of forest disturbance based on Landsat and MODIS. *Remote Sensing of Environment* 113(8): 1613-1627.

Hietz, P., G. Buchberger, and M. Winkler. 2006. Effect of forest disturbance on abundance and distribution of epiphytic bromeliads and orchids. *Ecotropica* 12(2): 103-112.

Hollander, M., D. A. Wolfe, and E. Chicken. 2013. *Nonparametric statistical methods*. Vol. 751. John Wiley & Sons.

Huang, C., S. N. Goward, J.G. Masek, N. Thomas, Z. Zhu, and J. E. Vogelmann. 2010. An automated approach for reconstructing recent forest disturbance history using dense Landsat time series stacks. *Remote Sensing of Environment* 114: 183–198.

Huang, C., K. Song, S. Kim, J. R. G. Townshend, P. Davis, J. G. Masek, and S. N. Goward. 2008. Use of a dark object concept and support vector machines to automate forest cover change analysis. *Remote Sensing of Environment* 112: 970–985.

Huete, A., K. Didan, T. Miura, E. P. Rodriguez, X. Gao, and L. F. Ferreira. 2002. Overview of the radiometric and biophysical performance of the MODIS vegetation indices. *Remote sensing of environment 83*(1-2): 195-213.

Hughes, M.J. 2014. *New Remote Sensing Methods for Detecting and Quantifying Forest Disturbance and Regeneration in the Eastern United States*. Ph.D. Thesis, University of Tennessee, Knoxville, TN, USA.

INEGI. 2005. *Land use and vegetation map, serie III (2002), scale 1: 250,000.* National Institute of Statistics and Geography. Mexico.

------. 2017. *Land use and vegetation map, serie VI (2014), scale 1: 250,000.* National Institute of Statistics and Geography. Mexico.

Iordanova, T. 2009. "Introduction to Stationary and Non-Stationary Processes". http://www.investopedia.com/articles/trading/07/stationary.asp (last accessed 3 January 2019).

IPCC. 2014. Climate change 2014: Synthesis Report. Contribution of Working Group I, II, and III to the Fifth Assessment Report of the Intergovernmental Panel on Climate Change. New York. Cambridge University Press.

ITTO. 2005. Revised ITTO criteria and indicators for the sustainable management of tropical forests including reporting format. International Tropical Timber Organization Policy development series No. 15.

IUFRO. 1994. *International Guidelines for Forest Monitoring*. International Union of Forest Research Organizations. World Series.

Jacquin, A., D. Sheeren, and J. P. Lacombe. 2010. Vegetation cover degradation assessment in Madagascar savanna based on trend analysis of MODIS NDVI time series. *International Journal of Applied Earth Observation and Geoinformation* 12: S3-S10.

Jenkins, M. and B. Schaap. 2018. *Forest Ecosystem Services*. Background study prepared for the thirteenth session of the United Nations Forum on Forests.

Jensen, J. L., K. S. Humes, A. T. Hudak, L. A. Vierling, and E. Delmelle. 2011. Evaluation of the MODIS LAI product using independent lidar-derived LAI: A case study in mixed conifer forest. *Remote Sensing of Environment* 115(12): 3625-3639.

Jiang, B., S. Liang, and W. Yuan. 2015. Observational evidence for impacts of vegetation change on local surface climate over northern China using the Granger causality test. *Journal of Geophysical Research: Biogeosciences 120*(1): 1-12.

Jin, S., and S. A. Sader. 2005. MODIS time-series imagery for forest disturbance detection and quantification of patch size effects. *Remote Sensing of Environment 99*(4): 462-470.

Joshi, N., E. T. A. Mitchard, N. Woo, J. Torres, J. Moll-Rocek, A. Ehammer, M. Collins, M. R. Jepsen, and R. Fensholt. 2015. Mapping dynamics of deforestation and forest degradation in tropical forests using radar satellite data. *Environmental Research Letters* 10(3): 1-13.

Julien, Y., and J. A. Sobrino. 2009. The Yearly Land Cover Dynamics (YLCD) method: An analysis of global vegetation from NDVI and LST parameters. *Remote Sensing of Environment* 113 (2):329–334.

Kant, P. 2006. Definition of Forests Under Kyoto Protocol; Choosing Appropriate Values for Crown Cover, Area and Tree Height for India. Indian Forester 132(5): 632.

Karl, T. R., J. M. Melillo, T.C. Peterson, T. C., and S. J. Hassol (Eds.). 2009. *Global climate change impacts in the United States*. Cambridge University Press.

Kaufmann, R. K., K. C. Seto, A. Schneider, Z. Liu, L. Zhou, and W. Wang. 2007. Climate response to rapid urban growth: Evidence of a human-induced precipitation deficit. *Journal of Climate* 20 (10):2299–2306.

Kaufmann, R. K., L. Zhou, R. B. Myneni, C. J. Tucker, D. Slayback, N. V. Shabanov, and J. Pinzon. 2003. The effect of vegetation on surface temperature: A statistical analysis of NDVI and climate data. *Geophysical Research Letters* 30 (22):3–6.

Kauppi, P. 2003. Low estimate for carbon stock in global forest vegetation based on inventory data. *Silva Fennica* 37(4): 451-457.

Kendall, M.G., 1955. *Rank Correlation Methods*. Griffin, London.

Kennedy, R. E., Z. Yang, and W. B. Cohen. 2010. Detecting trends in forest disturbance and recovery using yearly Landsat time series: 1. LandTrendr—Temporal segmentation algorithms. *Remote Sensing of Environment* 114(12): 2897-2910.

King, M. D., S. Platnick, W.P. Menzel, S. A. Ackerman, and P. A. Hubanks. 2013. Spatial and temporal distribution of clouds observed by MODIS onboard the Terra and Aqua satellites. *IEEE Transactions on Geoscience and Remote Sensing* 51(7): 3826-3852.

Klooster, D., and O. Masera. 2000. Community forest management in Mexico: carbon mitigation and biodiversity conservation through rural development. *Global Environmental Change* 10(4): 259-272.

Knyazikhin, Y., J. V. Martonchik, D. J. Diner, R. B. Myneni, M. Verstraete, B. Pinty, and N. Gobron. 1998. Estimation of vegetation canopy leaf area index and fraction of absorbed photosynthetically active radiation from atmosphere-corrected MISR data. *Journal of Geophysical Research Atmospheres* 103 (D24):32239–32256.

Kovacs, J. M., J. Wang, and M. Blanco-Correa. 2001. Mapping disturbances in a mangrove forest using multi-date Landsat TM imagery. *Environmental Management* 27(5): 763-776.

Kumar, D., and S. Shekhar. 2015. Statistical analysis of land surface temperature-vegetation indexes relationship through thermal remote sensing. *Ecotoxicology and Environmental Safety* 121:39–44.

Kwiatkowski, D., P. C. Phillips, P. Schmidt, and Y. Shin. 1992. Testing the null hypothesis of stationarity against the alternative of a unit root: How sure are we that economic time series have a unit root?. *Journal of econometrics* 54(1-3): 159-178.

Lambin, E. F., and D. Ehrlich. 1996. The surface temperature-vegetation index space for land cover and land-cover change analysis. *International Journal of Remote Sensing* 17(3):463–487.

Lambin, E. F., and D. Ehrlich. 1997. Land-cover changes in Sub-Saharan Africa (1982-1991): Application of a change index based on remotely sensed surface temperature and vegetation indices at a continental scale. *Remote Sensing of Environment* 61(2):181–200.

Liu, Z., M. Notaro, J. Kutzbach, and N. Liu. 2006. Assessing global vegetation-climate feedbacks from observations. *Journal of Climate* 19 (5):787–814.

Loboda, T. V., Z. Zhang, K. J. O'Neal, G. Sun, I. A. Csiszar, H. H. Shugart, and N. J. Sherman. 2012. Reconstructing disturbance history using satellite-based assessment of the distribution of land cover in the Russian Far East. *Remote sensing of environment* 118: 241-248.

Lucas, R.M., D. Clewley, A. Accad, D. Butler, J. Armston, M. Bowen, P. Bunting, J. Carreiras, J. Dwyer, T. Eyre, A. Kelly, C. McAlpine, S. Pollock, and L. Seabrook. 2014. Mapping forest growth and degradation stage in the Brigalow Belt Bioregion of Australia through integration of ALOS PALSAR and Landsat-derived foliage projective cover data. *Remote Sensing of Environment* 155: 42–57.

Lütkepohl, H. 2005. *New introduction to multiple time series analysis*. Springer Science & Business Media.

Mann, H. B. 1945. Nonparametric tests against trend. *Econometrica: Journal of the Econometric Society* 13(3): 245-259.

Mariano, D. A., C. A. C. do. Santos, B. D. Wardlow, M. C. Anderson, A. V. Schiltmeyer, T. Tadesse, and M. D. Svoboda. 2018. Use of remote sensing indicators to assess effects of drought and human-induced land degradation on ecosystem health in Northeastern Brazil. *Remote Sensing of Environment* 213 (April):129–143.

Matricardi, E. A. T., D. L. Skole and M. A. Pedlowski. 2010. Assessment of tropical forest degradation by selective logging and fire Landsat imagery. *Remote Sensing of Environment* 114: 1117-1129.

Matsushita, B., W. Yang, J. Chen, Y. Onda, and G. Qiu. 2007. Sensitivity of the Enhanced Vegetation Index (EVI) and Normalized Difference Vegetation Index (NDVI) to topographic effects. :2636–2651.

Menzel, A., and P. Fabian. 1999. Growing season extended in Europe. *Nature* 397 (6721):659.

Metternicht, G., Zinck, J. A., Blanco, P. D., and H. F. Del Valle. 2010. Remote sensing of land degradation: Experiences from Latin America and the Caribbean. *Journal of environmental quality* 39(1): 42-61.

Mildrexler, D. J., M. Zhao, F.A. Heinsch, and S.W. Running. 2007. A new satellite-based methodology for continental scale disturbance detection. *Ecological Applications* 17(1): 235-250.

Mildrexler, D.J., M. Zhao, and S. W. Running. 2009. Testing a MODIS Global Disturbance Index across North America. *Remote Sensing of Environment* 113: 2103–2117.

Moisen, G. G., M. C. Meyer, T. A. Schroeder, X. Liao, K. G. Schleeweis, E. A. Freeman, and C. Toney. 2016. Shape selection in Landsat time series: A tool for monitoring forest dynamics. *Global change biology* 22(10): 3518-3528.

Morales-Baquero, L., A. Borrego, M. Skutsch, C. Kleinn, and J. R. Healey. 2015. Identification and quantification of drivers of forest degradation in tropical dry forests: a case study in Western Mexico. *Land Use Policy* 49: 296-309.

Morales-Barquero, L., M. Skutsch, E. J. Jardel-Peláez, A. Ghilardi, C. Kleinn, and J. R. Healey. 2014. Operationalizing the Definition of Forest Degradation for REDD+, with Application to Mexico. *Forests* 5: 1653-1681.

Myneni, R. B., C. D. Keeling, C. J. Tucker, G. Asrar, and R. R. Nemani, R. R. 1997. Increased plant growth in the northern high latitudes from 1981 to 1991. *Nature 386*(6626): 698.

Myneni, R. B., S. Hoffman, Y. Knyazikhin, J. L. Privette, J. Glassy, Y. Tian, Y. Wang, X. Song, Y. Zhang, G. R. Smith, A. Lotsch, M. Friedl, J. T. Morisette, P. Votava, R. R. Nemani, and S. W. Running. 2002. Global products of vegetation leaf area and fraction absorbed PAR from year one of MODIS data. *Remote Sensing of Environment* 83(1): 214-231.

Na-U-Dom, T., X. Mo, and M. García. 2017. Assessing the Climatic Effects on Vegetation Dynamics in the Mekong River Basin. *Environments* 4 (1):17.

Nason, G. P. 2003. Chapter 11 Stationary and non-stationary time series. *Statistics in Volcanology* (1994):1–29.

Nemani, R. R., C. D. Keeling, H. Hashimoto, W. M. Jolly, S. C. Piper, C. J. Tucker, R. B. Myneni, and S. W. Running. 2003. Climate-driven increases in global terrestrial net primary production from 1982 to 1999. *Science* 300 (5625):1560–1563.

Notaro, M., Z. Liu, and J. W. Williams. 2006. Observed vegetation - Climate feedbacks in the United States. *Journal of Climate* 19 (5):763–786.

Ogbodo, J. A., D. O. Oke, and B. I. Dagba. 2015. The potential of synthetic aperture radar (SAR) imagery in automated detection of forest degradation features using visual and semi-automated analyses. *Land Use, Land-Use Change and Forestry* 57-77.

Pfaff, B. 2008a. *Analysis of Integrated and Cointegrated Time Series with R*. Second Edition. Springer, New York. ISBN 0-387-27960-1

----------2008b. "VAR, SVAR and SVEC Models: Implementation Within R Packag vars". Journal of Statistical Software 27(4): 1-32.

Papagiannopoulou, C., Di. G. Miralles, S. Decubber, M. Demuzere, N. E. C. Verhoest, W. A. Dorigo, and W. Waegeman. 2017. A non-linear Granger-causality framework to investigate climate-vegetation dynamics. *Geoscientific Model Development* 10 (5):1945–1960.

Patakamuri, S. K., and N. O'Brien. 2019. modifiedmk: Modified Versions of Mann Kendall and Spearman's Rho Trend Tests. R package version 1.3.0. https://cran.r-project.org/web/packages/modifiedmk/modifiedmk.pdf (last accessed 11 November 2019)

Penman, J., M. Gytarsky, T. Hiraishi, T. Krug, D. Kruger, R. Pipatti, L. Buendia, K. Miwa, T. Mgara, K. Tanabe, and F. Wagner. 2003. Definitions and methodological options to inventory emissions from direct human-induced degradation of forests and devegetation of other vegetation types. Intergovernmental Panel on Climate Change (IPCC) National Greenhouse Gas Inventories Programme.

Potter, C., P. N. Tan, M. Steinbach, S. Klooster, V. Kumar, R. Myneni, and V. Genovese. 2003. Major disturbance events in terrestrial ecosystems detected using global satellite data sets. *Global Change Biology* 9(7): 1005-1021.

Potter, C., P. N. Tan, V. Kumar, C. Kucharik, S. Klooster, V. Genovese, W. Cohen, and S. Healey. 2005. Recent history of large-scale ecosystem disturbances in North America derived from the AVHRR satellite record. *Ecosystems* 8(7): 808-824.

Potter, C., V. Kumar, S. Klooster, and R. Nemani. 2007. Recent history of trends in vegetation greenness and large-scale ecosystem disturbances in Eurasia. *Tellus B : Chemical and Physical Meteorology* 59(2): 260-272.

Pouliot, D., R. Latifovic, R. Fernandes, and I. Olthof. 2009. Evaluation of annual forest disturbance monitoring using a static decision tree approach and 250 m MODIS data. *Remote Sensing of Environment* 113(8): 1749-1759.

Powers, J. S., and W. H. Schlesinger. 2002. Relationships among soil carbon distributions and biophysical factors at nested spatial scales in rain forests of northeastern Costa Rica. *Geoderma* 109(3): 165-190.

Putz, F. E., and K. H. Redford. 2010. The Importance of Defining 'Forest': Tropical Forest Degradation, Deforestation, Long-term Phase Shifts, and Further Transition. *Biotropica* 42: 10–20.

Ramachandran, A., S. Jayakumar, R. M. Haroon, A. Bhaskaran, and D. I. Arockiasamy. 2007. Carbon sequestration: estimation of carbon stock in natural forests using geospatial technology in the Eastern Ghats of Tamil Nadu, India. *Current Science* 323-331.

R Core Team. 2018. "R: A language and environment for statistical computing". R Foundat ion for Statistical Computing, Vienna, Austria. https://www.R-project.org/ (last acc essed 10 January 2019).

Romero-Sanchez, M., and R. Ponce-Hernandez. 2017. Assessing and monitoring forest degradation in a deciduous tropical forest in Mexico via remote sensing indicators. *Forests* 8(9): 302.

Roy, D. P., P. Kennedy, and S. Folving. 1997. Combination of the normalized difference vegetation index and surface temperature for regional scale european forest cover mapping using AVHRR data. *International Journal of Remote Sensing* 18 (5):1189–1195.

Ryan, C.M., T. Hill, E. Woollen, C. Ghee, E. Mitchard, G. Cassells, J. Grace, I. H. Woodhouse, and M. Williams. 2012. Quantifying small-scale deforestation and forest degradation in African woodlands using radar imagery. *Global Change Biology* 18: 243–257.

Sasaki, N., and F. E. Putz. 2009. Critical need for new definitions of "forest" and "forest degradation" in global climate change agreements. *Conservation Letters* 2: 226–232.

Scheffer, M., J. Bascompte, W. A. Brock, V. Brovkin, S. R. Carpenter, V. Dakos, H. Held, E. H. Van Nes, M. Rietkerk, and G. Sugihara. 2009. Early-warning signals for critical transitions. *Nature* 461 (7260):53–59.

Schmidt, M., R. Lucas, P. Bunting, J. Verbesselt, and J. Armston. 2015. Multi-resolution time series imagery for forest disturbance and regrowth monitoring in Queensland, Australia. *Remote Sensing of Environment* 158: 156-168.

Schoene, D., W. Killmann, H. Von Lüpke, and M.L. Wilkie. 2007. *Definitional issues related to reducing emissions from deforestation in developing countries*. Vol. 5. Food and Agriculture Organization of the United Nations. Rome.

Schroeder, T. A., K. G. Schleeweis, G. G. Moisen, C. Toney, W. B. Cohen, E. A. Freeman, Z. Yang, and C. Huang. 2017. Testing a Landsat-based approach for mapping disturbance causality in US forests. *Remote Sensing of Environment 195*: 230-243.

Schucknecht, A., S. Erasmi, I. Niemeyer, and J. Matschullat. 2013. Assessing vegetation variability and trends in north-eastern Brazil using AVHRR and MODIS NDVI time series. *European Journal of Remote Sensing* 46(1): 40-59.

Seddon, A. W. R., M. Macias-Fauria, P. R. Long, D. Benz, and K. J. Willis. 2016. Sensitivity of global terrestrial ecosystems to climate variability. *Nature* 531 (7593):229–232.

SEMARNAT. 2007. *Manual of Forest Health*. Secretariat of Environment and Natural Resources. Mexico. http://www.conafor.gob.mx:8080/documentos/docs/15/810 Manual%20de% 20sanidad%20forestal.pdf (last accessed 23 October 2019).

Sen, P. K. 1968. Estimates of the regression coefficient based on Kendall's tau. *Journal of the American statistical association 63*(324): 1379-1389.

Sharma, C. M., S. Gairola, N.P. Baduni, S. K. Ghildiyal, and S. Suyal. 2011. Variation in carbon stocks on different slope aspects in seven major forest types of temperate region of Garhwal Himalaya, India. *Journal of Biosciences* 36(4): 701-708.

Shoch, D., J. Eaton, and S. Settelmyer. 2013. *Project developer's guidebook to VCS REDD methodologies*. Versión 2.0 February 2013. Conservación Internacional. https://www.conservation.org/docs/default-source/publication-pdfs/ci_redd-developers-guidebook.pdf (last accessed 11 November 2019).

Skutsch, M., C. Simon, A. Velazquez, J. C. Fernández. 2013. Rights to carbon and payments for services rendered under REDD+: Options for the case of Mexico. *Globlal Environmental Change* 23: 813–825.

Sofan, P., Y. Vetrita, F. Yulianto, and M. R. Khomarudin. 2016. Multi-temporal remote sensing data and spectral indices analysis for detection tropical rainforest degradation: case study in Kapuas Hulu and Sintang districts, West Kalimantan, Indonesia. *Natural Hazards* 80: 1279–1301.

Souza, C.M., J. V. Siqueira, M. H. Sales, A.V. Fonseca, J. G. Ribeiro, I. Numata, M. A. Cochrane, C.P. Barber, D. A. Roberts, and J. Barlow. 2013. Ten-Year Landsat Classification of Deforestation and Forest Degradation in the Brazilian Amazon. *Remote Sensing* 5: 5493-5513.

Stevens, A., B. Van Wesemael, G. Vandenschrick, S. Touré, and B. Tychon. 2006. Detection of carbon stock change in agricultural soils using spectroscopic techniques. *Soil Science Society of America Journal* 70(3): 844-850.

Strahler, A., D. Muchoney, J. Borak, M. Fried, S. Gopal, E. Lambin, and A. Moody. 1999. *MODIS land cover product: Algorithm theoretical basis document*.Version 5.0. https://modis.gsfc.nasa.gov/data/atbd/atbd_mod12.pdf (last accessed 11 November 2019)

Sulla-Menashe, D., R. E. Kennedy, Z. Yang, J. Braaten,O. N. Krankina, and M. A. Friedl. 2014. Detecting forest disturbance in the Pacific Northwest from MODIS time series using temporal segmentation. *Remote Sensing of Environment* 151: 114-123.

Tanase, M.A., I. Ismail, K. Lowell, O. Karyanto, and M. Santoro. 2015. Detecting and Quantifying Forest Change: The Potential of Existing C- and X-Band Radar Datasets. *PloS One* 10(6): 1-14.

Theil, H. 1950. A rank-invariant method of linear and polynomial regression analysis. Part 3. In *Proceedings of Koninalijke Nederlandse Akademie van Weinenschatpen A*. Vol. 53: pp. 1397-1412.

Tian, H., J. M. Melillo, D. W. Kicklighter, A. D. Mcguire, J. V. K. Helfrich III, B. Moore III, and C. J. Vorosmarty. 1998. Effect of interannual climate variability on carbon storage in Amazonian ecosystems. *Nature 396*(6712): 664.

Toda, H. Y, and T. Yamamoto. 1995. Statistical inferences in vector autoregressions with possibly integrated processes. *Journal of Econometrics* 66: 225-250.

Tran, T. V., K. M. de Beurs, and J. P. Julian. 2016. Monitoring forest disturbances in Southeast Oklahoma using Landsat and MODIS images. *International journal of applied earth observation and geoinformation* 44: 42-52.

Ullah, M. R., M. Al-Amin. 2012. Above-and below-ground carbon stock estimation in a natural forest of Bangladesh. *Journal of Forest Science* 58(8): 372-379.

UNEP-CBD. 2001. Report of the Ad Hoc Technical Expert Group on Forest Biological Diversity. Subsidiary Body for Scientific, Technical and Technological Advice. Seventh Meeting, Montreal, 12-16 November 2001.

USDA. 2016. *Forest Inventory and Analysis Glossary*. USDA Forest Service. https://www.nrs.fs.fed.us/fia/data-tools/state-reports/glossary/ (last accessed 11 November 2019).

Vandecar, K. L., D. Lawrence, D. Richards, L. Schneider, J. Rogan, B. Schmook, and H. Wilbur. 2011. High mortality for rare species following hurricane disturbance in the Southern Yucatan. *Biotropica 43*(6): 676-684.

Verbesselt, J., R. Hyndman, G. Newnham, and D. Culvenor. 2010. Detecting trend and seasonal changes in satellite image time series. *Remote Sensing of Environment* 114(1): 106-115.

Vidal, O., J. López-García, E. Rendón-Salinas. 2014. Trends in deforestation and forest degradation after a decade of monitoring in the Monarch Butterfly Biosphere Reserve in Mexico. *Conservation Biology* 28(1): 177-186.

Vogelmann, J. E., G. Xian, C. Homer, and B. Tolk. 2012. Monitoring gradual ecosystem change using Landsat time series analyses: Case studies in selected forest and rangeland ecosystems. *Remote Sensing of Environment* 122: 92-105.

Wan, Z. 2013. *Collection-6 MODIS Land Surface Temperature Products Users' Guide*. Institute for Computational Earth System Science, University of California, Santa Barbara.

---------. 2014. New refinements and validation of the Collection-6 MODIS land-surface temperature/emissivity products. *Remote Sensing of Environment* 140: 36-45.

Wan, Z, and J. Dozier. 1996. A generalized split-window algorithm for retrieving land-surface temperature from space. *IEEE Transactions on Geoscience and Remote Sensing* 34 (4):892–905.

Wan, Z., P. Wang, and X. Li. 2004. Using MODIS Land Surface Temperature and Normalized Difference Vegetation Index products for monitoring drought in the southern Great Plains, USA. *International Journal of Remote Sensing* 25 (1):61–72.

Wan, Z., Y. Zhang, Q. Zhang, and Z. L. Li. 2004. Quality assessment and validation of the MODIS global land surface temperature. *International Journal of Remote Sensing* 25 (1):261–274.

Wan, Z., and Z. L. Li. 1997. A physics-based algorithm for retrieving land-surface emissivity and temperature from EOS/MODIS data. *IEEE Transactions on Geoscience and Remote Sensing* 35: 980–996.

Wang, W., B. T. Anderson, D. Entekhabi, D. Huang, Y. Su, R. K. Kaufmann, and R. B. Myneni. 2007. Intraseasonal interactions between temperature and vegetation over the boreal forests. *Earth Interactions* 11 (18):1–30.

Wang, W., B. T. Anderson, N. Phillips, R. K. Kaufmann, C. Potter, and R. B. Myneni. 2006. Feedbacks of vegetation on summertime climate variability over the North American grasslands. Part I: Statistical analysis. *Earth Interactions* 10 (17).

Weishampel, J. F. W., J. N. Hightower, A. F. Chase, and D. Z. Chase. 2012. Use of airborne LiDAR to delineate canopy degradation and encroachment along the Guatemala-Belize border. *Tropical Conservation Science* 5: 12-24.

Weng, Q., D. Lu, and J. Schubring. 2004. Estimation of land surface temperature-vegetation abundance relationship for urban heat island studies. *Remote Sensing of Environment* 89 (4):467–483.

Xin, Q., P. Olofsson, A. Zhu, B. Tan, and C. E. Woodcock. 2013. Toward near real-time monitoring of forest disturbance by fusion of MODIS and Landsat data. *Remote Sensing of Environment* 135*:* 234-247.

Yan, K., T. Park, G. Yan, Z. Liu, B. Yang, C. Chen, R. R. Nemani, Y. Knyazikhin, and R. B. Myneni. 2016. Evaluation of MODIS LAI/FPAR product collection 6. Part 2: validation and intercomparison. *Remote Sensing* 8(6): 460.

Yang, W., D. Huang, B. Tan, J. C. Stroeve, N. V. Shabanov, Y. Knyazikhin, Y., R. R. Nemani, and R. B. Myneni. 2006. Analysis of leaf area index and fraction of PAR absorbed by vegetation products from the terra MODIS sensor: 2000-2005. *IEEE Transactions on Geoscience and Remote Sensing* 44(7): 1829-1842.

Yue, W., J. Xu, W. Tan, and L. Xu. 2007. The relationship between land surface temperature and NDVI with remote sensing: Application to Shanghai Landsat 7 ETM+ data. *International Journal of Remote Sensing* 28 (15):3205–3226.

Zhou, L., R. K. Kaufmann, Y. Tian, R. B. Myneni, and C. J. Tucker. 2003. Relation between interannual variations in satellite measures of northern forest greenness and climate between 1982 and 1999. *Journal of Geophysical Research* 108 (D1):4004.

Zhu, Z., and C. E. Woodcock. 2014. Continuous change detection and classification of land cover using all available Landsat data. *Remote sensing of Environment 144*: 152-171.

Zivot, E., and J. Wang. 2006. Vector autoregressive models for multivariate time series. In *Modelin Financial Time Series with S-Plus® 385-429.* Springer Science & Business Media.